8-2023

Biomimetic Aerosol Exposure System for in vitro Human Airway Exposure Studies

Samantha Emma Sarles
ses9066@rit.edu

Biomimetic Aerosol Exposure System for in vitro Human Airway Exposure Studies

by

Samantha Emma Sarles

A dissertation submitted in partial fulfillment of the

requirements for the degree of

Doctor of Philosophy

in Biomedical & Chemical Engineering

Advised by: Dr. Edward C. Hensel, PE

Kate Gleason College of Engineering

Rochester Institute of Technology

Rochester, New York

August 2023

Dissertation title: Biomimetic Aerosol Exposure System for in vitro Human Airway Exposure Studies

By
Samantha Emma Sarles

Committee Approval:

Dr. Edward C. Hensel, Advisor — Date
Professor, Associate Dean of Graduate Studies
Kate Gleason College of Engineering, Rochester Institute of Technology

---

Dr. Risa J. Robinson, Committee Member — Date
Professor, Department Head of Mechanical Engineering
Kate Gleason College of Engineering, Rochester Institute of Technology

---

Dr. Karin Wuertz-Kozak, Committee Member — Date
Professor, Department of Biomedical Engineering
Kate Gleason College of Engineering, Rochester Institute of Technology

---

Dr. Nathan C. Eddingsaas, Committee Member — Date
Associate Professor, School of Chemistry and Materials Science
College of Science, Rochester Institute of Technology

Dr. Irfan Rahman, Committee Member — Date
Professor, Department of Environmental Health
School of Medicine and Dentistry, University of Rochester Medical Center

Certified by:

Dr. Thomas Gaborski, Director — Date
PhD in Biomedical & Chemical Engineering
Rochester Institute of Technology

BIOGRAPHICAL SKETCH

NAME: Sarles, Samantha Emma

eRA COMMONS USER NAME: SES9066@rit.edu

POSITION TITLE: Doctoral Candidate

EDUCATION/TRAINING

INSTITUTION AND LOCATION	DEGREE *(if applicable)*	Start Date MM/YYYY	Completion Date MM/YYYY	FIELD OF STUDY
Rochester Institute of Technology, Rochester, NY	BFA	08/2012	05/2017	Industrial Design
Rochester Institute of Technology, Rochester, NY	MS	08/2017	08/2019	Interdisciplinary: Medical Device Engineering & Biomaterials
Rochester Institute of Technology, Rochester, NY	MS	08/2020	12/2022	Industrial & Systems Engineering
Rochester Institute of Technology, Rochester, NY	PhD	08/2019	08/2023	Biomedical & Chemical Engineering

A. Personal Statement

Academic training spanning several disciplines provides me the ability to address complex problems through an interdisciplinary lens, which enables novel scientific innovation while facilitating communication with collaborators across diverse technical backgrounds. My transdisciplinary education in design, biomedical science, and engineering along with my research experience in biomedical instrumentation development, including instruments for *in vitro* models and for clinical studies, has provided me a strong scientific background in tissue engineering, mechanobiology, molecular biology, biofabrication, and biomaterials.

As an undergraduate student, I was involved in research and development projects focused on accessibility, which gave me experience in human subjects research, intellectual property, human centered design, and ergonomics. For nearly six years, I have worked as a Graduate Research Assistant under the mentorship of Dr. Edward C. Hensel, PE, PhD in the Respiratory Technologies Lab at Rochester Institute of Technology. We are a multidisciplinary lab who studies the influence of tobacco product characteristics on instantaneous smoking behavior (e.g. puff flow rate, duration, volume), on emissions produced, on consumption behavior (e.g. cumulative volume, cigarettes per day) and ultimately how these factors impact health outcomes of the tobacco user. I have developed research instruments for investigation into health effects of inhaled tobacco products, such as electronic cigarettes, including development, testing, and manufacturing of tools used in clinical studies and a biomimetic aerosol exposure system for *in vitro* analytical and biological testing of inhaled aerosols. These projects have given me extensive experience with cell-substrate interactions, engineering for biomimicry, working with quantitative data, and technical communication.

I am committed to diversity and inclusion in science and engineering. I am a founding member and Inclusivity Officer of my university's Women in Grad School organization, a club that provides mentorship and support to women and gender minority graduate students. I will be the first woman to graduate from the Biomedical and Chemical Engineering PhD Program at Rochester Institute of Technology. As a graduate researcher, I have mentored multiple students who belong to under-represented groups. I mentored five female students, one Black student, and one LGBTQ+ student. Being a woman in science and LGBTQ+ myself, I am passionate about creating access, recruiting, and retaining researchers who are traditionally underrepresented in science and engineering.

Citations:

1. **Sarles, S. E.,** Hensel, E. C., Robinson, R. J. Surveillance of U.S. Corporate Filings Provides a Proactive Approach to Inform Tobacco Regulatory Research Strategy*. Int. J. Environ. Res. Public Health.* 16 March 2021.
2. **Sarles, S. E.**, Hensel, E.C., Rahman, I., Robinson, R. J. Clinical Biomarkers to Evaluate Next Generation Inhaled Tobacco Products' Effect in the Oral Cavity: A Narrative Review. *Current Oral Health Reports.* Manuscript ID: ORAL-D-23-00052. *In Review.*
3. Hensel, E.C., Eddingsaas, N., Saleh, Q., Jayasekera S., **Sarles, S.E.,** DiFrancesco, G., Robinson R.J. Proposed Standard Test Protocols and Outcome Measures for Quantitative Comparison of Emissions from Electronic Nicotine Delivery Systems. *Int. J. Environ. Res. Public Health.* 14 February 2022.
4. Hensel, E.C., Eddingsaas, N., Saleh, Q., Jayasekera S., **Sarles, S.E.,** Thomas, M., Myers, B., DiFrancesco, G., Robinson R.J. Nominal Operating Envelope of Pod and Pen Style Electronic Cigarettes. *Frontiers in Public Health.* 17 August 2021.

B. Positions, Scientific Appointments and Honors

Positions

2023-Present	Operations Coordinator, LGBTQ+ Workgroup-Health Equity Network, Society for Research on Nicotine and Tobacco
2023-Present	Member, Society for Research on Nicotine and Tobacco
2022-Preset	Inclusivity Officer, Women in Graduate School, Rochester Institute of Technology
Spring 2022	Course Instructor, Rochester Institute of Technology
2021-Present	Member, Biomedical Engineering Society
2020-Present	Graduate Research Mentor, Rochester Institute of Technology
Fall 2018	Graduate Teaching Assistant, Rochester Institute of Technology
2017-Present	Graduate Research Assistant, Rochester Institute of Technology

Honors

2023	Biomedical & Chemical Engineering PhD Program Graduate Teaching Award
2023	Biomedical & Chemical Engineering PhD Delegate Nominee, Rochester Institute of Technology
2019	Commencement Graduate Delegate/Speaker, Rochester Institute of Technology
2017	National Fastpitch Coaches Association All-America Scholar-Athlete

Reviewer for Journals

2021-Present	International Journal of Environmental Research and Public Health
2021-Present	Toxics

C. Contributions to Science

1. **Early Career:** My undergraduate research was focused on engineering for accessibility. Along with a multidisciplinary engineering team, our work on The Overcomer™, an adapted fitness product designed to enable children with disabilities to participate in athletic actives, led to a commercialized product and a patent with the United States Patent and Trademark Office. During my undergraduate career I worked with Dr. Dan Phillips and Jade Myers on the development of a 3D printed transhumoral prosthetic device to be used in LimbForge software, a package that helps clinicians streamline development and fabrication of low cost prosthetic limbs for patients in developing countries. This project provided me with the opportunity to conduct human subjects research in a clinical setting with Healing Hands for Haiti in Port-au-Prince, Haiti.
    a. U.S. Patent Number 10932982, Kabes, J., Henry, R., Moore, J., **Sarles, S. E.,** Hughes, A., Folby, H., Nicolas, E., Fenn,C., Closson, J., Bureau, N., Arabadjis, I., Boudreau, C., Alshaikh, A., Hurd, N., Colosimo., G.; ADAPTED FITNESS EQUIPMENT. March 2, 2021.
    b. **Sarles, S.E.** Accessible Technology for Underserved Amputees, *Effective Access Technology Conference*, Rochester NY, April 2017. Poster, Demonstration, and Abstract.

2. **Tobacco Use Monitoring:** I have contributed to technology innovation in clinical trial instrumentation with the development of ambulatory (take-home) wPUM™ topography monitors used in clinical studies to record smoking/vaping behavior (puff flow rate, duration, volume) of inhaled tobacco users in their natural environment. I developed monitors for cigarettes, waterpipes, five types of electronic cigarettes, and a heated tobacco product. This work was supported by the National Institutes of Health and the Food and Drug Administration Center for Tobacco Products and has resulted in several publications, with a nicotine-switching clinical trial of electronic cigarette users underway. The results are intended to inform health effect/cessation studies and regulatory policy changes.
    a. Robinson, R. J., **Sarles, S. E.,** Jayasekera, S., Al Olayan, A., Difrancesco, A. G., Eddingsaas, N. C., Hensel, E. C. A Comparison between Cigarette Topography from a One-Week Natural Environment Study to FTC/ISO, Health Canada, and Massachusetts Department of Public Health Puff Profile Standards. *Int. J. Environ. Res. Public Health*. 15 May 2020**.**
    b. Hensel, E. C., **Sarles, S. E.,** al-Olayan, A., DiFrancesco, A. G. , Jayasekera, S., Eddingsaas, N. C., Robinson, R. J. A Proposed Waterpipe Emissions Topography Protocol Reflecting Natural Environment User Behaviour. *Int. J. Environ. Res. Public Health*. 10 January 2020.
    c. Hensel, E. C., **Sarles, S. E.,** Nuss, C., Terry, J., Polgampola Ralalaga, C., DiFrancesco, A. G. , Walton, K., Eddingsaas, N. C., Robinson, R. J., Effect of Third Party Components on Emissions from a Pod Style Electronic Cigarette. *Toxicological Sciences.* Manuscript ID: TOXSCI-23-0251. *In Review.*
    d. Lin, W., Ogura, T., Augustine, F., O'Sullivan, S., Hill, T., Jabba, S., Robinson, R. J., Hensel, E., **Sarles, S.E.**, Nuss, C., Rahman, I., Stroup, A. An In-Depth Review: State of the Art of Sensory System Toxicology Testing for Chemical Constituents from Electronic Cigarettes. *Toxicological Sciences. In Preparation.*

3. **Biofabrication:** My graduate project for an MS in Industrial and Systems Engineering was with Dr. Iris Rivero in the iMED lab at Rochester Institute of Technology, which

focuses on development of bioinks and biofabrication techniques using additive manufacturing. I worked on the development and parametric analysis of a composite layering process to manufacture hybrid material, multi-cell type, full thickness skin models. A combination of 3D bio-printed scaffolds and cell laden hydrogel produced a living skin model with tunable layer stiffness and thickness. The results of this work enable low cost and repeatable manufacturing of full thickness skin models.

   a. **Sarles, S.E**., Lazarus, E., Widom, L., Wuertz-Kozak, K., Rivero, I. Hydrogel Composite Layering Process for Full Thickness Skin Models. *IISE Annual Conference and Expo*; Seattle, WA 23 May 2022. Proceedings Paper.

4. **Airway Modeling:** My innovative contribution to *in vitro* airway modeling is development and validation of a biomimetic aerosol exposure system (BAES) for testing of inhaled aerosols. In my dissertation work, I designed and fabricated the BAES, characterized mass distribution, flow rate, and wall shear stress throughout the system, and demonstrated emissions testing and biological exposure capabilities of BAES. Introducing physiologically relevant fluid shear and increasing accuracy of aerosol mechanics and dose delivered to cultures contributed to the objective of improving *in vitro* airway models to enable investigation of cellular mechanisms and disease pathophysiology. I adapted my previously developed process for fine tuning the vertical thickness of hydrogel scaffolds to control the magnitude of fluid shear exerted on cell cultures inside of a custom mesoscale cell culture system. A first principles model was developed to theoretically model the fluid mechanics inside of the system where *in situ* tools are not easily placed. The automated data acquisition system integrated into the system records large amounts of quantitative data which I organized, analyzed, and prepared for academic publications and for use in grant proposals.
   a. **Sarles, S. E.**, Hensel, E., Terry, J., Nuss, C., Robinson, R. J., Flow Rate and Wall Shear Stress Characterization of a Biomimetic Aerosol Exposure System. *Toxicological Sciences.* Manuscript ID: TOXSCI-23-0253. *In Review.*
   b. **Sarles, S. E.**, Hensel, E., Terry, J., Nuss, C., Robinson, R. J., Characterization of Mass Distribution in a Biomimetic Aerosol Exposure System. *Inhalation Toxicology. In Preparation.*
   c. **Sarles, S. E.**, Hensel, E., Terry, J., Nuss, C., Wagner, G., Robinson, R. J., Transverse Flow Effects Cell Viability in a Meso-Scale Flow Exposure Chamber for Inhalation Toxicology Testing. *Toxicology In Vitro. In Preparation.*
   d. Miller, L., Hill, T., Rahman, I., Hensel, E., Robinson, R., **Sarles, S. E**., Jabba, S., Muthumalage, T., Stroup., A., In Vitro Assessments of ENDS Toxicity in the Lung: Are We There Yet? *Toxicological Sciences. In Preparation.*

Complete List of Published Work in My Bibliography:
https://www.ncbi.nlm.nih.gov/myncbi/emma.sarles.1/bibliography/public/

ABSTRACT

Tobacco use remains the number one cause of preventable death in the United States, disproportionately affecting residents of rural areas, people who are financially disadvantaged, and adults who identify as gay, lesbian, or bisexual. The impact that electronic cigarettes will have on public health is not yet fully understood. Combinations of electronic cigarette products, human airway geometries, and user behaviors create barriers to understanding products' interaction with the human airway and their health effects. Current *in vitro* emissions systems, also called smoking robots, lack biomimicry, use unrealistic flow conditions, produce unrealistic aerosol dose, and provide inaccurate bio-mechanical cues to cell cultures, limiting ability to correlate *in vitro* outcomes with *in vivo* health effects.

A Biomimetic Aerosol Exposure System, which includes an electronic cigarette adapter, an Oral Cavity Module, and a Bifurcated Exposure Chamber, was designed, manufactured, and characterized. Mass distribution, flow rate, and cell viability were studied as a function of puffing and respiration topography and system location. Accuracy of flow rate throughout the system was within 5% of programmed flow rate. Mass deposition was significantly different between the Puff Only condition and topography profiles that include ambient air inhalation cycles between puffs. Proof of concept cell culture in the system was performed with 3T3 fibroblasts cultured at an air-liquid interface and exposed to transverse aerosol flow in the Bifurcated Exposure Chamber.

The Biomimetic Aerosol Exposure System was developed to increase biomimicry at three levels: the systems level, the macroscale level, and the cellular level. BAES achieves biomimicry at the systems level with the ability to perform puffing and ambient air inhalation between puffs, mimicking how a human uses an electronic cigarette. At the macroscopic level, the flow path to emissions/characterization and biological exposure subsystems utilize geometries that mimic the human airway, including surface topographies, turns, and a bifurcation. At the cellular level, the free stream angle of aerosol induces fluid shear on cells, mimicking physiological conditions. This system may broaden the utility of an emissions system to generate physiologically relevant *in vitro* models of exposure to inhaled aerosols.

ACKNOWLEDGEMENTS

I would like to extend my sincerest thanks to my committee for their guidance and expertise. Words cannot express my gratitude to my Lab Director, Dr. Risa Robinson, and advisor, Dr. Edward Hensel; they boldly took on a student without an engineering background and have supported and advocated for me over the past six years. It has been a privilege to be under Dr. Robinson's leadership. I could not have undertaken this journey without Dr. Hensel, who has spent hours teaching me engineering and science skills to ensure that my untraditional background was never a hindrance. I had the pleasure of collaborating with past and present Respiratory Technologies Lab members. Special thanks to Gary DiFrancesco for contributing to system fabrication and to Shehan Jayasekera for supporting this work through software development. I would like to express my appreciation to Caleb Nuss and Janessa Terry who conducted many, many, (many!) repeated experiments and were quick to detect and mitigate errors. I'd like to also acknowledge Tirzah Pilet whose medical illustrations are throughout this dissertation. Many thanks to Dr. Iris Rivero and iMed Lab for supporting biomaterials aspects of this work and for advising my Industrial and Systems Engineering MS project, an important milestone on my quest to a doctorate. Special thanks to Gabbie Wagner and the Tissue Regeneration & Mechanobiology Lab for executing biological studies. I must acknowledge Rahman Lab at the University of Rochester Medical Center for their resources and expertise.

I am deeply grateful to Jade Myers for first exposing me to biomedical research and who has been a source of encouragement. To my big brother Barry, who we lost to cancer in 2018; in the last conversation we had in person he motivated me to pursue a PhD. To my wife Emily who tolerates ceaseless conversations about science and supports me always and to Skylar Andie, who enriches my life every day. Thank you to my entire family, biological, by marriage, and chosen, who have provided support in many ways.

Research reported in this publication was supported by the Rochester Institute of Technology internal funds, the National Institute on Drug Abuse of the National Institutes of Health (NIH) and the Food and Drug Administration's (FDA) Center for Tobacco Products (CTP) under Award Number R21DA050852, and by the National Institute Of Environmental Health Sciences of the NIH and FDA CTP under Award Number R21ES029984. The content is solely the responsibility of the authors and does not necessarily represent the official views of the NIH or the FDA. This research is not involved in or related to any commercial entity and findings do not support the use of any tobacco or non-tobacco product.

TABLE OF CONTENTS

LIST OF FIGURES

LIST OF TABLES

NOMENCLATURE

3D – three dimensional

ALI – Air-liquid interface

BAES – Biomimetic Aerosol Exposure System

BEC – Bifurcated Exposure Chamber

BSR – Biomimetic Smoking Robot

$CaCl_2$ – Calcium Chloride

CAD – computer aided design

CBD – cannabidiol

CDC – Centers for Disease Control

CFD – Computational Fluid Dynamics

CFP – Cambridge filter pad

CI – confidence interval, +/- 95% on a mean unless noted otherwise

CSC – cigarette smoke condensate

CT – computed tomography

CTP – Center for Tobacco Products

DAC – data acquisition and control

DI – deionized

DUT – device under test

e-cigarette – electronic cigarette

ECM – extracellular matrix

ENDS – electronic nicotine delivery system

ETP – emissions topography profile

EVALI – electronic cigarette, or vaping, product use-associated lung injury

FDA – Food and Drug Administration

GL– glycerin

HPHC – harmful and potentially harmful constituents

HUMITIPAA – human vaping mimetic real-time particle analyzer

InHALES – Independent Holistic Air-Liquid aerosol exposure system

L_{OCM} – length of the Oral Cavity Module

LP – linear programming

MRTP – modified risk tobacco product

nAChRα7 – α7 nicotinic acetylcholine receptor

NIH – National Institutes of Health

OCI – Oral Cavity Insert

OCM – Oral Cavity Module

PAR – puff associated respiration

PBS – phosphate buffered saline

PCU – power control unit

PDA – Phase Doppler Anemometry

PDMS – polydimethylsiloxane

PG – propylene glycol

PLA – polylactic acid

PM – particulate matter

PMI – Phillip Morris International

RIT – Rochester Institute of Technology

RTL – Respiratory Technologies Lab

SA – surface area

SARS-CoV-2 – severe acute respiratory syndrome coronavirus 2

SD – standard deviation

SLA – stereolithography

THC – tetrahydrocannabinol

THP – tobacco heating products

TPM – total particulate matter

US – United States

V – volume

WSS – wall shear stress

CHAPTER 1. INTRODUCTION

1.1 Field of Study

This work is related to better understanding the three-way relationship between (1) the characteristics of aerosol inhalant devices (such as electronic cigarettes), (2) the way such products are used (particularly user puffing and breathing behavior) and (3) key geometric features of the human airway (Figure 1). The characteristics of products influence how users consume them, including puffing and respiration topography. The human airway is made up of a continuous flow path that constricts, turns, and branches into millions of small airway structures. Product characteristics, behavior of a user, and the anatomical structure of the human respiratory tract affect what, how much, and where emissions from an inhaled aerosols deposit and interact with airway tissue. The objective of this work is to advance the state of knowledge about how product characteristics and user behavior affect tobacco related injury and disease.

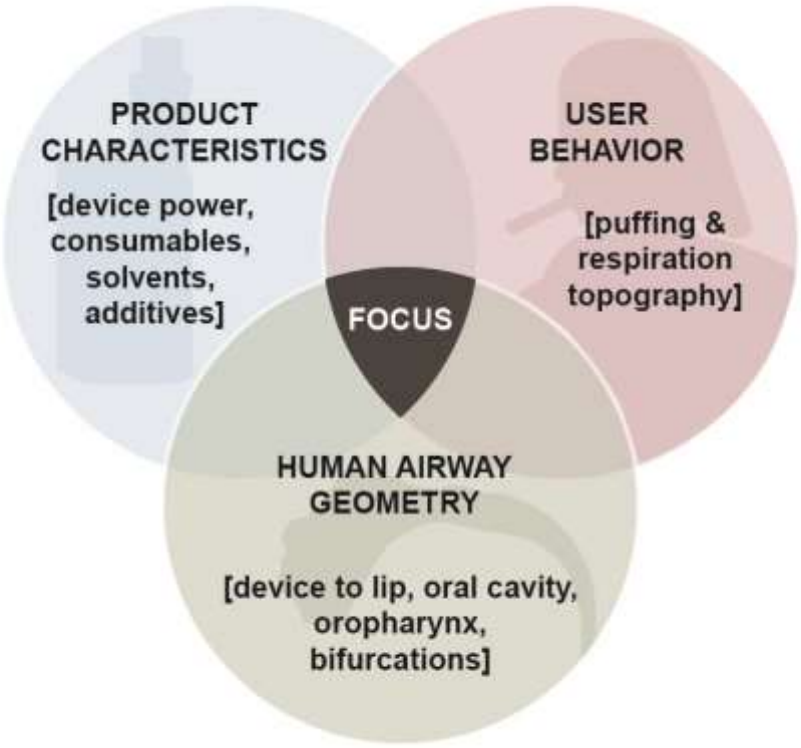

Figure 1 *This dissertation focuses on the interaction between product characteristics of inhaled nicotine products, user behavior, and key features of human airway geometry.*

A variety of exposure systems have been used for toxicity testing of aerosols. At one end of the spectrum, *in vitro* toxicology testing systems bear little resemblance to the geometric and flow conditions of the human airway. At the other end of the spectrum organ-on-a-chip systems seek to achieve high fidelity local conditions, but do not capture a systems level view of either the airway or the flow conditions (Figure 2).

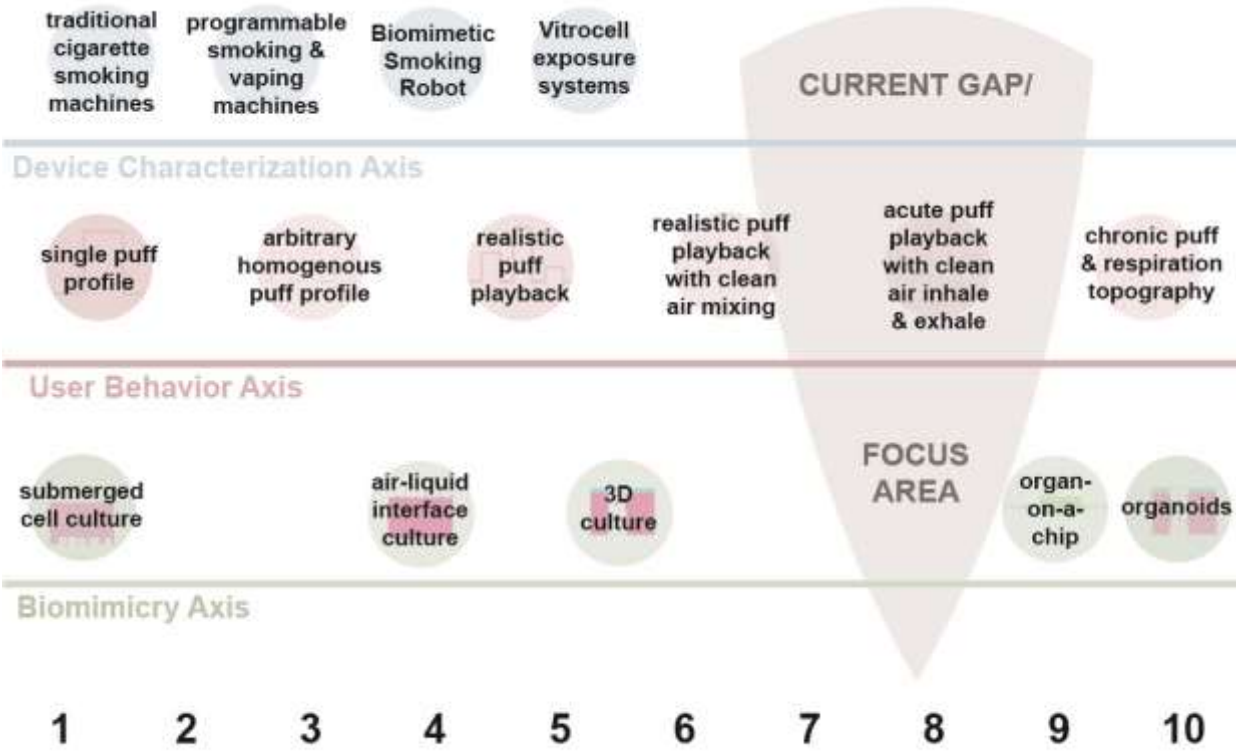

Figure 2 *A graphical representation of the past and present state of the art.*

Current emissions systems do not have the ability to mimic both user behavior and geometric biomimicry for biological exposure (Figure 3). The only system used in current literature with ability to mimic both user informed behavior and biomimicry is the Independent Holistic Air-Liquid Aerosol Exposure System (InHALES) [1], which is still in the prototyping stage by a tobacco company, and has failed to demonstrate accuracy and repeatability.

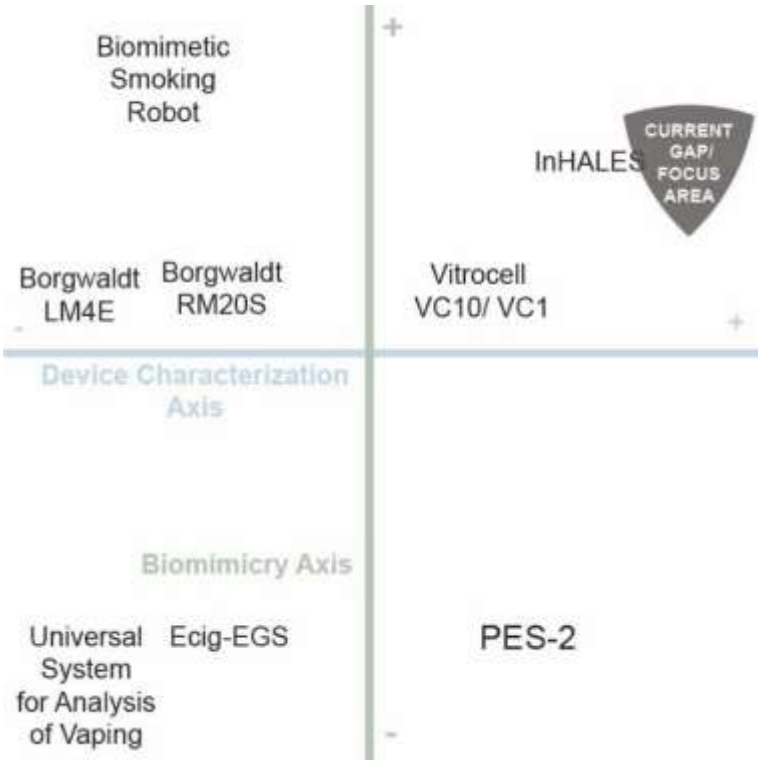

Figure 3 *Emissions systems shown on horizontal (user behavior) and vertical (biomimicry) axis show the strengths and weaknesses of current systems.*

1.2 Premise

An *in vitro* Biomimetic Aerosol Exposure System (BAES) will enhance the ability of respiratory health experts to better understand causes of e-cigarette associated lung injuries and other adverse health impacts associated with inhaled nicotine, cannabidiol (CBD), gases, solvents, chemicals, pathogens, and irritants. The BAES will exhibit enhanced biomimicry in comparison to traditional smoking machines and exposure systems from three perspectives: airway particle deposition and dosimetry, improved correlation between *in vitro* and *in vivo* local environment conditions, and more realistic interactions between the flowing aerosol and biological samples.

Aerosol generation will be accomplished with state-of-the-art commercially available electronic nicotine delivery system (ENDS). We use a JUUL® electronic cigarette (e-cigarette) as the aerosol source to demonstrate interoperability. Aerosol delivery and exposure is accomplished by modifying an existing programmable puffing system. Two aspects of the aerosol delivery system must be improved to enhance the realism of *in vitro* emissions and toxicology testing systems: geometry and system flow capabilities.

CHAPTER 2. SPECIFIC AIMS AND STUDY OBJECTIVES

This work is presented as five inter-related aims, each composed of several objectives. The first aim focuses on emission system geometry, the second focuses on realistic system flow conditions, the third addresses dosimetry as a function of geometric location and local flow conditions in the emission system, the fourth demonstrates feasibility of using live cell cultures for acute exposure studies, and the fifth demonstrates the utility of using the system to conduct comparative evaluations of exposure and cell response.

Aim 1. Demonstrate a geometrically bio-inspired aerosol exposure system

Hypothesis

Aerosol particle deposition, and hence dose, in aerosol exposure systems depend upon the flow path geometry. This is true under both transient and steady state system flow conditions.

Gap

The deposition of aerosol along the respiratory tract (between the mouth and the location of study) obscures the relationship between *in vivo* and *in vitro* dosimetry.

Approach

We address this gap by developing four geometric components to improve biomimicry of *in vitro* exposure systems.

Objective 1.1 Integrate an airtight streamlined connection between the ENDS device under test (the aerosol generator) and the inlet to the exposure system.

Objective 1.2 Integrate a human oral cavity mimetic exposure chamber.

Objective 1.3 Integrate an oropharynx model to emulate parallel flow paths from the oral cavity and nasal cavity into the pharynx.

Objective 1.4 Integrate modular exposure chambers with bifurcations in the flow path reminiscent of the upper airway in the lung for conducting aerosol deposition, cell exposure, and toxicity studies of relevant cell lines and/or tissues.

Aim 2. Demonstrate a human behavior-inspired aerosol delivery and distribution system

Hypothesis

Aerosol particle deposition and local flow conditions in machine puffing systems depend upon puff and respiration topography, referred to as the “system flow conditions.” This is true both in simple and complex system flow paths geometries.

Gap

Differences between the *in vivo* inhalation and *in vitro* machine puffing conditions limit the extrapolation of laboratory findings to human respiratory exposure and cell response. In addition to the issue of geometry induced deposition (and hence dosimetry) raised in Aim 1, this gap addresses issues related to local flow conditions experienced by cell cultures, such as wall shear stress.

Approach

We address this gap by modeling human behaviors to improve fidelity of *in vitro* exposure systems.

Objective 2.1 Integrate human puffing behavior with the exposure system of Aim 1. This objective employs the existing PES-2 control system.

Objective 2.2 Integrate a human puffing behavior and inhalation behavior using an oropharynx model to extend the PES-2 control system of Objective 2.1.

Objective 2.3 Develop system architecture for post-inhale breath hold and exhalation behavior by modifying the oropharynx model and PES-2 control system of Objective 2.2

Aim 3. Quantify the dose and flow conditions throughout the exposure system

Hypothesis

The aerosol particle deposition which naturally occurs in machine-puffing systems can be used to mimic particle deposition in the human respiratory tract. Characterizing the local deposition patterns and flow conditions will enable assessment of the bio-relevance of the local cell culture environment.

Gap

Differences between the *in vivo* and *in vitro* local cell environment limit the extrapolation of laboratory findings to human respiratory exposure and cell response.

Approach

We address this gap by modeling three human behaviors to improve fidelity of *in vitro* exposure systems.

Objective 3.1 Quantify the mass dose distribution as a function of geometric position (developed in Aim 1) and flow conditions (implemented in Aim 2) for an ENDS.

Objective 3.2 Quantify the local flow conditions (mass flow rate and mean aerosol velocity) as a function of geometric position and system flow conditions in the system.

Aim 4. Demonstrate proof of concept to conduct acute biological response of living cells in the aerosol generation, delivery, and exposure systems.

Hypothesis

The viability of cells under no flow conditions, transverse flow of clean air, and transverse flow of ENDS aerosol will not be equal.

Gap

Current exposure systems do not provide realistic dose or mechanical cues to cell cultures during exposure.

Approach

We address this gap by demonstrating and validating a proposed biological outcome measure for conducting relative risk assessment between inhaled tobacco product exposure conditions.

Objective 4.1 Propose standard input measures for reporting dose delivered to biological samples during cytotoxicity testing.

Objective 4.2 Quantify the response of 3T3 fibroblasts in the BAES at one or more geometric locations exposed to clean air as function of system flow conditions (no flow, puff).

Objective 4.3 Quantify the response of 3T3 fibroblasts in the BAES at one or more geometric locations exposed to ENDS aerosol as function of system flow conditions (no flow, puff).

Objective 4.4 Report inferential statistics of the outcome measure(s) with appropriate error bars as a function of aerosol condition (no load, clean air, toxicant puff) for each flow condition and observation location.

Aim 5 Report inferential statistics for the effect of input parameters and system response

Hypothesis

The BAES can be used for acute exposures of cell cultures under higher fidelity dose, geometry and flow conditions in comparison to traditional machine puffing emissions systems.

Gap

Current emissions and exposure systems do not provide risk assessment between inhaled tobacco products in a physiologically relevant environment.

Approach

We address this gap by demonstrating dose and a biological outcome measure as a function of system parameters for conducting relative risk assessment between inhaled tobacco products.

Objective 5.1 Demonstrate system level response as a function of location for a clean air puff

Objective 5.2 Demonstrate system level response as a function of location for one puff profile from one ENDS

Objective 5.3 Demonstrate system level response as a function of location for one puff profile from an ENDS accompanied by one puff associated respiration (PAR) diluting clean air inhale and followed by multiple tidal clean air inhales.

Objective 5.4 Demonstrate the ability to accelerate the pace of scientific discovery by reporting statistically significant findings as a function of location (dose and local flow conditions reminiscent of human exposure) and as a function of system flow conditions (puff, Puff+PAR+Tidal inhale) reminiscent of human puff and respiration behavior.

CHAPTER 3. BACKGROUND AND SIGNIFICANCE

3.1 Tobacco Related Disease & Public Health

Post-colonial tobacco smoking has been described as “a tragic accident of history” [2]. The role of commercial tobacco in American slavery [3], the prolific rates of lung cancer throughout the 20th century [4], the abrupt rise in adolescent nicotine use in the United States (US) in 2018 [5], and tobacco’s disproportionate effect on residents of rural areas, people who are financially disadvantaged, those uninsured or enrolled in Medicaid, and adults who identify as gay, lesbian, or bisexual [6] are a few of the devastating impacts which have grown out of the only legally marketed consumer product which demonstrably kills its users. While scientific advancement cannot undo years of complacency of world leaders or malice of tobacco industry, evidence based public health initiatives, driven by discoveries of independent researchers, might decrease morbidity for the world’s 1.3 billion tobacco users [7] through better understanding of tobacco related disease and alternative tobacco products. The history of tobacco use in humankind is vast, but the extensive scientific work on the topic converges to one conclusion: any known benefit of commercial tobacco use does not justify its danger to its users or those around them [4]. Yet, there is insufficient political will to ban this substance. However, most countries around the world have authorized various government agencies to regulate the manufacturing, sale, and use of tobacco and nicotine products. A timeline with key events related to history of the manufacture, marketing, and regulation of tobacco products is given in Figure 4.

Tobacco plants, native to the Americas, were discovered 18,000 years ago when humans migrated to the Americas from Asia. Cultivation of *Nicotiana tabacum* and *Nicotianarustica* began between 5000 and 3000 BC and use of the plant spiritually and medicinally by indigenous people was widespread across the American continents by the time colonists arrived in 1492. In precolonial times, tobacco was snuffed, chewed, consumed, and applied to the skin and eyes, however, smoking tobacco was most popular. Tobacco smoking was an important artifact of social life and spiritual rituals for indigenous people. Soon, tobacco was brought to Europe, and while not immediately accepted in the region, it eventually became popular. In the 1850s, manufactured cigarettes became available in England, providing an opportunity for tobacco manufacturers to manipulate what went into cigarettes [4]. Meanwhile, the tobacco industry had taken off in America where one half of American tobacco was grown domestically and relied almost exclusively on the labor of enslaved people [3]. Approximately

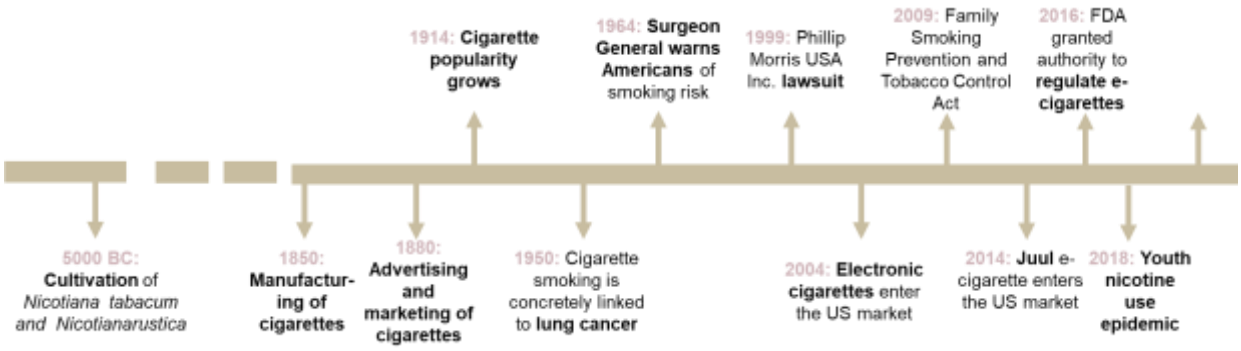

Figure 4 *A brief history of the manufacture, marketing, and regulation of tobacco products.*

8,500 enslaved people were forced to work as tobacco hands in the state of Virginia alone by 1860 [3]. Cigarettes grew in popularity in the US during the next several decades and in the 1880s packaging and advertising became relevant in the tobacco industry. This drove competition and narrowed price [8]. In 1890, American Tobacco Co., which was made up of five companies and produced around 90% of cigarettes made in the US, was worth over $316,000,000 [8]. The company was one of the original twelve members of the Dow Jones Industrial Average [9]. In 1907 American Tobacco Co. was found in violation of antitrust law and dissolved into three separate companies: American Tobacco Co., P. Lorillard, and R. J. Reynolds, Liggett & Meyers. All three companies were eventually acquired by British American Tobacco (SEC 1-32258, SEC 56-0950247).

The convenience of manufactured cigarettes contributed to their rise in popularity during the First World War. Smoke from pipes and cigars, which were previously popular, allowed uptake of nicotine through the oral mucosa. In contrast, cigarettes produce smoke with higher acidity, requiring inhalation to the lungs for effective uptake [4]. Inhalation into the lungs provides greater surface area for absorption and nicotine is more readily delivered to the brain compared to absorption through oral mucosa [4].

In the years following, the prevalence of lung cancer increased. From 1939-1964 there were 29 retrospective studies of lung cancer internationally [10]. The 1950s brought publications that concretely linked lung cancer to cigarette smoking. Skepticism and criticism surrounding these findings arose [11-15]. In 1954 the Tobacco Industry Research Committee was formed by tobacco industry leaders, which provided funding to scientists to investigate the impact of tobacco on human health [16]. In 1956, the US Public Health Service began to review available data and a scientific Study Group was formed cooperatively by the National Cancer Institute, the National Heart Institute, the American Cancer Society, and the American Heart Association. At

least sixteen studies were conducted over 18 years [10]. At the conclusion of the project, the Study Group concluded that “there is a causal relationship between excessive smoking of cigarettes and lung cancer” [10]. On July 12, 1957, US Surgeon General Leroy E. Burney issued a statement that “excessive smoking is one of the casuistic factors in lung cancer” [10]. This gave way to the first Surgeon General’s report on Smoking and Health in 1964 [10], where for the first time, the US public was warned by their government about the dangers of smoking cigarettes.

Tobacco companies continued to deny these claims and defy the public. In 1999, the US brought a lawsuit against tobacco company Philip Morris USA, Inc [17]. The charges, as described by US District Judge Gladys Kessler of the District of Columbia who heard the case, were for “engaging in a lengthy, unlawful conspiracy to deceive the American public about the health effects of smoking and environmental tobacco smoke, the addictiveness of nicotine, the health benefits from low tar, ‘light’ cigarettes, and their manipulation of the design and composition of cigarettes in order to sustain nicotine addiction.” The Judge found that “Defendants Have Falsely Denied that They Can and Do Control the Level of Nicotine Delivered In Order to Create and Sustain Addiction.” The damage was done. The US Surgeon General declared that “tobacco related disease was the most significant cause of disease ever documented [17]” and at the start of the 21st century, tobacco related disease remained the leading cause of preventable death worldwide [18]. In 2009 the Family Smoking Prevention and Tobacco Control Act gave the US Food and Drug Administration (FDA) the regulatory authority to oversee manufacture, marketing and distribution of tobacco products [19]. Less than 15 years after the US Surgeon General sounded the alarm on tobacco related disease, a new product would enter the world market with the intent of having a positive impact on public health [20]. Instead, it would fuel the next nicotine powered epidemic in the United States [5].

3.2 Emergence of Novel Inhaled Tobacco Products

Youth tobacco use had been steadily declining for three years before a spike in 2018, when the former US FDA commissioner declared “youth use of electronic cigarettes has reached an epidemic proportion” [21]. Electronic cigarettes (e-cigarette) deliver nicotine to a user through inhalation of a vaporized liquid that generally consists of propylene glycol, vegetable glycerin, flavor additives, and nicotine. The liquid, “e-liquid,” is heated and aerosolized by a metallic coil that is supplied with energy from a battery. From the time electronic cigarettes entered the US market in 2004, they steadily rose in popularity yet remained unregulated until 2016 when the FDA was granted regulatory authority [22] based on a US Court of Appeals

Decision [23] that determined that electronic cigarettes fall under the authority of the FDA as a "tobacco product". In 2020, Centers for Disease Control (CDC) reported that 4.47 million children under the age of 18, including 23.6% of American high school students, identified as "current e-cigarette users" [24]. A bill passed in 2022 gave the FDA the authority to regulate synthetic nicotine not derived from tobacco under the Family Smoking Prevention and Tobacco Control Act [25].

Researchers have studied e-cigarettes and their consumable e-liquid, nicotine and flavor dissolved in a liquid carrier, often propylene glycol and glycerin, with studies into cytotoxicity [26-31], cytokine secretion [32-35], cell morphology [32], the oral microbiome [36], and wound healing [37, 38]. Despite widespread publication of e-cigarette related work, many studies fail to directly link results to predicted health effects or to regulatory outcomes, particularly due to non-repeatable results, lack of standardization across studies, and unrealistic methods of exposure *in vitro.* Countless combinations of device flow path geometries, consumables, operating parameters of e-cigarette products, and patient specific biological responses have created limitations in understanding, diagnosing, and predicting e-cigarette related injury and disease [39]. Further, the market for novel inhaled tobacco products is rapidly evolving.

In the early years of e-cigarettes their design was reminiscent of combustible cigarettes (Figure 5a). Devices were disposable or rechargeable and cartridges contained pre-filled e-liquid surrounding a heating element. They came to be referred to "cig-a-likes" and "first generation e-cigs" [40, 41]. The market quickly matured and "second generation" devices

a) A cig-a-like (First Generation) electronic cigarette.

b) An NJOY e-cigarette, a pen style (Second Generation) product.

c) A SMOK box mod (third generation) style e-cigarette.

d) A JUUL (pod style) e-cigarette.

***Figure 5** Photos of electronic cigarettes. Photographs of commercial products by the Respiratory Technologies Laboratory, Rochester, NY.*

(Figure 5b), which had refillable tanks, larger batteries, more advanced heating elements, and the form factor of a pen gained popularity. Third generation devices (Figure 5c) introduced new challenges for research and regulation with customizability by the user. They have been termed “box mods” because of their ability to be modified with ease and for their boxy form factor (a result of large batteries). These products use high power, interchangeable coils, and temperature and wattage control [40]. Between 2014 and 2016, the market trended toward customizable products [41]. In 2015 the JUUL® e-cigarette entered the market (Figure 5d) and not only created a product that crept into social media and pop culture of adolescents and young adults, but also created an entirely new category of electronic vaporizers, “pod style”, when other manufacturers began to make similar products [42]. Within less than four years on the market, one in five high school students claimed to have seen someone using a JUUL e-cigarette in school [43]. The JUUL e-cigarette and similar products use a “rechargeable lithium cell battery to provide energy to a heating element which heats nicotine carrying liquid, vaporizing it into an aerosol, which a user inhales. The heating element and nicotine containing liquid, e-liquid, are housed in disposable units JUUL Labs® Inc. called a ‘JUULpod®’. Many users refer to these as “pods.” The device is recharged with a connection to a power source” [41].

While early investigation has supported lower cytotoxicity of e-cigarette aerosol compared to combustible cigarettes [44, 45], specific factors that contribute of cytotoxicity e-cigarette emissions and their impact on long-term health effects are not known. Urena *et al.* [46] provided a comprehensive assessment of the effect of various e-cigarette product parameters on biological response in a 2020 study that found that cytotoxicity, oxidative stress, and radical levels increase with atomizer age and that intracellular factors other than oxidative stress play a role in cytotoxicity. Authors observed obvious charring of a third-generation e-cigarette’s wick as the atomizer was used repeatedly. Cell viability decreased as the atomizer was aged. Formaldehyde, acetaldehyde, and acrolein were present in the aerosols from all e-liquids when puffed with a new atomizer and concentrations increased with atomizer age. Fruit flavors generated significantly higher levels of acetaldehyde than tobacco flavors. The study also found that e-liquid marketed as the same flavor from the same manufacturer, but at different nicotine levels, produced observable differences in cytotoxicity. There was an observable relationship between e-liquid cytotoxicity and oxidative stress; however, antioxidant treatment did not eliminate the cytotoxic effect of e-liquid, suggesting that intracellular mechanisms other than oxidative stress play a role in cytotoxicity. The authors [46] recommend that future work identify

and quantify reactive species deposited on cell cultures, identify source of toxicants, and study the role of nicotine in cytotoxicity.

The high levels of nicotine in some e-cigarette products raise concerns about their impact on addiction. A 2011 article [48] quantified salivary cotinine, a metabolite of nicotine, of smokers, former smokers, e-cigarette users, and former smokers who use nicotine medication with liquid-chromatography tandem mass-spectrometry. The study found that cotinine in e-cigarette users was higher than levels found in former smokers who use nicotine medications. In e-cigarette users, correlations between cotinine level and e-liquid concentration, puffs per day and duration of e-cigarette use were all weak. User behavior was all self-reported via a mail in survey and authors suggest that difference in cotinine levels may be a result of factors not measured in the study such as “electric power of the device, vapour temperature and density, nicotine concentration in the vapour (versus in liquids), volume of puffs, depth of inhalation, duration of apnoea between inhalation and exhalation and each individual’s specific nicotine metabolism[48].” This study highlights challenges e-cigarettes pose for research and regulation with their highly variable parameters and dependence on user operation.

In 2019, what was once a concerning trend of an under-regulated product transformed into a public health emergency. On August 1, 2019, the first cases of electronic cigarette, or vaping, product use-associated lung injury (EVALI), were reported to the US CDC [49]. As of February 18, 2020, the latest reported data from the CDC, there were 2,807 reported hospitalized cases of EVALI, including 68 deaths (Figure 6) [49]. While long term effects of EVALI are unknown, a one year retrospective study shows high rates of hospital readmission and emergency department visits in EVALI patients [50]. Patients also reported fatigue, labored-


The New York Times

Vaping Kills a 15-Year-Old in Texas

The teenager was the youngest to die so far in the outbreak of lung illnesses that affected thousands of people.

Figure 6 *A New York Times headline from January 2020 reads “Vaping Kills a 15-Year-Old in Texas”. The child’s death was a result of electronic cigarette, or vaping, product use-associated lung injury and a co-morbidity [47].*

breathing, decreased exercise capacity, cough, anorexia, and abdominal pain at outpatient follow-up visits. 80% of EVALI patients had reported using e-cigarette products that contain tetrahydrocannabinol (THC). A study by the CDC found vitamin E acetate in the bronchoalveola lavage fluid of 48 of 51 (94%) EVALI patients, while 100% of samples from healthy participants were negative for vitamin E acetate [51]. The study concludes that vitamin E acetate may play a role in EVALI patients. A study published in August 2020 revealed a possible mechanism of EVALI. DiPasquale [52] reports that Vitamin E acetate causes increase in membrane fluidity contributing to pulmonary surfactant failure and collapse of the epithelial monolayer. This tissue damage may be consistent with signs and symptoms of EVALI. This important finding was achieved using a setup that lacks realistic exposure. The model used lipid-only pseudo-pulmonary surfactant exposed to pure vitamin E acetate. The model also uses a much lower concentration of vitamin E acetate than preliminary work broadly estimates may be exposed to lung tissue [51, 52]. Another study [53] found that vitamin E acetate particle size and deposition patterns are dependent on user puffing topography, especially flow rate, which is not considered in the study. In 2021, Kaiser and colleagues used a biomimetic smoking robot with real-time optical particle analysis capabilities to demonstrate that the addition of Vitamin E acetate to e-liquid increases number of particles inhaled from an electronic vaporizer while altering the particle size distribution of the aerosol [54]. A necessity for an emissions system that can both accurately recreate user puffing topographies and expose biological samples in a way that promotes accurate dosimetry, flow mechanics, and particle distribution is further demonstrated by the EVALI public health crisis.

Just as FDA regulatory authority and actions began to catch up with the transformative e-cigarette market by banning flavored products and limiting marketing activities [20], tobacco heating products (THP), which had gained popularity internationally in the past decade [55], made their way into the US market. In July 2020, the US FDA approved the marketing of a THP product, the IQOS (Figure 7a) and its consumable tobacco sticks, HeatSticks™ (Figure7b), as a “reduced exposure” product based on a modified risk tobacco product (MRTP) application [56]. Karma *et al.* [55] showed that “reduced exposure” marketing of the IQOS will be misleading for consumers. The product was the first tobacco product to receive this type of authorization from the FDA [56]. The authorization was granted based on scientific data from Phillip Morris International (PMI) that supports fewer harmful and potentially harmful constituents (HPHCs) produced by the IQOS than in 3R4F reference cigarettes and that all constituents were lower in IQOS emissions than in 3R4F reference cigarette smoke [57]. However, the majority of scientific

data on THP is from the tobacco industry with limited independent validation [58]. According to St. Helen *et al.* [57], levels of "56 other constituents in the IQOS, which are not included in…FDA's list of HPHCs, were higher in IQOS emissions [than in 3R4F reference cigarettes]". There are at least 20 studies published from PMI about the IQOS supporting claims of reduced harm [59].

a) An IQOS power control unit, charger, and cleaning accessories.

b) A package of HeatSticks™, the tobacco consumable used in IQOS products.

Figure 7 *An IQOS Tobacco Heating Product, its consumables, and charging accessories. Photos of commercial products by the Respiratory Technologies Laboratory, Rochester, NY.*

Current data about THP, such as IQOS, is primarily limited to machine puffed emissions using parameters that have not been tested for relevance to human THP use and appear to be unreliable, underestimating toxicant exposure [58]. Available data shows concerning trends such as the IQOS delivering more nicotine than some types of electronic cigarettes [60] and the IQOS having a higher nicotine transfer rate than cigarettes [61]. Statistically significant discrepancies exist between independent and manufacturer funded machine puffing studies [58, 61-66]. Preliminary data from the Respiratory Technologies Lab (RTL) shows that variable device operation of the IQOS may affect emissions. Data in the MRTP application does not consider puffing topography, device operation, or user behavior. There has been limited work published regarding the toxicity of IQOS aerosol. Leigh 2018 [67] reported IQOS exposure reduced viability of cells and produced less cytokines excreted by IQOS exposed cells than Marlboro Red smoke exposed cells. Nabavizadeh 2018 [59] showed that IQOS exposure impairs endothelial function in a rat model, even at low exposures. The study also found that blood nicotine levels were ~4.5-fold higher for IQOS compared to cigarette smoke, despite nicotine emissions being 63% lower, and concluded IQOS may not reduce risk of adverse cardiovascular effects.

Particular concern has been expressed about e-cigarette use amid the COVID-19 pandemic [68, 69]. Specifically, preliminary work by Rahman *et al.* [70] shows that e-cigarette

induced pulmonary inflammation may upregulate the angiotensin-converting enzyme 2 receptor, a severe acute respiratory syndrome coronavirus 2 (SARS-CoV-2) receptor, through dysregulation of extracellular matrix (ECM) repair mediated by α7 nicotinic acetylcholine receptor (nAChRα7). These results were achieved by exposing adult C57BL/6 J (WT) mice and nAChR α7 knockout mice to e-aerosol using a commercially available SCIREQ “InExpose” smoking system (SCIREQ Inc., Montreal, Canada). Rahman’s study agrees with similar findings where gene expression and cytokine profile of e-cigarette users exposed to live attenuated influenza virus vaccine were shifted, indicating suppression of host anti-viral response [71]. It is possible that a similar phenomenon could occur that would affect the efficacy of the SARS-CoV-2 vaccine in e-cigarette users since response to viral pathogens tend to be similar [71]. The authors of the influenza vaccine study highlight the need for investigation into viral susceptibility and course of infection in inhaled tobacco users by using live viruses in “physiologically relevant models such as the air-liquid interface (ALI) human airway epithelial cells [71]”. Furthermore, a study found that COVID-19 diagnosis is five times more likely in adolescents who have ever used e-cigarettes, seven times more likely in youth who ever dual-used cigarettes and e-cigarettes and past 30 days youth dual-users were 6.8 times more likely to receive a COVID-19 diagnosis [70, 72]. Recent work shows that users of any inhaled nicotine product may increase the risk of SARS-CoV-2 diagnosis [68, 70], compromises antiviral response [71], and leads to more severe clinical outcomes [73].

While alternative tobacco products, such as e-cigarettes and THPs, may improve health outcomes for established adult smokers, long term effects of chronic e-aerosol exposure are not known. Further, accessibility, marketing, and sweet flavors of ENDS has created a new generation of nicotine users.

3.3 Tobacco Regulatory Science and the role of geometry in machine puffing systems

Analytical emissions testing includes the capture and analysis of aerosol or smoke from a tobacco product. Emissions testing is a recommended by the FDA for a product’s Premarket Tobacco Applications [74], documentation that initiates the path to approval for sales and marketing of a product by the FDA. Biological testing includes the exposure of biological samples, such as mammalian cells, bacteria, or animals, to emissions and conducting analyses including toxicity, oxidative stress, genotoxicity, screening biomarkers, and other biological endpoints. Both types of testing require emissions systems, which apply vacuum pressure to an

aerosol generator (tobacco product) and carry the aerosol to an emissions capture or biological exposure subsystem. Flow rates and puff intervals can be programmed into many systems. A timeline with early emissions systems for tobacco product screening is given in Figure 8. Emissions systems have been used for many decades [28, 75-80] with the first smoking machine being used in 1892 when the Connecticut Agriculture Experiment Station was used to puff a cigar using a siphon [81]. Between 1939 and 1971, several smoking machines were developed [81]. Borgwaldt developed the first smoking machine capable of *in vitro* toxicity testing with captured smoke condensate and described a protocol for preparing smoke condensate for a mouse skin bioassay published in 1968 [82]. The development and validation of an ALI in 1979 [81] opened new doors for tobacco research. Culturing at an ALI is more mimetic of the physiological microenvironment of airway cells [81]. In 2002, Aufderheide *et al.* published methods for integrating a modular ALI chamber into an emissions system. Aufderheide *et al.* demonstrated the chamber by exposing human cell lines (bronchial epithelial cells HFBE21 and human lung fibroblasts LK004) to three environmental atmospheres, including side-stream cigarette smoke [79]. The exposure chamber was designed for use with multiple aerosol generating machines [79]. ALI exposure chambers connected to emissions systems have become standard for biological testing of tobacco smoke and e-aerosol. The commercially available exposure systems most popular in the literature are Aufderheide's CULTEX® system, the Vitrocell® system, and British American Tobacco's exposure chamber coupled with Borgwaldt emissions systems (Figure 9a) [83]. Custom emissions systems, such as the RTL's PES-2 (Figure 9b) and the Biomimetic Smoking Robot (BSR) (Figure 9c) have been characterized [80, 84] and used for analytical testing of several tobacco products [85, 86]. Currently available emissions systems for biological and analytical testing are not designed to produce biomimetic deposition patterns [28, 75-80].

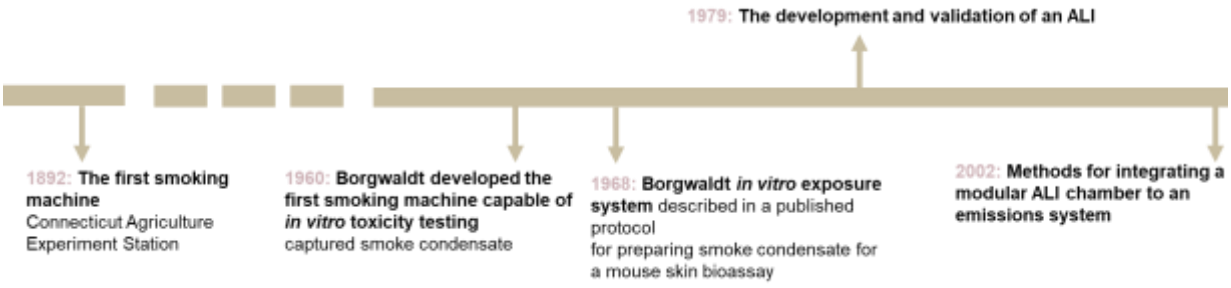

Figure 8 *A timeline of early emissions systems used for tobacco product screening [79, 81, 82].*

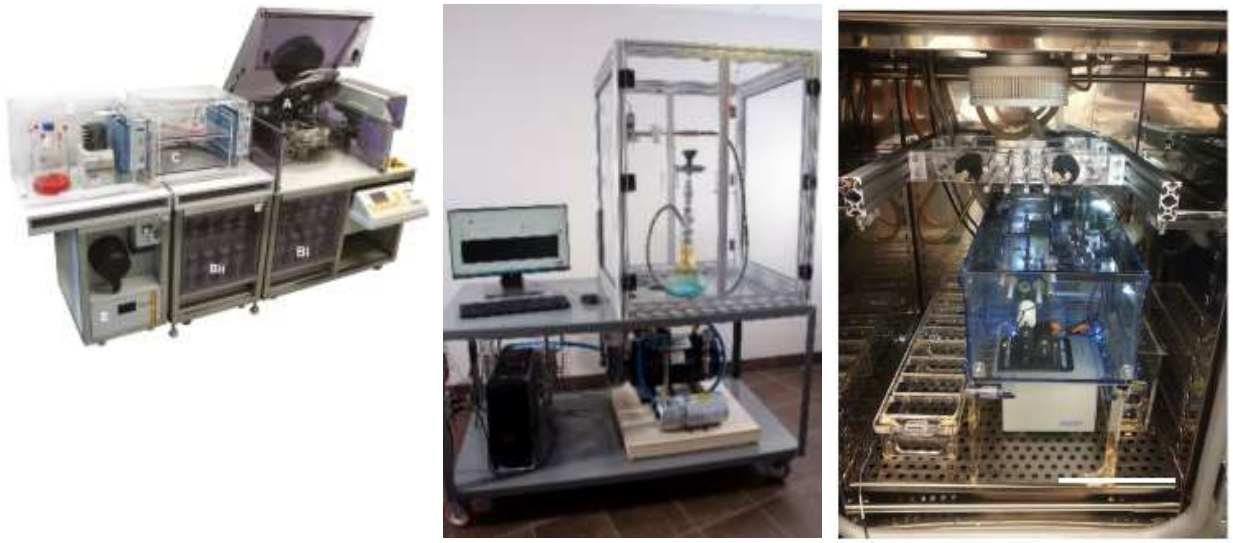

a) *A Borgwaldt RM20S 8 syringe smoking machine (A, B, E) with a British American Tobacco exposure chamber subsystem housed in an incubator (C-D) [76].*

b) *A photo of PES-2 (Respiratory Technologies Lab, Rochester, NY) with a water pipe.*

c) *Benam et al.'s Biomimetic Smoking Robot [84].*

Figure 9 *Emissions systems used in tobacco research and described in prior literature.*

A variety of three-dimensional (3D) lung model geometries [87-91] and 3D modeling techniques [90, 92] have been used in the literature for numerical [93], computer simulation [91, 94-96], and *in vitro* models [91, 97] . I*n vitro* experiments that use realistic lung geometry study particle deposition in physical 3D lung models, but there are no publications that use these lung models for analytical or biological studies, leaving a significant gap in the literature. The most common way to acquire airway geometry data is through medical imaging [92]. A major limitation of medical imaging of lung geometry is that image quality becomes poor after the third generation due to movement in the thoracic cavity caused by the heart beating. Therefore, methods that include medical imaging of lung casts have been employed and have allowed the production of digital models down to the 17th generation [92].

Two well-known and widely used models are Weibel's Model A [98] and the Horsfield model [89]. The Weibel model is an idealized symmetric model from the trachea to the alveoli based on a cast of a cadaver. The generations are numbered G0-G23, with G0 being the

trachea. The Horsfield model is a more realistic model that includes asymmetry of the bronchial branches and number the generations starting at terminal branches to accommodate asymmetry.

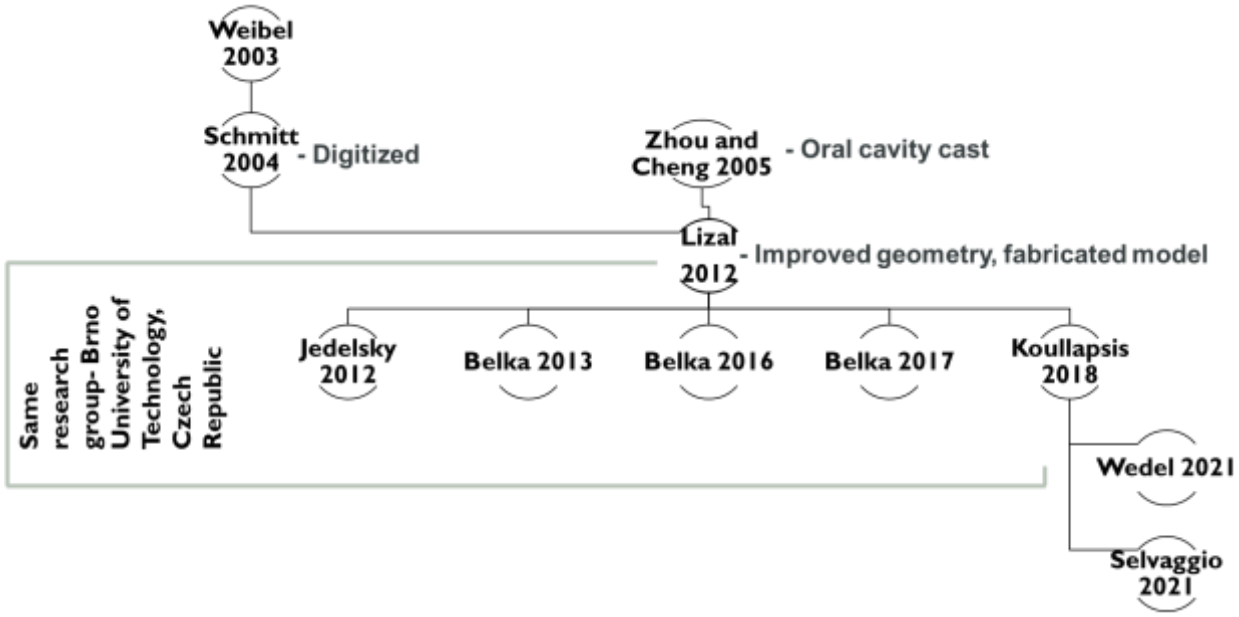

Figure 10 *A map of publications that describe improvements to and use of the Weibel model for computer simulation and in vitro particle deposition studies. Citations were traced back to Schmitt 2004 where the citation for the model is "Personal Correspondence" with Weibel in 2003, though the Weibel model was first described in 1963 [87].*

Neither model includes surface roughness nor protrusions found in the airway and are idealized geometries. Figure 10 gives a brief overview of publications that describe improvements to and later use of a digitalized Weibel model. Weibel's lung model [87, 88] was digitized in 2004 by Schmidt *et al.* [99] with high-resolution computed tomography (CT) of a cast. The Schmidt model begins at the trachea and does not include the laryngopharynx or oral cavity. In 2011 Lizal *et al.* [92] digitally combined the Schmidt model to a laryngopharynx and tracheal airway model from a 3D CT scan of a human subject. A wax oral cavity was acquired from Lovelace Respiratory Research Institute, scanned with an Atos (GOM, Braunschweig, Germany) device, converted to STL format and attached to the rest of the model. The realistic model was fabricated with and without the oral cavity via additive manufacturing for deposition studies and by brushing silicone on a sacrificial core for optical measurements. The realistic model was validated using Phase Doppler Anemometry (PDA) and Computational Fluid Dynamics (CFD) and showed good agreement at five out of six locations measured. A fifth

model was made with a simplified lung geometry that consisted of glass tubes to increase PDA measurement locations. This model was not validated in the 2011 article.

Inclusion of realistic geometry for anatomical structures should be included in particle deposition studies. The structure of the larynx is a determinant of flow mechanics and therefore particle deposition in the extrathoratic airway. Larynx anatomy includes the glottal aperture, tissue folds that form a triangular or elliptical cross section. This cross-sectional area varies with flow rate and oscillates during a breathing cycle. The structure is the greatest flow constriction in the upper airway and creates the laryngeal jet [100]. Prior work has demonstrated that the laryngeal jet has a significant impact on downstream particle deposition, especially in the tracheobronchial region. Xi [100] used CFD to show that inclusion of a laryngeal jet impacts airflow and aerosol dynamics including more mixing, increased particle deposition in the trachea, and deeper penetration of gaseous and particulate matter in further generations. Current emissions and exposure apparatuses fail to mimic the geometry and flow mechanics of the larynx.

Currently, two novel emissions systems described in the literature use a biomimetic system design. Both systems also include integrated environmental control. Benam *et al*. [84] designed, built, and validated the BSR (Figure 9c), which addresses several shortcomings of commercially available systems including particle deposition in transit to an exposure chamber, lack of control over dose, inability to precisely mimic human puff-inhale breath patterns, and aerosol exposure is not mechanically memetic of *in vivo* exposure. The BSR is also the first system in the literature to deliver volumes small enough for organ chips. Authors observe that particle distribution is uniform throughout the exposure region, however particle deposition is likely non-uniform throughout human airway and it is not clear how smoke particles are distributed through the airway *in vivo*. The dose exposed to the organ chip in the BSR does not represent the entire human airway and is limited to geometries and flow conditions of lower lung generations. Other limitations of the BSR include that the BSR cannot puff at variable flow rates in a single trial because the air pump flow uses an on/off signal instead of variable voltage to a valve. The currently validated BSR configuration has a maximum puff volume of 80mL and does not allow microbiome, migration studies, or low-cost toxicity studies that can be done without an airway chip. In 2021, Benam and colleagues published an updated architecture of BSR, naming the new iteration “human vaping mimetic real-time particle analyzer” (HUMITIPAA) [54]. In this new configuration, the addition of an optical particle sensor enables real-time particle analysis,

binning particle size frequency between four size fractions, 300 nm–1 µm, 1 µm–2.5 µm, 2.5 µm–4 µm, and 4 µm–10 µm, but does not include the airway chip.

InHALES is the first emissions system with the ability to simulate regular breathing between puffing. The system was first described in at the 2018 European Society of Toxicology and claimed to allow researchers to study exposure and particle deposition throughout the human respiratory tract [101]. This system appeared in peer reviewed literature for the first time in *Toxicology In Vitro in* June 2020 [1]. The authors use a flow path that resembles *in vivo* geometry, including number of bronchial branches and branch diameters, to represent six generations of the human airway. Flow is achieved through primary and secondary pumps that represent the mouth and lungs and the opening and closing of valves are used to achieve bidirectional breathing. The multi-pump design allows the system to simulate different puffing behaviors and allows clean air to enter the system after a puff, similar to a person inhaling cigarette smoke into their mouth and then taking a second breath to transport it to the lungs. The InHALES is capable of variable flow rates within a puffing trial. The system has culture devices throughout the flow path where cells cultured on hydrogel are placed flush with the flow path, mimicking shear stress on cells that occurs *in vivo.* The system is in the prototyping and proof of concept stage and has not yet been fully characterized or validated.

3.4 Human Behavior and Tobacco Use

Characteristics of commercial inhaled nicotine delivery systems, such as aerosol outlet hydraulic diameter, power, and e-liquid pH vary significantly. These product attributes may change puffing topography of users [41, 86, 102-104]. This is important because puffing topography, including flowrate and puff duration have an effect on emissions and should be considered in both analytical and biological testing of inhaled tobacco emissions [85]. Prior work of the RTL includes the development of topography monitors (Figure 11**)**, including monitors for cigarettes, hookah, and JUUL e-cigarettes, for ambulatory monitoring of instantaneous behavior (puff topography) including flow rate of aerosol, puff volume, time of day of puffs, and frequency of puffs across a range of products [41]. Recent technology development also allows monitoring of respiration topography using a Hexoskin smart garment [105]. Topography monitoring gives valuable data for policy making decisions and provides a starting point for more sophisticated *in vitro* models. Although it is well documented that use topography effects emissions and that users puff at variable flow rates within a session [106, 107], most emissions systems used in the literature are not capable of variable flow rates, inhales between puffs or exhales. In fact,

InHALES is the only system capable of inhales between puffs and BSR is the only fully characterized system capable of exhale breaths.

Figure 11 *A model demonstrating use of a JUUL® e-cigarette (a) and the same model demonstrating use of a JUUL e-cigarette with a wPUM™ JUUL topography monitor.*

3.5 Limitations of comparing human health response to in vivo and in vitro studies of health effects.

Biological studies related to tobacco use in humans are limited to non-invasive, low risk observation. Saliva and oral swabs are used as bio samples for human subjects research since they are easily accessible and because oral health gives insight into systemic health. It is well documented that poor oral health has negative consequences on systemic homeostasis [36, 108, 109]. Specifically, an imbalance of bacteria in the oral cavity can lead to an inflammatory state resulting in adverse effects on systemic health [109]. The oral cavity immune system consists of resident immune cells in the salivary glands, immune cells that migrate from systemic circulation, and the mucosal immune system. The immune system of the oral cavity is in bidirectional communication with the gut and systemic immune systems. However, the current state of knowledge indicates that levels of *some* biomarkers in salvia do not correlate well with levels in systemic circulation and therefore may not be a good measure of systemic health [110]. Further, salivary biomarkers such as pro-inflammatory cytokines and immunoglobulins are associated with chronic and acute stress and may confound results [110]. The use of animal models is not ideal for mechanistic studies involving the human airway. First, most small animals are nose breathers [84], therefore the impact of aerosol passing through the oral cavity cannot be assessed. Also, the makeup and structure of airway epithelium differs significantly between humans and other species, including mice [111].

In vitro models are used for screen cytotoxicity [26-30, 112, 113], genotoxicity [83, 114], inflammatory effects [32, 33, 115] and induced oxidative stress [32, 34, 113, 115, 116] of

tobacco products by exposing cultures to emissions via emissions systems with biological exposure subsystems. Despite the impressive advances in technologies that allow more realistic exposure such as ALI and organ-on-a-chip, studies that use unrealistic exposure techniques, arbitrary doses, and non-relevant cell lines continue to be published. Submerged cell culture (Figure 12, left panel) is not appropriate for screening of inhaled environments for a variety of reasons. Cigarette smoke, e-cigarette aerosol, and other aerosols consist of constituents in multiple phases. Hydrophobic and volatile components may not reach cells submerged in cell culture media. Further, primary human airway cells in submerged culture do not possess characteristics of *in vivo* airway epithelial cells [117], so their biological response to chemical species is not representative of *in vivo* airway tissue. Basal cells in human bronchial epithelium possess stem cell qualities and have the ability to differentiate into other cell types,

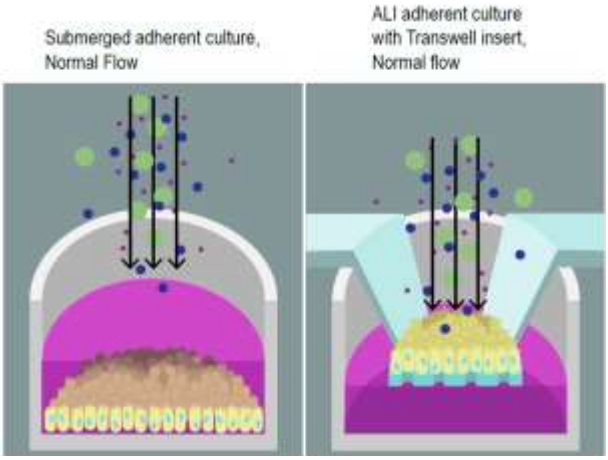

Figure 12 *This graphic shows culture techniques used in biological exposure studies for tobacco product screening. (Graphic by Tirzah Pilet for the Respiratory Technologies Lab).*

including ciliated cells, Clara cells, and goblet cells [111]. Submerged culture of primary cells inhibits ciliogenesis [118]. Mature muccociliated, pseudostratified, columnar epithelium can be achieved in culture through culture of primary airway cells with a combination of retinoic acid, a collagen substrate, and importantly, an ALI (Figure 12, right panel) [117]. Despite this knowledge and the availability of ALI culture systems, a portion of recent tobacco regulatory science literature contains published results and conclusions that are found using cells exposed to chemical inhalants in submerged culture [26, 33, 119, 120]. For example, in August 2020, an article assessed a THP compared to combustible cigarettes using a micronucleus assay [120]. Authors used a commercially available emissions system to puff each product and collect particulate matter on Cambridge filter pads. The cigarette smoke condensate (CSC) was

extracted, prepared and exposed to Chinese hamster lung V79 cells, human lymphoblastoid TK6 cells, and Chinese Hamster Ovary cells in submerged culture. Cells were stained, imaged with fluorescence microscopy, and scored. Results show less genotoxicity in cells exposed to THPs compared to cigarettes. The article concludes that “THPs are less risky than conventional cigarettes and that 21st century screening techniques can be employed to support product design and decision making, as a potential 1st screen prior to more traditional assessments [120].” It can be argued that such conclusions should not be made from this study as human puffing behavior between products, compensatory behavior, mechanical cues, and a physiologically relevant culture environment were not considered. Further, cell lines do not produce realistic cell responses and tend to be less sensitive to stimuli than primary cells, therefore they are not good candidates for *in vitro* models for product screening.

ECM stiffness is another a parameter to consider when striving for realistic culture conditions. Fibroblasts, epithelium, and endothelial cells in the lung have been shown to exhibit fundamental cellular changes based on ECM stiffness [121]. Culture techniques that better mimic the *in vivo* structure of airway tissue, just as 3D culture on soft scaffold materials, promote realistic *in vitro* response and increase the body of knowledge of disease pathogenesis. By using a 3D human upper airway epithelia reconstituted *in vitro* (MucilAir™, Epithelix, Geneva, Switzerland), Tapparel *et al.* [122] found that a primary ALI culture system allowed growth of several clinical strains of human rhinoviruses, a virus that cannot be supported with standard cell lines. The culture technique also allowed for the finding that the viruses tend to enter and exit at the apical side of the tissue. These findings would not have been possible without a realistic 3D culture setup that mimics the physiological microenvironment of cells. The field of tobacco research is lagging in the development of realistic *in vitro* setups that broaden the capabilities of cell exposure studies and allow researchers to ask more complex questions related to tobacco related injury and disease.

Great strides were made with the introduction of the ALI in tobacco research [78, 79], however there has been little innovation in cell culture techniques specific to exposing biological samples to inhaled environments in nearly 20 years. Meanwhile, the field of tissue engineering and applications of mechanobiology have matured quickly. Mechanical cues, such as fluid shear, have shown to alter protein expression [123], yet only two studies account for effects of fluid shear on biological response to tobacco aerosol. InHALES [1] introduced a novel method for culturing cells at an ALI while eliminating the adversities of the cell culture insert. Epithelium was cultured on cell culture inserts until maturity, then the membrane was punched from the

insert with the tissue culture attached and cultivated on hydrogel. The hydrogel was placed in cavities of a pipe of an exposure system with the tissue culture flush with the pipe inner wall. This method is a promising technique for culturing airway cells at an ALI, while eliminating the non-physiologically relevant attributes of a cell culture insert. However, results from this study showed lack of repeatability and poor cell survival when exposed to lab air at appropriate flowrates. Organ-on-a-chip technology has demonstrated impressive replication of the microenvironment of small airway tissue [84, 124, 125]. The BSR [84] established shear stress on cells during cigarette smoke and e-cigarette aerosol exposure with an airway on a chip. However, airway on a chip is not practical for modeling the entire human airway. In addition to the high cost of fabrication, microfluidic devices cannot accurately represent the flow mechanics of early airway generations nor the upper respiratory system. While the technology is promising, organ-on-a-chip has not been validated for repeatability [126]. Further, organ-on-a-chip represents the smallest functional unit of an organ; not an entire organ [126]. Therefore, lung-on-a-chip cannot be used for mechanistic studies that aim to study biological response as a function of lung position. The ability to couple microfluidic devices to a modular airway model would be more useful for testing e-cigarette aerosol and other inhaled environments when appropriate, but organ-on-a-chip cannot achieve desired results alone.

Mechanical cues improve realism of *in vitro* studies and tend to have the greatest effect in primary cells. Yet, studies on cell lines are often used to draw conclusions about the relative risk of novel tobacco products. The epithelial lining of the human airway provides defense against the environment through several mechanisms, including providing a physical barrier, secretions that facilitate immunity, and through muccociliary clearance [117]. Chronic obstructive pulmonary disease, a common tobacco related disease, is associated with impaired muccociliary clearance, which fosters pathogen colonization [117]. Mucociliary cell differentiation and function are mediated by molecular mechanisms that can be altered with exposure to toxicants such as cigarette smoke [111] and is modeled *in vitro* best using primary cells. Gene expression profiling and protein analysis can show how aerosol exposure effects function of the airway's epithelial lining and give insight into mechanisms of disease. Schamberger *et al.* [111] found that cigarette smoke extract altered differentiation and function of primary human bronchial epithelial cells cultured at an ALI over a 28 day period. Acetylated-tubulin, a protein normally expressed in ciliary cells, decreased in differentiating primary bronchial epithelial cells after 21 days of chronic exposure to cigarette smoke extract, compared to an untreated control [111]. Protein analysis is preferred for characterization of epithelial

function over gene expression since prior work has indicated that ciliary cell fate may be regulated in a post-transcriptional manner [111]. These findings support the use of primary cells in screening tobacco products for toxicity, morphology, and function.

3.6 The lack of standard input measures (definitions of dose) and the need for standard (but multiple) outcome measures

A major limitation in translation of findings in tobacco regulatory science is lack of consistency in reporting. It is especially found in studies involving next generation alternative tobacco products such as electronic cigarettes and heat-not-burn products. This limitation may be partly attributed to the transition from using cigarette smoke extract and CSC in toxicology studies to direct aerosol exposure using an ALI. In the early days of e-cigarette research, cytotoxicity of e-liquid was studied by adding unvaporized liquid to cell cultures [26]. After data was published that supported that aerosolization of e-liquid produces harmful byproducts not found in e-liquid before heating it [127], the field largely transitioned to exposing cell cultures to aerosol. Biological studies of cigarette smoke generated from exposure systems have historically used diluted cigarette smoke [76, 77, 128, 129] because of the strong cytotoxic effect cigarette smoke has on cells [112, 130], but e-cigarette aerosol has been demonstrated to be less cytotoxic than cigarette smoke when puffed with standard protocols, so diluted aerosol is not always used [130]. This inhibits cross-product comparisons. Methods nor reported metrics have been consistent across studies [131, 132]. In literature published between 2016-2021, cytotoxicity results are reported as cell viability [44, 46], cytotoxicity [133], Lactate Dehydrogenase release [129], and IC_{50} [112, 134-136]. IC_{50} dose is reported in mass per unit volume [112, 134], exposure time [112], percent aerosol [27], and percent of puffs [136]. Without consistent methods and reporting of results, the repeatability of studies and the ability to relate them to human health and addiction is limited.

CHAPTER 4. INNOVATION

Aim 1: Demonstrate a geometrically bio-inspired aerosol exposure system

A variety of exposure systems have been used for testing aerosols. Table 1 compares the biomimicry of exposure systems used for toxicity and emissions testing. Each column of the table describes an aspect of geometry as it relates to biomimicry of the system. Each row of the table represents an existing emissions and exposure system. The entries each row and column can be compared to one another to assess the relative features and capabilities of available devices. The Transit Length column describes the distance between the device under test and emissions capture or biological exposure subsystem. Angle of Inclination denotes if the system set up allows a device under test to be inclined (filled circle), or not (open circle). Columns with headings describing specific airway geometries contain data about how closely a flow path and/or exposure apparatus resembles geometry of the human airway. An open circle means realistic geometry was not utilized or that the anatomical structure is not included in the system, a half-circle signifies that there were considerations toward biomimetic geometry, but the geometry is approximated or simplified. A filled circle denotes a system where medical imaging data or casts of a human airway were used for system geometry design. Small Airway is lung generation seven and later. A human airway model that has been used in prior studies [91, 137] is used as a starting point in this work. Figure 13 compares the airway model to human airway anatomy and introduces terminology which will be used throughout this work.

Table 1 *A comparison of biomimicry of emissions systems in the literature. Asterisk denotes that ability to modify this attribute requires optional hardware.*

Emissions System	Transit Length [cm]	Angle of Inclination	Oral Cavity Geometry	Nasal Cavity Geometry	Large Airway Geometry Gen 1-6.	Small Airway Geometry Gen. 7-22	Citation
PES-2	5	●	○	○	○	○	[80]
Biomimetic Smoking Robot	Not reported	○	○	○	○	●	[84]
InHALES	Not reported	○	◖	○	●	○	[1, 101]
Borgwaldt RM20S	~290	○	○	○	○	○	[44]
Borgwaldt LM4E	~130	○	○	○	○	○	[44]
Universal System for Analysis of Vaping	Not reported	●	○	○	○	○	[138]
Ecig-EGS	Not reported	○	◖	○	○	○	[139]
Vitrocell VC 10	~90	●*	○	○	○	○	[44]
Vitrocell VC1	~125	●*	○	○	○	○	[44]
Hosseini 2023 Mouth and Throat Model	19.9	●	●	○	●	○	[140]

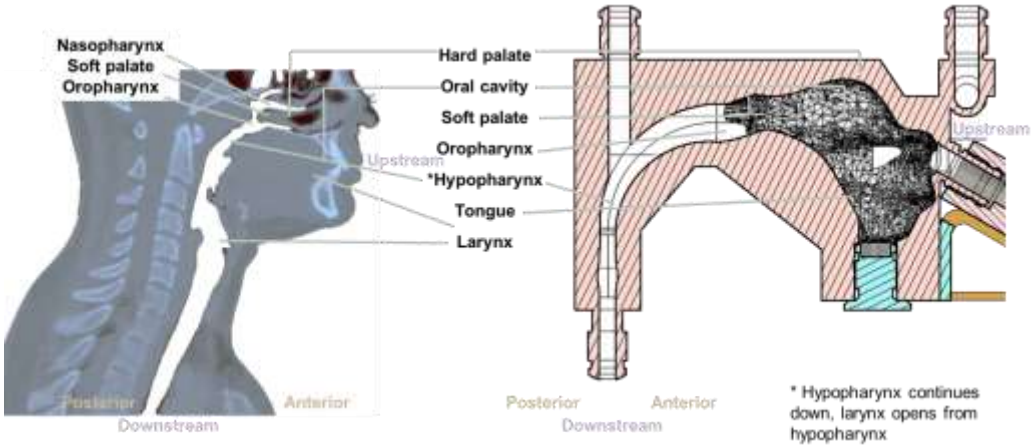

Figure 13 *A comparison of the geometry of the Oral Cavity Module to representative human anatomy from a 27 year old white female.*

Objective 1.1 Integrate an airtight connection between the ENDS device under test (the aerosol generator) and the inlet to the exposure system

The mounting and connection of a device under test to an emissions system is an undervalued subsystem (Figure 14a). Two commonly used emissions testing protocols [141, 142] describe briefly the necessity of product orientation. If an electronic cigarette (e-cigarette) is puffed horizontally or with the mouthpiece lower than the distal end, it increases the risk of "dry puffing". This phenomenon occurs when the wick of an e-cigarette's atomizer is not bathed in liquid and becomes dry. When power is delivered to the coil, the wick is burned instead of e-liquid being aerosolized. There has been some speculation that studies that report high levels of carbonyls are biased by dry puffing occurrences [143]. While these claims have been disputed, this criticism highlights the need for emissions testing setups that reduce risk of "dry puffing". Prior work has shown that 30 degrees from horizontal is an appropriate angle for testing of pod style e-cigarette products such as the JUUL e-cigarette [41].

The two standard emissions protocols aforementioned indicate the importance of an airtight seal at the connection between a device being tested and the emissions system. A tobacco product is often connected and disconnected by a laboratory technician several times throughout an experiment. It is important that this the airtight seal is repeatable. A repeatable seal can be achieved by placing a connector at the interface of a tobacco product and the system's flow path. Commercially available gaskets are generally circular and come in standard sizes. The variety of sizes and form factors of the tobacco products studied in the RTL requires custom gaskets or connectors to be made.

A current limitation of the PES-2 emissions systems is that the connections between test product and emissions capture subsystem contain geometry that increases the risk of deposition in transit to the emissions capture system, obscuring emissions results. Figure 14b-c shows the flow path of the PES-2 emissions system between a device under test and a filter pad used to capture emissions. Areas of the flow path that include geometry that may contribute to mass loss through impaction are circled. A-A is the cross section of a filter pad holder. B-B is the connection between a barb on the filter pad holder and flexible tubing. This interface poses a high risk for deposition through impaction. C-C is the interface between e-cigarette and tubing. We have observed that this interface has a high risk of leaking. D-D shows a cross section of exhaust of an e-cigarette. This geometry depends on the device under test.

Objective 1.1 will address the seal between the product under test and the emissions system, the ability to position a device under test at an appropriate angle of inclination and reducing deposition in transit to an emissions capture subsystem during emissions testing. This objective focuses on modifications to Section A of the airway geometry, shown in Figure 14d. Developments include modular adapters for a variety of emissions system inlet geometries and mold design and fabrication for high throughput manufacturing of adapters.

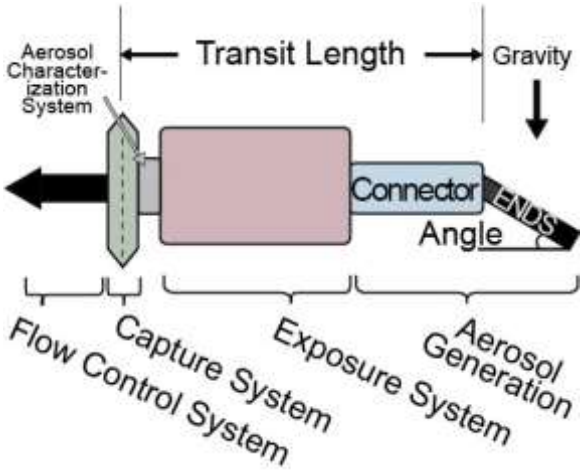

a) *A generalized schematic of typical attributes of emissions and exposure systems*

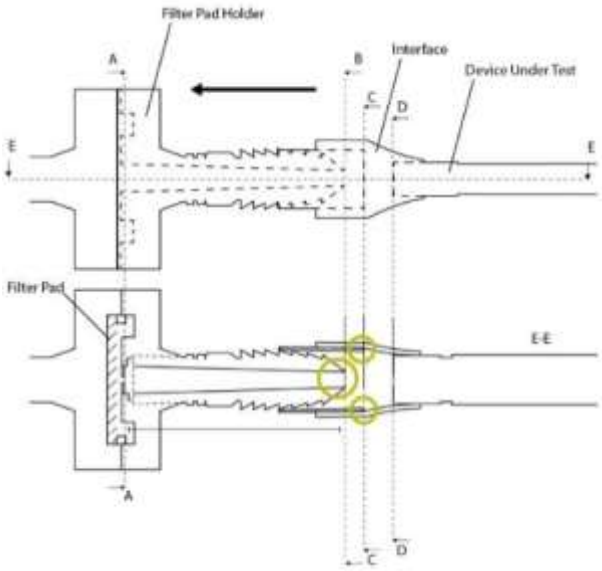

b) *The flow path between a device under test and a filter pad in a filter pad holder. Flow is from right to left. Areas that may contribute to mass loss through impaction are circled.*

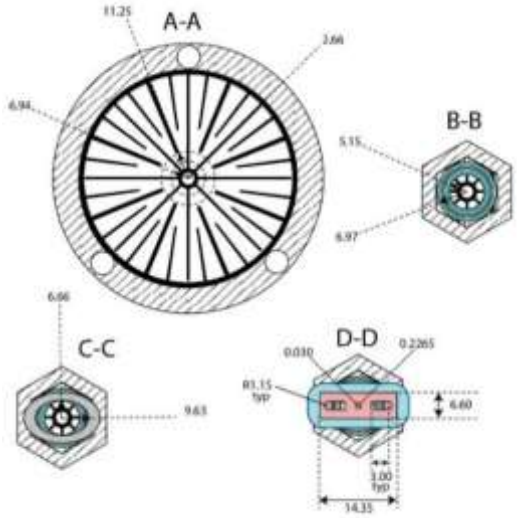

c) *A-A is the cross section of a filter pad holder. B-B is the connection between a barb on the filter pad holder and flexible tubing. C-C is the interface between e-cigarette and tubing.*

d) *The inlet to the oral cavity and mimics human lips.*

Figure 14 *The inlet geometry of PES-2. Schematics are not drawn to scale. Dimensions are given in millimeters.*

Objective 1.2 Integrate a human oral cavity mimetic exposure chamber appropriate for conducting aerosol deposition, cell exposure, and toxicity studies of relevant cell lines and/or tissues

The oral cavity is an important part of the human airway and a primary defense mechanism for the body. However, currently available emissions systems are not equipped for investigations into inhaled environments impact on oral health. The transit length to exposure chambers of commercially available exposure systems is not representative of transit to the oral cavity and therefore dosimetry and particle deposition is not representative of *in vivo* exposure. Few studies pertaining to oral health of inhaled tobacco users, including oral microbiome and dental hard tissue studies, appear in the literature. The oral microbiome is of interest because of the impact this environment has on overall human health [109]. While cytotoxicity studies and the development of dose response curves are valuable preliminary data in evaluating the immediate safety of an inhaled substance, studying abundance of bacteria and the mechanisms related to bacterial diversity may allow for predictions of long-term health effects, especially chronic disease. Zhang 2019 [108] found that shift in the salivary microbiome may play a pathogenic role in non-small cell lung cancer. Despite the important insights into health the microbiome gives, to date, few studies that investigate the microbiome of e-cigarette users have been published. Stewart *et al.* [36] was the first publication to study the effects of e-cigarettes on oral and gut microbiome of users. The study finds that there is no significant difference in the bacterial profile of e-cigarette users compared to non-users. Several limitations of this small-scale pilot study and inconsistencies in historical data of cigarette smoking's impact on the microbiome highlight the necessity for further research into the impact of inhaled tobacco product use on both microbial diversity and function. Another study [144] found that e-cigarette exposure reduced host anti-microbial activity against *Staphylococcus aureus. Roushdy et al.* [145] found that *Streptococcus mutans* count was higher in tobacco smoking groups than in non-smokers' saliva. Pushalkar *et al.* [146] found that e-cigarette users are generally more prone to infection. Conversely, a small scale pilot study [147] found that e-cigarettes may not shift oral and lung microbiome however, limitations of this study include small sample size (N=28) and metatranscriptome profiling of bacteria, which when used alone tends to lack reproducibility and widespread applicability [148]. Technologies that allow recreation of observed biological activities such as these should be developed to allow *in vitro* mechanistic studies.

The effect of inhaled tobacco on hard dental tissue is another area of research that might be improved with a biomimetic exposure system that considers the oral cavity. Cho *et al.* [149] found an association between adolescents who use e-cigarette products and experiencing cracked or broken teeth. Zhaoa *et al.* [150] studied the effects of discoloration of human premolars from cigarette smoke, e-cigarette aerosol, coffee, red wine, and soy sauce. The study used a VITROCELL exposure system for e-cigarette and cigarette exposure. Cigarette exposure was 20 cigarettes per day with Kentucky reference cigarettes, while e-cigarette exposure was 300 puffs per day using a MESH e-cigarette product in classic tobacco flavor. The paper does not specify puff topography other than session length. This is the first paper to study discoloration of human teeth using e-cigarettes and was the first to compare degree of discoloration across multiple common exposures. This is also the first study to capture these effects while incorporating daily brushing. Unfortunately, the dose of smoke or aerosol exposed to teeth is likely not representative of what is introduced to the mouth during regular use. This exposure could be made more realistic by performing the same experiment using a biomimetic exposure chamber and using user puffing topographies. Kumar *et al.* [151] compared cigarette exposure effects on surface roughness of different denture materials. Surface roughness impacts the accumulation of bacterial and formation of biofilms on teeth; bacteria tend to accumulate on uneven topographies. To study the impact of cigarette smoking on surface roughness of dentures, two diverse denture materials, heat-cured polymethylmethacrylate and flexible denture base material, were exposed to cigarette smoke in a custom-made exposure chamber. Results showed a significant difference between surface roughness of each material before and after exposure. There was also a significant difference between surface roughness of the two materials, with the flexible material surface roughness being more affected by smoke exposure. Studying hard dental tissue as a function of puffing topography (flow rate, puff duration, volume) and user behavior (mouth to lung versus direct to lung) would be valuable for informed regulation of product characteristics. For example, the exit diameter of an e-cigarette may have an impact on oral health by influencing the flow rate that a product is puffed.

Three-dimensional (3D) reconstruction of the oral cavity has been used widely in the field of dental surgery and patient education, but the technology has not been extended into inhalation research. A study that was part of The Visible Human Project [152] reconstructed the human face and oral cavity by using liner interpolation software (EIKONA 3D) on images transverse cryosections of a male head. A detailed 3D mesh was produced and can be edited for patient specific anatomies. A 2021 study [153] described *OralViewer,* the first 3D oral cavity

reconstruction technique that uses a 2D panoramic x-ray. *OralViewer* was developed for patient education of surgical procedures. Soft tissue and jaw bones are pre-defined and is adapted to patient specific tooth anatomy. The pre-built templates were constructed from computed tomography (CT) scan data. A focus group with experts who tested *OralViewer* described that using a CT scan for the jawbone and gum template limits the accuracy of the model. The expert recommendation was to improve the model by using intra-oral scans, which can capture details of soft tissue. 3D digital models have also been used in dentistry for appliance manufacturing by 3D scanning plaster casts and using the model in computer aided design (CAD) software as a design tool [154]. A standard workflow for many dental offices include sending a plaster model, cast, or intraoral scan data to proprietary companies who generate the digital model and make them available for download [155].

Much current literature exposes bronchial or lung epithelium to a dose that is indefinite and often not repeatable because of aerosol loss in transit. Results that quantify cytotoxicity [26-30, 112, 113], genotoxicity [83, 114], inflammatory response [32, 33, 115] and oxidative stress [32, 34, 113, 115, 116] are not representative of the entire airway. Neither mass loss nor biological response in the oral cavity have been studied widely. Current emissions systems so not provide the geometry to simulate deposition in the oral cavity. Objective 1.2 will focus on development of a biomimetic Oral Cavity Module. The module, focus Location B, is shown in Figure 15 and will both be equipped with emissions capture and biological exposure instruments as well as introduce inlet geometry to the emissions system that acts as a filter for downstream emissions characterization and exposure. The apparatus will exhibit enhanced biomimicry in comparison to traditional smoking machines and exposure systems from three perspectives: oral cavity particle deposition and dosimetry, improved correlation between *in vitro*, *in silico*, and *in vivo* conditions.

Figure 15
Location B of the airway geometry includes a realistic oral cavity.

Objective 1.3 Integrate an oropharynx model to control flow paths from the oral cavity and sinus cavity into the pharynx

Respiration of clean air is an aspect of human behavior that is often neglected in machine puffing systems. The Independent Holistic Air-Liquid aerosol exposure system (InHALES) is the first emissions system with the ability to simulate regular breathing between puffing. While the InHALES system is an impressive idea, proof-of-concept has not been effectively demonstrated. Aerosol delivery was validated inside of the pumps but not in the

entire airway model, where many cell cultures are exposed to test environments. Also, mass delivery (ng/cm^2) inside of the primary pump was not repeatable. Another concerning result given in the InHALES validation paper is that cells exposed to lab air flowing through the apparatus caused a significant difference in cell viability compared to an incubator control when a “deep inhale” (an inhale to the lungs) was simulated. Further, command flow was not achieved by the system when the resistance of a cigarette was added to the inlet. It is imperative that tobacco company-independent biomimetic exposure and deposition systems be developed to enable studies allowing us to better understand the biological mechanisms underlying inhaled toxicants on relevant human cell lines.

Objective 1.3 will focus on modifications to PES-2 that provide the ability to inhale clean air between puffs. The upper airway geometry currently used within our research group [91] uses a digitized 3D cast of an adult female’s oral cavity and a 3D reconstruction of the larynx and tracheal bronchial region from cryosections of an elderly female [137]. The geometry between the exhaust of the oral cavity and the inlet to the larynx was approximated with a spline curve (Location C in Figure 16) and lacks biomimicry. This is where we will make modifications to the oral cavity model to introduce a flow path to model the nasopharynx.

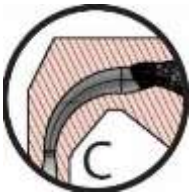

Figure 16
Location C is the approximated spline between the oropharynx and hypopharynx.

Objective 1.4 Integrate modular exposure chambers with bifurcations in the flow path reminiscent of the upper airway in the lung

Downstream from the oral cavity, an inhale moves through the pharynx, the larynx, and into the tracheobronchial region. The tracheobronchial region dominates particle deposition, protecting the fragile downstream airway, yet geometries that mimic this have not been used in analytical emissions work. Historically, realistic airway geometries have been used for computational fluid dynamics [95, 156] and *in vitro* optical analysis [92] of fluid flow and aerosol deposition in the human airway. However, this technique has not been used for emissions analysis or biological exposure until recently [1] with an article describing, but not fully validating, the biomimetic InHALES system. Introducing bifurcations into an emissions system flow path is a basic modification that may allow researchers to manipulate dose by adding or reducing flow path bifurcations and inducing deposition through impaction and sedimentation.

Objective 1.4 focuses on the design, fabrication, testing, and scaling of an apparatus that adds bifurcations to a flow path through a commercial multiple well plate. The module can be connected to the exhaust of the Oral Cavity Module (Figure 17). The Bifurcated Exposure Chamber (BEC) flow path is intended to mimic flow of generations one and two of the human airway. By mimicking lung geometry, mass transport to cell cultures and emissions capture instruments is more realistic; unintended mass loss through impaction on non-anatomical features is minimized. Development of modular enclosures for standard plates with inlets and outlets such that fluid flow is along the rows of each plate, a flow path insert with a bifurcation within a chamber splits one flow path into two, each with its own outlet will mitigate risk of non-physiological deposition. Tubing can be used to connect plates with one another and to other analytical instruments, such as sorbent tubes for volatile capture. The benefits of using multiple well plates as a capture medium are twofold. One, it allows for transverse flow, which is more memetic of how aerosol interacts with the walls of the human airway. Second, plates are versatile; cells can be cultured in wells for biological exposure, aerosol deposited in wells can be extracted with methanol and used for analytical chemistry, and optical evaluation techniques are possible, as the plate can be places onto a microscope stage. The addition of a flow path with a bifurcation built for commercially available multi-well plates offers versatility that is not available in current state of the art emissions systems and exposure apparatuses.

Figure 17
Location D is the module downstream from the oral cavity

Aim 2: Demonstrate a human behavior-inspired aerosol delivery and distribution system

A schematic of the architecture and signals of PES-2's configuration is given in Figure 18. The arrow identifies the section of the flow path that innovation will be made via the modules described in Aim 1. From upstream to downstream, the PES-2 system includes an aerosol generator (e-cigarette), an emissions capture subsystem (such as a filter pad holder and Cambridge filter pad), a system flow meter, a proportioning valve, a solenoid valve and a closed loop vacuum system. Aerosol that is generated by a test product flows through a pipe into the emissions capture subsystem, or other analytical instrument, to facilitate analysis of emissions and to protect the rest of the system from exposure downstream. The system flow meter is a calibrated orifice plate (Alicat Scientific, Tucson, AZ) serviced by a third-party vendor annually to ensure accuracy over the operating range 0 to 500 mL/s. At the exhaust of the flow meter is a proportioning valve that controls flow rate through close-loop control with the data acquisition

and control (DAC) system. The flowmeter sends a digital flow rate signal to the DAC and the DAC sends a voltage to the proportioning valve modulating it at 100Hz to maintain the command flow rate. At the exhaust of the proportioning valve is a solenoid valve that is given an on/off signal from the controller at the start and end of an inhale. Downstream from the solenoid valve is the inlet to a vacuum tank with an integrated closed-loop control vacuum system, including an inlet from atmosphere, a vacuum pump, and exhaust. The system is only capable of producing vacuum pressure with its current configuration and control code[80].

Table 2 gives a comparison of system flow attributes of emissions systems in the literature. Puffing Profile refers to the ability to puff at a variable flow rate within a trial. An open circle signifies that a system only has ability to puff at one flow rate in a trial. A filled circle is a system that can puff as an infinite number of flow rates within a trial, within the limits of its pump. The Clean Air Inhale column describes if a system can bring clean air into the system flow path. An open circle indicates that there is not a mechanism for bringing clean air into the system. A half circle signifies that clean air can be mixed with aerosol in the system. A filled circle indicates that a system can puff clean air through the entire flow path upon a command. A filled circle in the Exhale column describes a system with bidirectional flow while an open circle is unidirectional flow. A goal for this dissertation is that each column will contain a filled circle for our emissions system at its completion.

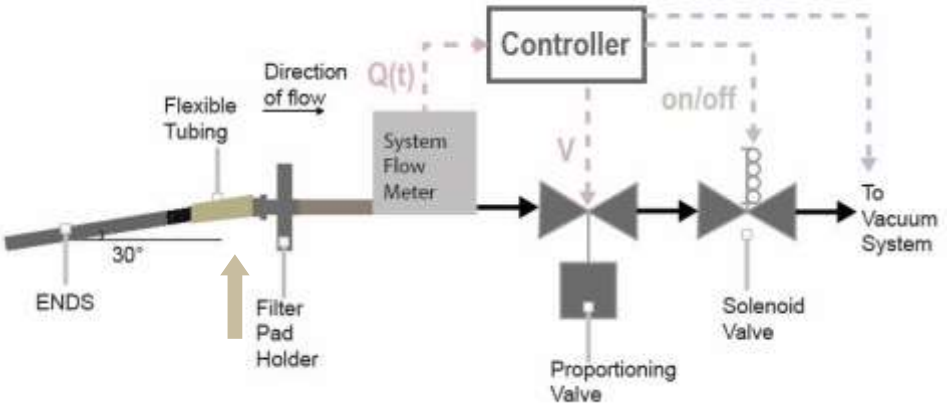

Figure 18 *A schematic of PES-2 before any modifications were made. The tan arrow calls out where areas of innovation will be made, including Locations A, B, C, and D, identified in Aim 1.*

Table 2 *A comparison of attributes of emissions systems in the literature.*

Emissions System	Puffing Profile	Clean Air Inhale	Exhale	Flow Rate Range [mL/s]	Citation
PES-0	●	○	○	0-80	-
PES-1	●	○	○	0-150	-
PES-2	●	○	○	0-450	[80]
Biomimetic Smoking Robot	○	●	●	Not reported	[84]
InHALES	○	●	●	Not reported	[1, 101]
Borgwaldt RM20S	○	◖	○	Not reported	[76]
Borgwaldt LM4E	○	○	○	Not reported	[44]
Universal System for Analysis of Vaping	○	○	○	Not reported	[138]
Ecig-EGS	○	◖	○	Not reported	[139]
Vitrocell VC 10	●	○	○	Not reported	[157]
Vitrocell VC1	●	○	○	Not reported	[158]
Hosseini 2023 Mouth and Throat Model	●	○	●	0-4500	[140]

Objective 2.1 Integrate human puffing behavior with the exposure systems from Aim 1. This objective employs the existing PES-2 control system

The importance of using human puffing topography in emissions testing is well established [41, 86, 102-104]. There are few emissions systems in the literature are capable of puffing at variable flowrates [80, 112]; the only biomimetic emissions system validated in the literature is not [84]. PES-2 can be programmed to playback inhalation profiles observed from users through topography monitoring. The green line on Figure 19 shows a puffing profile from a real user, obtained with concurrent puff and respiration topography monitoring.

Objective 2.1 integrates the modules described in Aim 1 into PES-2 system architecture and control code. Integration of these subsystems allows unidirectional puffing at variable flowrates, puff durations, post-puff intervals, and session lengths. Variable flow rate human puffing topography is used to quantify aerosol deposition in each module and to measure flow rate throughout the emissions system flow path.

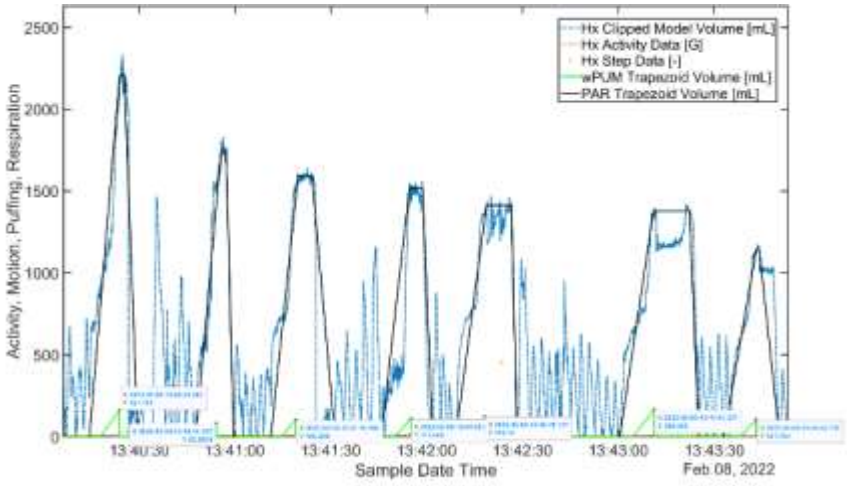

Figure 19 *An excerpt from participant OS7-21 baseline (usual product) puffing and inhalation topography from an ongoing clinical study. Puff profiles are observed from tobacco users in the natural environment using topography monitoring, then simulated on PES-2 by programming topography parameters into a control code through a graphic user interface.*

Objective 2.2 Integrate a human puffing behavior (mouth inlet or aerosol) and inhalation behavior to extend the PES-2 control system of Objective 2.1

It is important to mimic natural environment topographies of users because e-cigarettes produce different aerosol constituents depending on how a device is used [116, 159], especially at higher flow rates when aspiration has been demonstrated by our lab to occur with some e-cigarette devices. Breaths of clean air between puffs of a tobacco product may affect retention and clearance of deposited matter. Before the era of electronic nicotine delivery systems (ENDS), tobacco smoke was often diluted to mimic the act of inhaling smoke from mouth to lung with a breath of clean air. Dilution of cigarette smoke was necessary to increase resolution of data in dose response curves in biological testing because cigarette smoke is highly cytotoxic. E-cigarettes have shown lower cytotoxicity than cigarette smoke [130]. In response, several articles [28, 45, 160-163] have reported modifying emissions systems to produce undiluted aerosol. Interestingly, nearly all publications that discuss use of undiluted aerosol come from tobacco industry research labs. Adamson 2018 [44] (British American Tobacco) is the first publication to use an unmodified commercially available emissions system to produce undiluted aerosol, followed a few months later by Thorne *et al.* [130] (British American Tobacco), who made a case for studying e-cigarette exposure under undiluted conditions while cigarette aerosol should be diluted to prolong exposure time and produce a valid dose-response curve.

Researchers at Phillip Morris [133] exposed human organotypic oral epithelial cultures to undiluted tobacco heated product (THP, also referred to as ‘Heat Not Burn’) smoke or cigarette smoke. The study reported reduction in biological response in THP exposed cells compared to cigarette exposed samples [133]. Bishop *et al.* (British American Tobacco) used undiluted e-cigarette aerosol in 2019 to show that diluted versus undiluted aerosol does not affect distribution of aerosol and asserting undiluted aerosol permits dose extrapolation for human exposure [112].

Prior work supports the use of undiluted aerosol to generate dose response curves but does not acknowledge how clean air respiration may affect dose distribution as a function of lung location, an important detail in understanding mechanisms of tobacco related disease. Preliminary clinical data, shown in Figure 19, indicates that users take a high volume, high flow rate, “deep” inhale immediately following a puff. This deep inhale will be referred to as Puff Associated Respiration (PAR). Following a PAR, users return to their regular tidal breathing that tends to be smaller in volume than PAR. Objective 2.2 focuses on modifying PES-2 architecture and control code to incorporate PAR and tidal clean air inhales into puffing protocols.

Objective 2.3 Develop system architecture for post-inhale breath hold and exhalation behavior by modifying the oropharynx model and PES-2 control system of Objective 2.2

As of 2023, the only emissions system in the literature capable of simulating a breath hold, lung reserve volume, and exhalation is the InHALES, shown in Figure 20 [1]. There is one system capable of exhalation [84], the Biomimetic Smoking Robot (BSR), but it is not capable puffing at variable flow rates. InHALES is still in the prototyping phase and faces several limitations. Variable puffing profiles have not been demonstrated. Also, command flow was not maintained with the added resistance of a tobacco product. Fluid shear of air on cells damaged cell membranes and reduced viability. Other than these limitations, it is important for testing setups to be developed independent of tobacco companies to avoid bias.

Objective 2.3 includes designing modification of PES-2 architecture and control code to incorporate the necessary hardware and control code logic for breath holds and bidirectional flow through the system, including exhale through a nasal cavity.

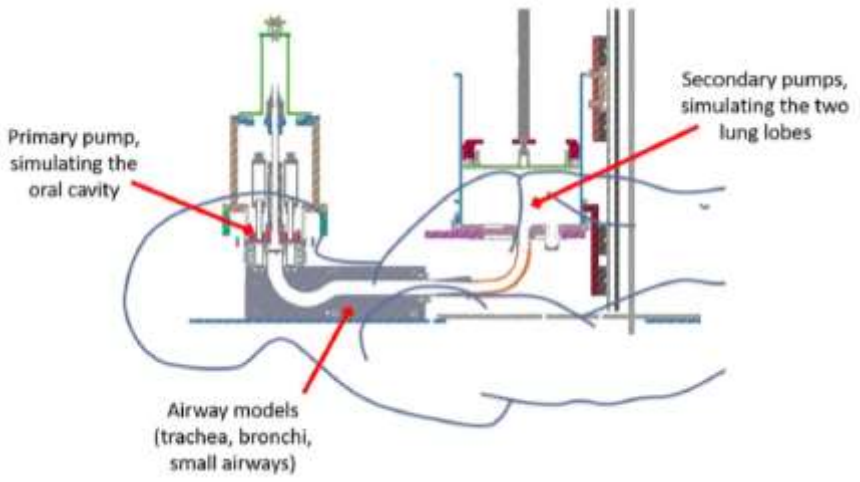

Figure 20 *A graphic of architecture of the independent holistic air-liquid exposure system presented in Steiner, 2020 [1].*

Aim 3: Quantify the dose and flow conditions throughout the exposure system

Aerosol is a mixture of particulate matter (PM) and gas phase constituents. Analytical emissions systems should have the ability to capture and quantify emissions in both phases. A major limitation in the state of the art is that lack of biomimicry in flow path geometries obscures the ability to draw relationships between measured dose and airway location, an important relationship for studying particle retention and mechanisms of airway injury. PM can be captured on filter pads (Figure 21a). Hydrophilic PM and some gas phase constituents can be captured in liquid (Figure 21b), though one standard protocol for analytical testing of e-cigarettes [164] requires a filter as an “aerosol trap” while other protocols [141] do not specify capture material. Volatile phase constituents are captured by placing sorbent tubes in the flow path of an emissions system (Figure 21c). Sorbent tubes contain solid absorbent material, such as activated charcoal or silica gel, to trap compounds until they are extracted for analysis using gas chromatography–mass spectrometry. Before *in vitro* biological exposure systems were developed, cigarette smoke condensate (CSC) was prepared by passing cigarette smoke through a liquid, capturing hydrophilic constituents, and exposing biological samples [82]. This practice is less common with the availability of equipment for direct biologic exposure [79]. Nonetheless, not all emissions systems are equipped to expose biological samples. A schematic that generalizes an *in vitro* exposure set up is given in Figure 21d. *In vivo* exposure (Figure 21e), the direct exposure of an animal and analysis of physiological response, is not the

focus of this dissertation. The use of animal models is not ideal for mechanistic studies involving the human airway. Most small animals are nose breathers [84], therefore the impact of aerosol passing through the oral cavity cannot be assessed. Also, the makeup and structure of airway epithelium differs significantly between humans and other species, including mice [111]. Table 3 compares emissions capture and exposure capabilities of emissions systems described in the literature. For PM, hydrophilic, and volatile capture, a filled circle means that the system has the capability throughout the system while an open circle denotes that it does not. A half circle denotes that capture is possible but is limited to certain locations in the flow path. For *in vivo* and *in vitro* exposure, full and empty circles signify the same as the other columns and a half circle means that the system is capable of the exposure type with the addition of a compatible exposure module.

The deposition of aerosol along the respiratory tract (between the mouth and the location of study) obscures the relationship between *in vivo* and *in vitro* dosimetry. Sosnowski *et al.* [165] estimated that 15-45% of main stream e-cigarette aerosol is deposited into the lungs, depending on the user's breathing. Emissions capture for analysis is often an arbitrary distance or minimized distance from a device under test. Standardized puffing protocols for emissions testing does not accurately represent human puffing behavior. Moreover, biological exposure chambers often utilize different flow path geometries than emissions capture subsystems, introducing obscurities between estimated dose delivered and biological response. The ability to capture emissions with accepted techniques, such as with filters, liquid, and sorbent tubes, in realistic geometry identical to geometry used for *in vitro* biological sample exposure provides data about how mass dose is distributed throughout the airway.

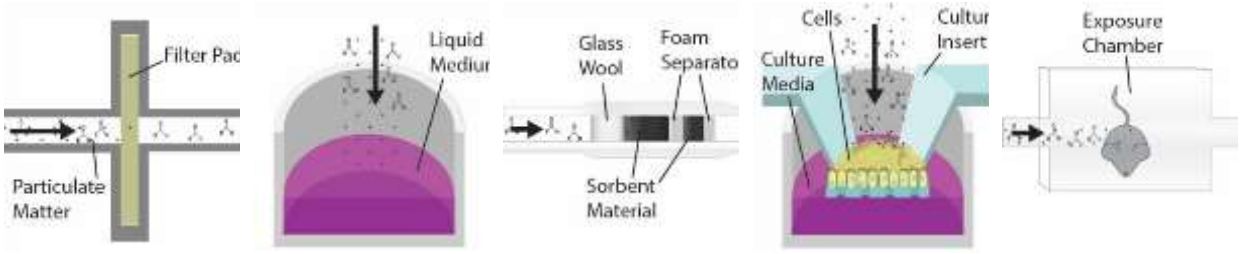

Particulate matter capture with a filter pad. | *Capture of hydrophilic compounds with a liquid.* | *Gas phase capture with a sorbent tube.* | *In vitro exposure of cells at an air-liquid interface.* | *In vivo exposure with an exposure chamber.*

Figure 21 *Cross-sectional schematics of emissions capture and exposure methods used in tobacco research.*

Table 3 *Comparison of emissions capture and exposure capabilities of current emissions systems.*

Emissions System	Particulate Matter Capture by a Filter	Hydrophilic Compound Capture by Liquid	Volatile Capture by Sorbent Tube	*In Vitro* Exposure	*In Vivo* Exposure	Citation
PES-2	●	○	●	○	○	[80]
Biomimetic Smoking Robot	○	○	○	●	○	[84]
InHALES	○	◖	○	●	○	[1, 101]
Borgwaldt RM20S	●	●	○	◖	○	[76]
Borgwaldt LM4E	●	●	○	◖	○	[44]
Universal System for Analysis of Vaping	N/A	N/A	○	○	○	[138]
Ecig-EGS	●	○	○	○	○	[139]
Vitrocell VC 10	●	●	●	●	○	[157]
Vitrocell VC1	●	●	●	●	○	[158]
Hosseini 2023 Mouth and Throat Model	●	○	○	○	○	[140]

Objective 3.1 Quantify the mass dose distribution as a function of geometric position (developed in Aim 1) and system flow conditions (implemented in Aim 2) for one or more ENDS

The deposition of aerosol along the respiratory tract (between the mouth and the location of study) obscures the relationship between *in vivo* and *in vitro* dosimetry. Sosnowski *et al.* [165] estimated that 15-45% of main stream e-cigarette aerosol is deposited into the lungs, depending on the user's breathing. Emissions capture for analysis is often an arbitrary distance or minimized distance from a device under test. Standardized puffing protocols for emissions testing does not accurately represent human puffing behavior. Moreover, biological exposure chambers often utilize different flow path geometries than emissions capture subsystems, introducing obscurities between estimated dose delivered and biological response. The ability to capture emissions with accepted techniques, such as with filters, liquid, and sorbent tubes, in realistic geometry identical to geometry used for *in vitro* biological sample exposure provides data about how mass dose is distributed throughout the airway.

Objective 3.1 quantifies mass deposited in modules described in Aim 1 and as a function of flow conditions described in Aim 2. Mass balance for each module is performed using filter pads (Figure 21a) at the exhaust of each module. Mass [mg] of deposited aerosol is reported for modules of the emissions system.

Objective 3.2 Quantify the local flow conditions (mass flow rate and mean aerosol velocity) as a function of geometric position and system flow conditions for one or more ENDS

When a particle deposits in the airway, clearance and retention processes begin immediately and are dependent on size and anatomical location of the particle. When a particle deposits and is retained in the lung, it becomes coated in or absorbs surfactant, which may provide immune privilege and aid in absorption and translocation through the blood-brain barrier increasing uptake efficiency of aerosol deposited in the lungs compared to other parts of the airway [166]. Particle size and deposition patterns are dependent on user puffing topography, especially flow rate [53]. Objective 3.2 uses calibrated instruments to measure flow rate at system locations. Modules in Aim 1 and measurement instruments are modular allowing measurements throughout the system. Flow conditions in Aim 2 are exercised and local flow conditions are quantified at number of locations throughout the system for a given flow condition.

Aim 4: Validate the acute response of living cells in the aerosol generation, delivery and exposure systems

Dosimetry has been a challenge in airway exposure and toxicity studies that utilize emissions systems [83]. Inaccurate dose arising from the exposure systems obscures comparisons between studies and translation of results into public health initiatives*[84].* Current culture systems for air-liquid interface (ALI) exposure fails to maintain realistic aerosol particle deposition mechanics in the human airway. Current low-cost, high throughput ALI culture systems do not allow cultures to be exposed to shear stress from transverse flow (Table 4). There is a need for systems which better replicate *in vivo* exposure for more accurate models of biological activity. In parallel, development of techniques for extrapolating dose of aerosol exposure to airway tissues allows researchers to create more accurate *in vitro* models of human airway exposure. A biomimetic exposure chamber with precise dosimetry might allow recreation of epithelial barrier and inflammatory response to toxicants and lung injury in a laboratory

environment, allowing researchers to study mechanisms related to various chemical inhalation related oral, nasal, and respiratory diseases and injuries.

Table 4 *A comparison of exposure techniques for biological studies of tobacco product aerosol in the literature.*

Emissions System	Transverse Flow	Air-Liquid Interface	3D Culture	Organ-on-a-chip	Citation
PES-2	○	○	○	○	[80]
Biomimetic Smoking Robot	●	●	○	●	[84]
InHALES	●	●	●	○	[1, 101]
Borgwaldt RM20S	○	◖	○	○	[76]
Borgwaldt LM4E	○	◖	○	○	[44]
Vitrocell VC 10	○	●	●	○	[157]
Vitrocell VC1	○	●	●	○	[158]

Objective 4.1 Propose standard measures for reporting dose delivered to biological samples during cytotoxicity testing

There has been a lack of consistency in reporting of methods and results in testing alternative tobacco products. The tobacco research field's transition from using CSC to aerosol exposure at an ALI for *in vitro* testing makes it difficult to compare results between historical studies [83] and makes cross product comparisons between combustible cigarettes and alternative tobacco products challenging. Without standardized reporting, repeatability, translation and evidence-based regulation implementation is hindered. Objective 4.1 gives recommendations for standard input and outcome measures for testing and reporting cytotoxicity of tobacco product aerosol based on literature of the field and results from Aim 3. The results of this objective are used in subsequent aims and objectives.

Objective 4.2 Quantify the response of a living cell culture of 3T3 fibroblasts in the BAES for one or more puffing profiles, using clean air, as function of system flow conditions

Limitations in current state of the art exposure systems are related to the lack of biomimicry, especially relating to fluid mechanics of aerosol exposed to cell cultures. In traditional cell exposure methods, aerosol is exposed with the free stream perpendicular to cell cultures [83, 167] (Figure 22, panel a-b). *In vivo,* air flows transverse to epithelial tissue causing

fluid shear on cells. Cell culture inserts, such as Transwell® inserts used in multiple well plates (Figure 22, panel c), contain dips and edges that may result in non-physiological mechanical cues [1]. Tissue engineering techniques can be applied to an exposure chamber to increase similarity to *in vivo* cell exposure. Innovation in culture substrates and techniques for mimicking *in vivo* mechanical cues can be applied to an exposure system for more realistic cell responses.

Two emissions systems described in the literature consider the effect of fluid shear on cell cultures with transverse flow exposure [1, 84] (Table 4). Fluid shear from transverse flow in the InHALES disrupted the integrity of the cell membrane. Figure 23, from Steiner 2020, shows stained EpiOral cultures after exposure to clean air, propylene glycol, and 3R4F reference cigarettes for two puffing regimes [168]. The paper reports that EpiOral cultures exposed to lab air under “shallow inhalation” showed altered morphology with disturbance to the cell membrane and decreased viability. Visual analysis of images presented in the paper shows disturbance to cell membranes are annotated in Figure 23. Three out of six of the conditions studied, including under both shallow and deep inhale, appear damaged. Refinement of culture techniques for exposure to transverse flow (Figure 22, panel d) at relevant local flow conditions are needed to improve the biomimicry of *in vitro* airway models. The BSR exposed samples to aerosol via transverse flow, but the organ-chip used is not representative of the entire airway.

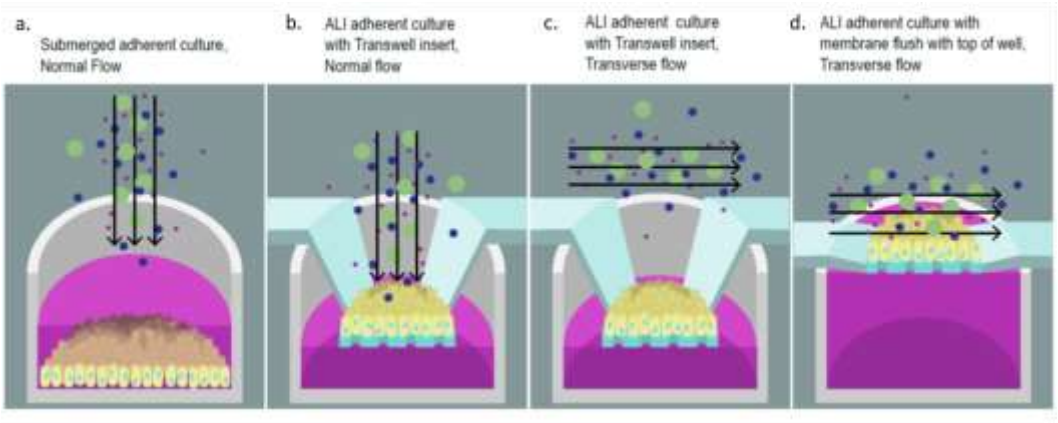

Figure 22 *The possible effect of free stream angle and culture surface height on aerosol concentration on the culture surface. Graphic by Tirzah Pilet for the Respiratory Technologies Lab.*

Objective 4.2 studies cytocompatibility of cells on custom scaffolds [169] an ALI without a culture insert and tests the effect of transverse flow of clean air at user informed system flow conditions on cell viability. Biological response of cell cultures placed in the modules described

in Aim 1 and exposed to the flow conditions described in Aim 2 is reported as a function of flow conditions, calculated from measurements made in Aim 3.

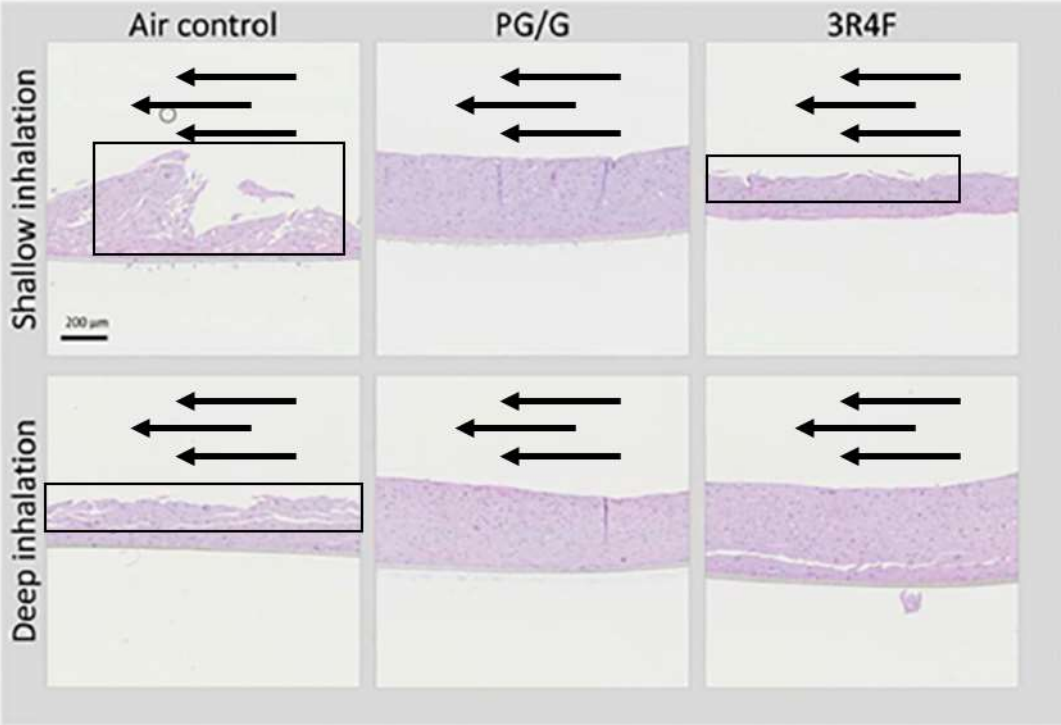

Figure 23 *An annotated figure from Steiner 2020, hematoxylin, eosin- and Alcian blue-stained EpiOral cultures after exposure to air, propylene glycol, and 3R4F cigarettes for two puffing regimes [1]. Arrows show expected flow direction based on histology. Boxed areas show damage to the cell membrane.*

Objective 4.3 Quantify the response of a living cell culture of 3T3 fibroblasts in the BAES to one or more ENDS as function of system flow conditions

Objective 4.3 uses the same setup as Objective 4.2 to test the effect of transverse flow of ENDS aerosol at user informed system flow conditions on cell viability. Biological response of cell cultures placed in the modules described in Aim 1 and exposed to the flow conditions described in Aim 2 is reported as a function of flow conditions and dose of aerosol, calculated from measurements made in Aim 3.

Objective 4.4 Report inferential statistics of the outcome measure(s) with appropriate error bars as a function of condition (no load, clean air, toxicant puff) for a given location

For one or more locations in the system cell viability from the Clean air condition, ENDS aerosol condition, and incubator control are tested for statistical significance.

Aim 5: Report inferential statistics for the effect of input parameters and system response

Results that quantify cytotoxicity [26-30, 112, 113], genotoxicity [83, 114], inflammatory response [32, 33, 115] and oxidative stress [32, 34, 113, 115, 116] are not representative of the entire airway. Biomimicry of the emissions system and cell cultures throughout the flow path may provide more realistic doses for a given tissue type and culture location. To study the effect of emissions system parameters, statistical comparisons from results from Aim 4, can provide insight on which input parameters (Aim 1-3) have an effect on cell viability and dose.

Given the high throughput nature of the Biomimetic Aerosol Exposure System (BAES), multiple datasets, with replicates for each, are produced for a single condition. Inferential statistics reports which system attributes (location, system flow conditions) have a significant effect on dose delivered and cell viability and should be considered in emissions exposure of biological samples.

CHAPTER 5. APPROACH

Aim 1: Demonstrate a geometrically bio-inspired aerosol exposure system

ENDS Adapter Design and Fabrication

Mass loss between e-cigarette and biological exposure or emissions capture is a significant barrier in quantification of biological response and emissions. The adapter used to connect the device under test (DUT) to the emission system may induce deposition within the flow path or the system before the aerosol ever arrives at the exposure chamber or the capture system, potentially under-reporting fundamental emissions outcomes. An approach to design of an adapter specific to a device under test is presented here. The design objectives for the adapter were to minimize abrupt changes in cross sectional area of the flow path and reduce the cumulative flow path volume between the exit plane of the DUT and emissions system entrance. The flow outlet of a JUUL e-cigarette (JUUL Labs, Washington D.C., USA) is approximately elliptical in shape, while the compression fitting used at the inlet to the filter pad holder has a circular cross section. The transition in flow path diameter between the tobacco product exit and emissions system inlet was designed to minimize mass loss. A sigmoid function was used to identify the radii of coincident ellipses, whose tangent functions exhibit C^1 continuity. The spline connects the outlet of the e-cigarette to the inlet of a coupling on the filter pad holder. The radii are calculated as:

$$f = \frac{1}{1+e^{-z}} \quad (1)$$

where

$$z = G\pi\left(\frac{x-0.5}{L}\right) \quad (2)$$

G=x/L

L= transition path distance

x=plane distance

Points for line segments of horizontal and vertical ellipse radii were calculated by:

$$P_x = x_0(1-f) + f x_L \quad (3)$$

In Fusion 390 (Autodesk, San Rafael, CA) computer aided design (CAD) software, planes were created at x_0 and x_L and segmented with planes every 10% of L. Ellipses with radii P_y and P_x, as calculated above, are placed on each plane. Figure 24 shows an annotated sketch of the major axis of ellipses that make up the flow path transition of the streamlined adapter for a JUUL e-cigarette. Using these profiles, a cut was lofted through a solid block to create a continuous flow path. Receivers for a JUUL e-cigarette mouthpiece and a mechanical coupling (MSC Industrial Direct, Melville, NY) were modeled at the entrance and exit of the flow path producing a digital model of a custom ENDS adapter. From this, a mold was digitally modeled by subtracting the digital part from a solid block to create the mold's core. A hallow box was modeled around the core to create the walls of the mold. The core was scaled to 0.85 in the x and y directions so that the final part applies squeeze to the inserted components. Molds were fabricated in aluminum by the Mechanical Engineering Department Machine Shop at Rochester Institute of Technology (Rochester, NY). Two-part 20A *Let's Resin* silicone rubber (Shenzhen E4ulife Technology Co., Ltd) was mixed following manufacturer instructions and poured into the mold. The part was cured at room temperature for at least 24 hours and removed from the mold. After fabrication, the part was evaluated for an airtight seal.

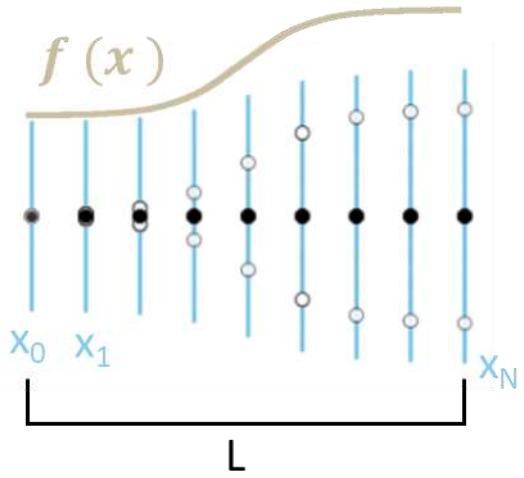

Figure 24 *An annotated sketch of the major axis of ellipses that define the flow path transition of the streamlined adapter for a JUUL electronic cigarette.*

ENDS Adapter Leak Test

The ENDS adapter was leak tested to ensure an airtight seal under negative pressure. The ENDS adapter was placed onto PES-2 with its outlet connected to a filter pad holder. In

place of an e-cigarette at the inlet, a “mock JUUL”, an aluminum bar machined to the same dimensions of a JUUL device, was used to obstruct the flow path. The mock JUUL was inserted into the adapter and the entire assembly was supported to avoid cantilevering between the ENDS adapter and the mock JUUL. A puff profile consisting of 5 second puffs at 50 mL/sec was used to test for leaks. Measurements taken by the system flow meter were visually monitored in real time on the PES software’s graphical user interface. A flow rate of 0 mL/s at steady state with the system inlet is fully obstructed indicates that the system is airtight.

Oral Cavity Module Design and Fabrication

A previously described [91] digital model of the human airway from the mouth to the sixth lung generation was used as a starting point for the Oral Cavity Module (OCM). Using Fusion360 CAD software the model was modified to create the biomimetic OCM. First, the airway model was segmented to include the lips to the larynx. A mechanical connector compatible with the outlet of the ENDS adapter described above was modeled onto the “lips” of the model. The mechanical connector was rotated 30 degrees from horizontal to reflect the angle that a user might hold an e-cigarette in their mouth. An inter-module sampling insert was designed to be placed in the wall of the OCM. A flow channel connecting the oral cavity to a second system inlet was added to enable additional pumps to be connected to the model. A third system inlet, mimicking the inlet from the nasopharynx to the oropharynx was added approximately at the soft palate. The flow path of the OCM is illustrated in Figure 25. Key anatomical dimensions of the OCM including volume (V), surface area (SA), and length of the OCM (L_{OCM}) are: V= 49.62 cm^3, SA= 152.98 cm^2, and L_{OCM}= 13.20 cm. The green line on the Section View of Figure 25 shows the center line, L_{OCM}, used to denote the nominal OCM length.

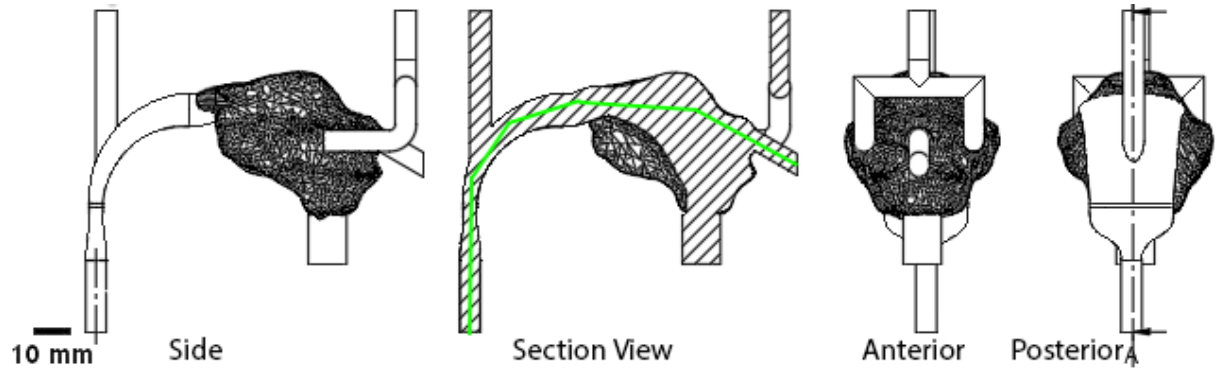

Figure 25 *A schematic of the fluid space of the Oral Cavity Module.*

OCM geometry and inserts were exported as a mesh. The OCM was fabricated in stereolithography by Trimech (Glen Allen, VA) in Somos® 11122XC with an engineering clear finish. OCM Inserts were prepared for printing in PreForm (Formlabs, Sommerville, MA) software and were printed in BioMed Amber Resin (Formlabs, Somerville, MA) on a Formlabs 3 SLA printer. Post-processing steps, including removal of support material and sanding, were performed. A positioning jig designed to hold an e-cigarette at the inlet of OCM to prevent cantilevering of the pod and disruption to the electrical connection between pod and device was 3D printed in Polylactic acid (PLA) (MatterHackers, Lake Forest, California) on an Ultimaker S5 (Utrecht, Netherlands) and mounted to the OCM. An ENDS adapter was connected to the inlet of the OCM.

Oral Cavity Module Usability Testing

An assembly procedure for the OCM was developed and tested by giving all necessary parts and a written procedure to a lab technician. The technician performed the procedure while compliance and/or difficulties were documented with notes and photography. After following the procedure, the technician graded the clarity and detail or the procedure using a Likert Scale. A score of three or better means the procedure was deemed sufficient, while a score below three required a revision to the procedure to address the shortcoming identified.

Bifurcated Exposure Chamber Design and Fabrication

A Bifurcated Exposure Chamber (BEC) designed to create a transvers flow path over a standard multiple well plate and be integrated into the system downstream from the OCM was designed and fabricated. BEC was modeled in Fusion 360 using an iterative process that included prototyping and computational modeling of each iteration. A rendering of the BEC assembly in an exploded view is given in Figure 26. A physical BEC assembly includes stainless steel tubing, an aluminum BEC enclosure, an aluminum BEC lid with a rubber gasket, a multiple well plate, 12 custom BEC Inserts, and a silicone rubber BEC bifurcated flow path part.

A BEC enclosure and lid were milled from aluminum. The lid includes a gasket, which was cut to the size of the lid from 1/16” thick silicone sheet of hardness 60D. Undersized holes were drilled for inlet and outlets to the chamber and 50.8 mm long steel tubing was permanently attached to the chamber using a compression fit. A thin coating of Hylomar Universal Blue Sealant (Hylomar LLC, Center Point, Texas, USA) was applied to the end of the tubing before it was cooled with dry ice for 30 min. The aluminum chamber was heated to approximately 125°C

for 30 min in an oven. The chamber was removed from the oven, the tubing was removed from the dry ice, and the sealant coated end of the tubing was driven into the holes of the chamber. Upon returning to room temperature, a secure attachment and seal were achieved.

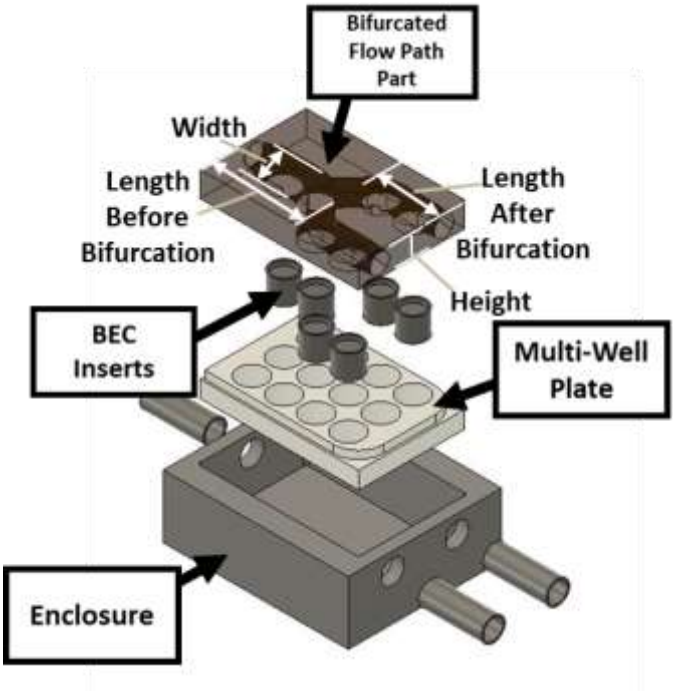

Figure 26 *An exploded view of a Bifurcated Exposure Chamber (BEC) assembly that includes the BEC enclosure, a multiple well plate, BEC Inserts and a bifurcated flow path part. A lid (not pictured) is placed over the flow path part to make the assembly airtight.*

A bifurcated flow path part is intended to lay on top of the multi-well plate and guide the aerosol flow tangentially across the cell culture exposure surfaces within the BEC using physiologically relevant geometry and flow conditions. Geometric relevance was implemented using an idealized model of a symmetric lung with branching angles identical to Lizal 2012's adaption of the original Weibel lung [92] and with hydraulic diameters ±0.2 cm of the original Weibel lung model [87]. Bifurcated flow path channels with rectangular cross sections were modeled in CAD software such that the flow path of each generation was aligned along the centerline of wells in a traditional multi-well plate. The flow path was 3D printed in PLA on Prusa i3 MK3S+ (Czech Republic) 3D printer and used as a casting mold. For mass balance experiments, two-part 20A Let's Resin silicone rubber was mixed following manufacturer instructions and poured into the casting mold and cured for at least 24 hours. When the silicone rubber was removed from the mold, the impression of the rectangular cross section flow path

were revealed as open channels in the bifurcated flow path part. For biological exposures, a bifurcated flow path part was made from polydimethylsiloxane (PDMS), which is well documented to be biocompatible and inert to ethanol and ultraviolet sterilization methods [170]. DOW SYLGARD™ 184 SILICONE ENCAPSULANT CLEAR (Ellsworth Adhesives, Germantown, WI) was mixed according to manufacturer instructions and cast as described above. The bifurcated flow path part was used in lieu of a standard multi-well plate cover during exposure.

BEC Inserts were developed to measure mass deposition or to culture cells in each well of the multi-well plate, which would be exposed to the open channels beneath the bifurcated flow path part. BEC Inserts for mass balance studies were 3D printed on a Formlabs 2 printer in clear resin. Inserts used for cell culture were machined from 7/8” 316 Stainless steel rod on a lathe in the Brinkman Lab at Rochester Institute of Technology (RIT) (Rochester, NY). BEC was assembled by placing BEC Inserts into six wells of a 12-well plate, the 12-well plate into the chamber with the bifurcated flow path part on top of the plate, and tightening the BEC lid on the chamber using thumb screws. The part was assembled into BAES and assessed for an airtight seal. BAES is modular, components can be attached in a variety of configurations with analytical instruments inserted into the flow path at several locations.

Aim 2: Demonstrate a human behavior-inspired aerosol delivery and distribution system.

Comprehensive System Architecture for a Biomimetic Aerosol Exposure System

A schematic of comprehensive BAES architecture is given in Figure 27. State numbers are shown inside of circles and given throughout the system to identify key system locations. Room air enters the system at primary inlet, State 0, or secondary inlet, State 200. “ENDS” is the DUT and aerosol generator. States 200-290 are the Nasal Cavity Subsystem. A ‘T’ shaped pipe extends upward from the oropharynx flow path with one side of the pipe an inlet for ambient air (State 200) through a solenoid valve (S2). The other arm of the ‘T’ (State 260) is in fluid communication with the vacuum system. A solenoid valve at the primary system inlet (S4) is used to prevent activation of an ENDS during a clean air puff. Modules and measurement instruments between State 2 and 490 can be added, removed, and interchanged. The number of BECs, which are individually labeled with Greek letters, can be reduced or expanded. The vacuum system has its own closed loop flow path that takes in room air and exhausts to a building exhaust handling system.

Demonstrate Human Puffing Behavior

The existing PES-2 control software can perform discrete puffs with programmable human topography parameters. The existing software supports homogeneous (repeated identical puffs) and heterogeneous (observed user puff topography playback) profiles. Integration of modules described in Aim 1 and the addition of new subsystems require additional functions in the control code. Table 5 describes the process logic required to implement discrete puffing with an updated BAES. Flowrate, puff duration, and post-puff gap are programmed for a specific Emissions Topography Profile (ETP).

Demonstrate Human Puffing and Inhalation Behavior

ETPs that include both discrete puffs and clean air inhales through the Nasal Cavity Subsystem use the same control logic as discrete puffing with additional processes for clean air inhales. Inhalation is achieved by opening valves that allows room air to flow into the secondary system inlet (State 200), while closing a valve at the primary system inlet (State 0) to prevent flow through the ENDS, which would actuate the device. Not every inhale cycle includes a puff, but every puff is followed by an inhale. Table 6 describes processes for ETPs that include discrete puffing and clean air inhalation. Puff flowrate and duration, post-puffing interval, inhale flow rate and duration, and post-cycle interval are programmed by an operator for each ETP.

Control Code Logic for Puffing, Inhalation, Breath Hold, and Exhalation

Discrete puffing, clean air inhalation, breath hold, and exhalation ETPs require coordination of all subsystems shown in Figure 27. Exhales require a second flow path to the vacuum subsystem and coordination between valves. Table 7 describes processes for ETPs that include exhales. Puff flowrate and puff duration, post-puff interval, inhale flowrate and duration, post-inhale breath hold, exhale flowrate and duration, and inter-cycle interval are programmed by an operator for each ETP. A cycle is defined by a discrete puff, followed by an inhale, followed by an exhale, based on preliminary respiration topography data [105]. Not every inhale cycle includes a puff, but every puff is followed by an inhale.

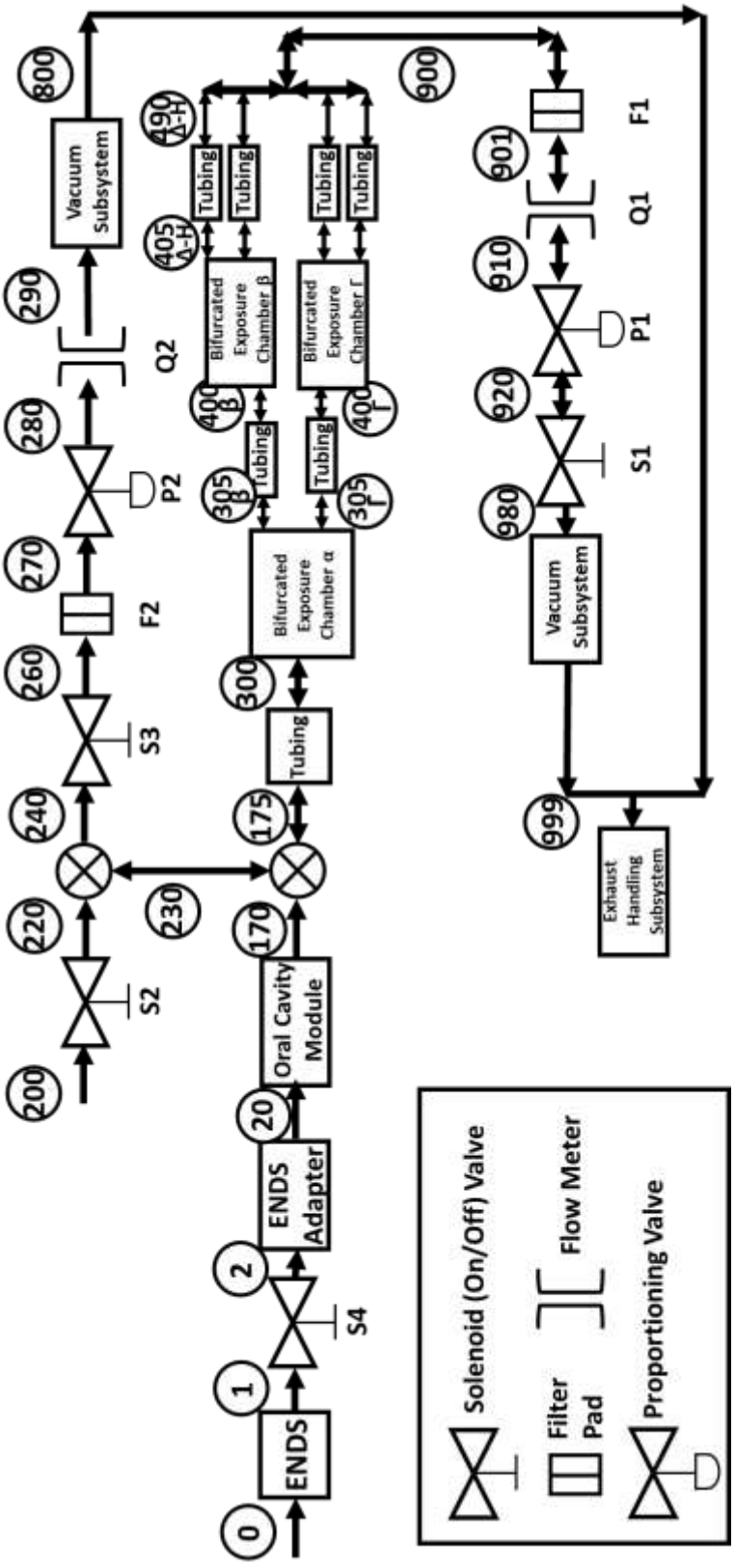

Figure 27 *A schematic of Biomimetic Aerosol Emissions System. State numbers are identified inside of circles, labels not enclosed in circles reflect component names.*

Table 5 *Process logic for an Emissions Topography Profile with discrete puffs. Values for flowrate, puff duration, and post-puff gap are programmed by system operator.*

System Flow Condition	Process Description	S1	S2	S3	S4	Q1	Q2	P1	P2
Discrete Puff	Prior to Puff	Open	Close	Close	Open	-	-	-	-
	During Puff	Open	Close	Closed	Open	Measure at 901, signal to controller	-	Modulate, signal from controller	-
	End Puff	Close	Close	Close	Close	-	-	-	-
	Post-Puff Interval	Close	Close	Close	Close	-	-	-	-
	Count Puffs	Close	Close	Close	Close	-	-	-	-

Table 6 *Process logic for an Emissions Topography Profile with discrete puffs followed by inhales. Values for puff flowrate, puff duration, post-puff gap, inhale flowrate, and inhale duration are programmed by system operator.*

System Flow Condition	Process Description	S1	S2	S3	S4	Q1	Q2	P1	P2
Discrete Puff	Prior to Puff	Open	Close	Close	Open	-	-	-	-
	During Puff	Open	Close	Closed	Open	Measure at 901, signal to controller	-	Modulate, signal from controller	-
	End Puff	Close	Close	Close	Close	-	-	-	-
	Post-Puff Interval	Close	Close	Close	Close	-	-	-	-
Nasal Inhale	Prior to Inhale	Open	Open	Close	Close	-	-	-	-
	During Inhale	Open	Open	Close	Close	Measure at 901, signal to controller	-	Modulate, signal from controller	-
	End Inhale	Close	Close	Close	Close	-	-	-	-
	Post-Inhale Breath Hold	Close	Close	Close	Close	-	-	-	-
	Count Cycles	Close	Close	Close	Close	-	-	-	-

Table 7 *Process logic for an Emissions Topography Profile with discrete puffs followed by inhales and exhales. Values for puff flowrate, puff duration, post-puff gap, inhale flowrate, inhale duration, breath hold, exhale flowrate, exhale duration, and inter-cycle gap are programmed by system operator.*

System Flow Condition	Process Description	S1	S2	S3	S4	Q1	Q2	P1	P2
Discrete Puff	Prior to Puff	Open	Close	Close	Open	-	-	-	-
	During Puff	Open	Close	Closed	Open	Measure at 901, signal to controller	-	Modulate, signal from controller	-
	End Puff	Close	Close	Close	Close	-	-	-	-
	Post-Puff Interval	Close	Close	Close	Close	-	-	-	-
Nasal Inhale	Prior to Inhale	Open	Open	Close	Close	-	-	-	-
	During Inhale	Open	Open	Close	Close	Measure at 901, signal to controller	-	Modulate, signal from controller	-
	End Inhale	Close	Close	Close	Close	-	-	-	-
	Post-Inhale Breath Hold	Close	Close	Close	Close	-	-	-	-
Exhale	Prior to Exhale	Close	Close	Open	Close	-	-	-	-
	During Exhale	Close	Close	Open	Close	-	Measure at 280, signal to controller	-	Modulate, signal from controller
	End Exhale	Close	Close	Close	Close	-	-	-	-
	Post-Exhale Breath Hold	Close	Close	Close	Close	-	-	-	-
	Count PAR Cycles	Close	Close	Close	Close	-	-	-	-
	Count Sedentary Cycles	Close	Close	Close	Close	-	-	-	-
	Count Active Cycles	Close	Close	Close	Close	-	-	-	-

Computational Model of Wall Shear Stress

Wall shear stress (WSS), an important parameter to model in biological testing, is not easy to measure within any *in vitro* system. Therefore, we modeled WSS with a first principles linear programming (LP) model to establish a design target for inlet flow conditions which simultaneously perform within limits of a device under test and mechanical requirements related to physiological relevance for a given system geometry. The program mathematically models the branching airway using arcs and nodes, where each node is a bifurcation and each arc is a branch within a lung generation. A model that assumes conservation of mass, an

incompressible fluid, an idealized symmetric lung, and air as the fluid was formulated. The empirical equation used for WSS [171] in a rectilinear channel was:

$$\tau = \frac{\mu 6Q}{wh^2} \quad (4)$$

where τ is WSS, μ is dynamics viscosity of air (μ_{air} =1.79 x 10^{-5} Pa s), Q [m^3/s] is volumetric flow rate, the variable being optimized (the objective function), w is width of the channel, and h is the height of the channel. Channel dimensions the BEC bifurcated flow path part in the final iteration of the LP model are given in Table 8.

Table 8 *Dimensions of flow channels by lung generation in a biomimetic aerosol exposure system.*

Generation	**Number of Channels**	**Minimum Target Wall Shear Stress (f_{min})**	**Maximum Wall Target Shear Stress (f_{max})**	**Given Channel Width (w)**	**Given Channel Height (h)**
[-]	[-]	[Pa]	[Pa]	[m]	[m]
1	1	0.0025	0.02	0.0166	0.0166
2	2	0.02	0.03	0.0150	0.0100
3	4	0.03	0.05	0.0081	0.0075
4	8	0.03	0.05	0.0075	0.0050

The flow rates at which e-cigarettes are puffed are small in comparison to the deep inhale users typically take following a puff or flow rates associated with tidal breathing. Tidal breathing flow rates are too high for most e-cigarettes, excluding high powered box-mod devices. In BAES, puffing is intended to generate aerosol from the e-cigarette under realistic device usage conditions and the subsequent clean air inhalation taken is intended to maintain a physiological environment (shear stress) in the system. Therefore, inhalation flow rate was maximized, subject to constraints on Reynolds number and WSS.

Global parameters are constraints that apply to all arcs in the linear system and therefore all flow paths in the physical lung model for a given breathing type. Global parameters are given in Table 9. Prior work from Mahto 2014 showed that cells remained viable after exposure to 2 Pa of shear stress for 20 minutes [172]. This result informs $fmax_{puff}$, the maximum WSS permitted at any point in the system. Meanwhile, $fmin_{puff}$ is 0 Pa because during puffing, the intention is to achieve aerosol exposure informed by user puffing behavior, not mechanical

cues. Puff flow rate was allowed to vary between 17 mL/s and 65 mL/s ($qmin_{puff}$ *and* $qmax_{puff}$) representing the operating range of a JUUL e-cigarette [173]. Inhalation flow rate constraints, $qmin_{inhale}$ *and* $qmax_{inhale}$, were determined based on prior computational work [97]. Inputs for minimum and maximum WSS for inhalation in generations 1-4 were based on computational fluid dynamics models and are given in Table 8 [91, 174]. The empirical equation used for WSS is only valid when flow is laminar, therefore, Reynolds Number was constrained below 2100, *ReMax,* the value where flow begins to transition from laminar to turbulent. The model was programmed into AMPL (Bell Labs, Holmdel, NJ, USA) and was run using the Gurobi Optimization solver. The LP provided a design target of ~510 mL/s for clean air inhalation to maintain a physiological environment between puffs for the e-cigarette. The corresponding WSS for generations 1-4 in a lung model with the dimensions given in Table 8 are given in Figure 28.

Table 9 *Global parameters for a first principles model of optimal inlet flow rate.*

Parameter	Value	Unit	Citation
$fmin_{puff}$	0	[Pa]	
$fmax_{puff}$	2	[Pa]	[172]
$qmin_{puff}$	1.7 x 10^{-5}	[m3/s]	[85]
$qmax_{puff}$	6.5 x 10^{-5}	[m3/s]	[85]
$qmin_{inhale}$	2.5 x 10^{-4}	[m3/s]	[97]
$qmax_{inhale}$	0.001	[m3/s]	[97]
rho	1.23	$[\frac{kg}{m^3}]$	
μ	1.79 x 10^{-5}	$[Pa * s]$	
ReMax	2100	[-]	

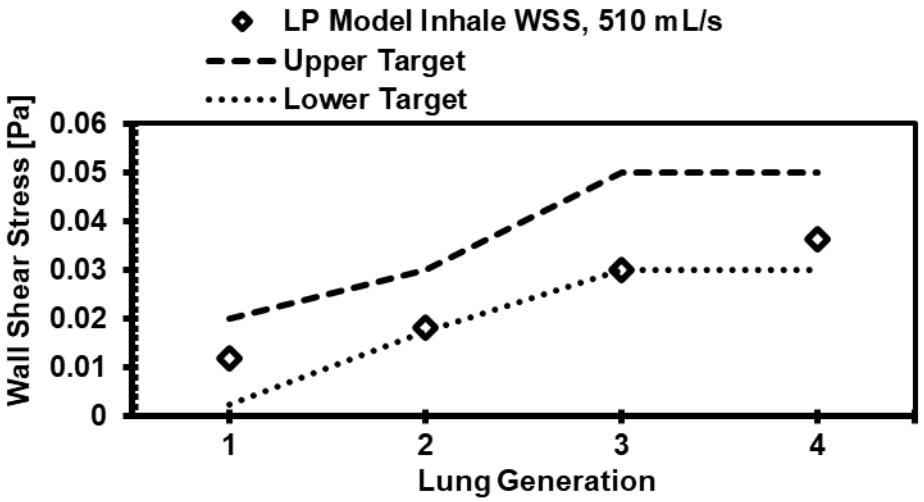

Figure 28 *Wall shear stress (WSS) at an optimized flow rate, 510 mL/s, which fulfills all constraints of the linear programming (LP) model of optimal inlet flow rate subject to constraints on WSS, Reynolds Number, and flowrate limits for a given lung model geometry.*

Simplified System Architecture for a Biomimetic Aerosol Exposure System Feasibility Assessment

Adapt the PES-2 as Biomimetic Aerosol Exposure System (BAES)

The Respiratory Technologies Lab has developed and validated [80] programmable emissions systems PES-0, PES-1, and PES-2 in accordance with good laboratory practices ISO IEC 17025 and exceeding those of ISO 3308:2012 routine analytical cigarette smoking machine. PES-2 was adapted by designing a manifold with an outlet that connects to the inlet to vacuum on PES-2. The manifold replaced the single inlet to vacuum with five inlets that can be blocked when not in use or connected to exposure modules and other subsystems. The manifold was milled from stainless steel by RIT's Mechanical Engineering Machine Shop (Rochester, NY) and mechanical couplings (MSC Industrial Direct, Melville, NY) were screwed into four the inlets. Filter pad holders were outfitted with male couplings on both sides. Brackets and shelving designed to hold custom exposure modules described in Aim 1 were built and placed inside of the emissions system. The configuration shown in Figure 29, which consists of ENDS, ENDS adapter, Oral Cavity Module, Bifurcated Exposure System, and filter pads at each of BEC's two outlets will be referred to as Full Assembly in following sections. Figure 29 illustrates the implemented BAES for which subsequent results will be reported, while Figure 27 provides a design roadmap for technology development beyond the implementation scope of this work.

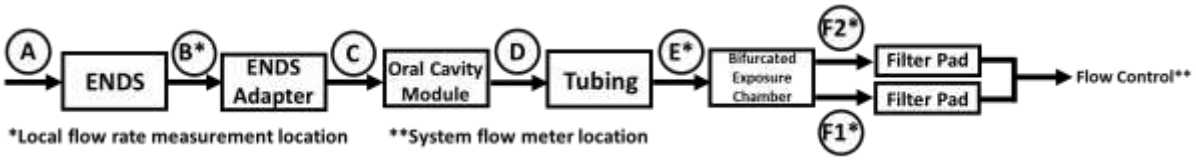

Figure 29 *A schematic showing Full Assembly a Biomimetic Aerosol Exposure System including ENDS, ENDS adapter, Oral Cavity Module, Bifurcated Exposure System, and filter pads.*

Oral Clean Air Inhalation Subsystem Design

To more accurately mimic actual user behavior, an inhalation subsystem was developed that inserts an e-cigarette into the ENDS adapter for an airtight connection to the OCM during puffing and retracts the e-cigarette at the conclusion of a puff for clean air inhalation through the same system inlet. An L12-R Micro Linear Servo (Actuonix Motion Devices, British Columbia, Canada) was mounted co-axially aligned with the OCM inlet. A connector that holds an e-cigarette onto the arm of the actuator was designed in Fusion360 software was 3D printed on an Ultimaker S5 in Semper-Flexx98 (Keene Village Plastics, Cleveland, Ohio). Petroleum jelly (Vaseline, Unilever, Englewood Cliffs, NJ) was periodically spread onto the inside surface of the ENDS adapter (about every 50 puffs) to reduce resistance from friction between the ENDS and ENDS adapter, ensuring that the e-cigarette moves in and out of the adapter with every puff. Five ETPs were developed based on clinically relevant puff and inhalation volumes of JUUL e-cigarette users and are given in Table 10 [175].

Table 10 *Emissions topography profiles based on clinically relevant puff, puff associated respiration (PAR), and tidal breathing volumes [175]. Profiles that include clean air inhalation are named with their PAR flow rates.*

		List of Topography Profiles		Puff Only	Puff Only	PAR150	PAR250	PAR350	PAR450
System Start-Up Protocol	Pre-Cleansing Breath	Flow Rate	[mL/s]	10	10	100	100	100	100
		Duration	[s]	10	10	4	4	4	4
		Volume	[mL]	100	100	400	400	400	400
		Gap	[s]	10	10	20	20	20	20
		Repetitions	[-]	2	2	1	1	1	1
Puff and Respiration Cycle (PRC)	Puff	Flow Rate	[mL/s]	25	25	25	25	25	25
		Duration	[s]	3.5	3.5	3.5	3.5	3.5	3.5
		Volume	[mL]	87.5	87.5	87.5	87.5	87.5	87.5
		Post-Puff Gap	[s]	10	10	1	1	1	1
		Number of Puffs Per PRC	[-]	1	1	1	1	1	1
	Puff Associated Respiration (PAR)	Inhale Flow Rate	[mL/s]	0	0	150	250	350	450
		Inhale Duration	[s]	0	0	10	6	4.29	3.33
		Inhale Hold/Post-PAR Gap	[s]	0	0	2	2	2	2
		Volume	[mL]	0	0	1500	1500	1501.5	1498.5
		Exhale Flow Rate	[mL/s]	0	0	0	0	0	0
		Exhale Duration	[s]	0	0	0	0	0	0
		Exhale Hold	[s]	0	0	0	0	0	0
		Number of PARs Per PRC	[-]	0	0	1	1	1	1
	Tidal Breathing	Flow Rate	[mL/s]	0	0	150	250	350	350
		Inhale Duration	[s]	0	0	3.33	2	1.43	3.33
		Inhale Hold/Post-Tidal Gap	[s]	0	0	2	2	2	2
		Volume	[mL]	0	0	499.5	500	500.5	1165.5
		Exhale Flow Rate	[mL/s]	0	0	0	0	0	0
		Exhale Duration	[s]	0	0	0	0	0	0
		Exhale Hold	[s]	0	0	0	0	0	0
		Number of Tidal Breaths	[-]	0	0	5	5	5	5
		Inter-PRC Gap	[s]	0	0	3	3	3	3
		Number of PRCs	[-]	50	25	25	25	25	25
System Shut-Down Protocol	Post-Cleansing Breath	Flow Rate	[mL/s]	10	10	0	0	0	0
		Duration	[s]	10	10	0	0	0	0
		Volume	[mL]	100	100	0	0	0	0

Aim 3: Quantify the dose and flow conditions throughout the exposure system

Sample preparation

Lab made e-liquid was used to eliminate batch variation between commercial e-liquid products. 50:50 Propylene Glycol (PG): Glycerin (GL) (HiLIQ, Wan Chai, Hong Kong) by mass was mixed. Brilliant Blue FCF (Millpore Sigma, Darmstadt, Germany) was added to the solution

for mass characterization trials that include BEC in the BAES flow path. 5% nicotine (non-protonated, N3876 Sigma-Aldrich) by mass was added to the solution for cell exposure trials (0.475:0.475:0.05 PG:GL:Nic). E-liquid was kept at 4°C until use. BLANKZ! refillable pods (https://blankzpods.com/) with a JUUL (JUULLabs, Washington DC) e-cigarette were used for system characterization. For each trial, a pod was selected from inventory and given an identification number. A fully charged JUUL e-cigarette was removed from the charger and allowed to come to room temperature. The BLANKZ! pod was filled with e-liquid using a disposable pipette. After being filled, a pod was left for at least 15 minutes to ensure e-liquid had soaked the wick and to allow the e-liquid to reach room temperature. Pods were refilled every other trial (50 puffs) and were replaced after being used for 100 puffs (4 trials). If the coil became exposed to air during a trial or if the pod exhibited any evidence of burning, the pod was replaced and set aside for later inspection. To compare ENDS performance with third-party pods to intended pod for a JUUL power control unit (PCU), JUUL brand pods prefilled with 5% tobacco flavored nicotine, purchased at smoke shops and gas stations in the Rochester, NY area were used. A Mettler Toledo Model Number AE240-1 S/N J65956 analytical balance, with manufacturer reported readability of 0.1 mg, approximate accuracy of 0.4 mg, and range of 200 grams with a linearity of ±0.02 mg was mounted on a heavy work bench to minimize vibration effects. The “Before” mass of each pod and Cambridge filter pad (Performance Systematix Inc, Grand Rapids, MI) were measured using the analytical mass balance. A fully charged JUUL PCU was equilibrated with room temperature and the pod was assembled onto it.

Flow Rate Characterization

Flow rate characterization of BAES was conducted by measuring local volumetric flow rate at four locations in the system on the BAES Full Assembly, annotated in Figure 29, where asterisks denote flow rate measurement locations. An uncharged JUUL e-cigarette and empty BLANKZ! (blankzpods.com) pod were used to retain the flow resistance of placing a product in the system while measuring flow rate to illustrate the transient system response. System flow rate was measured downstream from the filter pads with a system flow meter (Alicat Scientific), a calibrated orifice plate, re-certified by a third-party vendor annually. We used internally manufactured orifice plates [41] calibrated against the system flow meter to measure local flow rate throughout the system. Initial flow rate characterization was conducted between the e-cigarette and the ENDS adapter (Figure 29, location B). The command flow rate was systematically varied from 25-50 mL/s in increments of 5 mL/s while varying system flow duration from 3.5-4.5 s in increments of 0.25 s. To further characterize repeatability at a

clinically relevant flow rate [175] the “Puff Only 50” profile, given in Table 10, was used to measure repeatability of puff flow rate at locations B, E, F1 and F2 shown on the schematic in Figure 29. Measurements at the BEC outlet (location F1 and F2) were measured simultaneously with a flow meter at each BEC outlet to maintain a symmetric flow path. For inhalation characterization, flow rates produced by PAR450 (given in Table 10) were measured at locations E, F1 and F2. Inhalation flow rate was not measured at location B because the geometry of the local flow meter is incompatible with the inhalation subsystem.

ENDS Adapter Mass Balance

To compare mass deposition in the connection between ENDS and system inlet, a representative traditional emissions set up that uses tubing to connect the ENDS to the system was compared to the ENDS adapter. Either an ENDS adapter or flexible tubing was connected to the ENDS by inserting the mouthpiece of the product into the ENDS adapter until hitting an internal wall or inserted into the tubing without covering air inlets on the pod. The exhaust of the adapter was connected to the inlet of a filter pad holder, which was connected to the emissions system. For trials using flexible tubing, a smaller diameter tube was inserted into a larger diameter tube to account for the change in outer diameter between the e-cigarette and the filter pad holder. The interface, which was 5 cm in length, was sealed with laboratory film (Parafilm™, Fisher Scientific, Pittsburgh, PA). BAES was programmed with “Puff Only” topography parameters, given in Table 10. After completion of puffing, the e-cigarette and filter pad were removed from the emissions system. The “After” mass of each pod and filter pad were measured and recorded. Between trials, the outside of the pod and the PCU were cleaned by wiping any e-liquid droplets with a paper towel.

BAES Mass Balance

Distribution of mass in BAES was studied using two BAES configurations. In the “Adapter + OCM” configuration, the path between the e-cigarette outlet and the filter pad included an ENDS adapter, the OCM, and inlet geometry of the filter pad holder upstream from the pad. The filter pad holder was connected to the exhaust of OCM, which falls in the laryngeal region. In the “Full Assembly” condition, 28.4 cm of polyethylene tubing was placed at the outlet of the OCM to connect it to a BEC with an internal flow path models the first lung bifurcation. In this condition, filer pads were connected at each of the two BEC outlets. In both configurations filter pad holders were connected to the flow control subsystem.

BEC Inserts were prepared for mass measurement by filling the custom inserts with deionized (DI) water before a trial and placing the inserts in wells of a 12-well plate. The OCM Insert was placed into the OCM receiver. BAES was programmed with Puff Only, PAR150, PAR250, PAR350, or PAR450, given in Table 10. After completion of a puffing protocol, the e-cigarette and filter pad were removed from the emissions system. “After” mass of each pod and filter pad were measured and recorded. Between trials, the outside of the pod and the PCU were cleaned by wiping any e-liquid droplets with a paper towel. Samples from BEC and the OCM Insert were taken after two runs of a puffing protocol. The aerosol exposed DI water in each insert was transferred to its own well in a 96-well plate. DI water was used to rinse the OCM and the tubing connecting the OCM to BEC and a sample of the water was added to the plate to quantify the mass concentration of aerosol deposited in the OCM and the tubing. A VersaMax microplate reader connected to SoftMax® Pro 6 software was used to measure absorbance in the samples from BAES. Absorbance data was processed into mass concentrations in Matlab.

Aim 4: Validate the acute bio-response of living cells in the aerosol generation, delivery and exposure systems

Tunable Scaffolds to Control Fluid Shear

Scaffolds with tunable height to place a cell monolayer in the flow path of BEC by placing scaffolds in steel BEC inserts were developed. Scaffold height can be tuned by varying the volume of reagents used to fabricate the scaffold. 7% alginate solution (m/v) was made by mixing Sodium alginate (W201502, Sigma-Aldrich) in DI water at 40°C until alginate was fully dissolved. 120 mM Calcium Chloride ($CaCl_2$) solution was made by mixing $CaCl_2$ dihydrate (C79-500, Fisher Chemical) with DI water until dissolved. Each solution was sterilized via autoclave and stored in sterile conditions at 4°C until use. To fabricate scaffolds, alginate was brought to room temperature. Using sterile technique, 10 mL of alginate was added to a 55 mm petri dish. $CaCl_2$ was added to a beaker. Using forceps, the petri dish full of alginate was carefully lowered into the $CaCl_2$ bath and placed in 4°C for 1 hour. The petri dish of alginate was removed from the bath and using a cork bore punch, scaffolds were punched from the alginate. Each scaffold was transferred to a 12-well plate using sterile forceps and rinsed phosphate buffered saline (PBS). Scaffolds were coated with 0.01 mg/mL fibronectin solution by incubating scaffolds with fibronectin for 30 minutes, then aspirating excess solution. Culture media was added to wells with scaffolds and incubated in 37°C 5% CO_2 overnight. Prior to cell seeding,

scaffolds were placed in sterilized 316 stainless steel BEC Inserts, described in Section 5.1, Bifurcated Exposure Chamber Design and Fabrication. The culture system is shown in the schematic in Figure 30. Scaffold dimensions were analyzed using photos of scaffolds taken with an Apple iPhone 11 (Apple Inc., Cupertino, California) and processed in ImageJ2 (https://imagej.net/software/imagej2/).

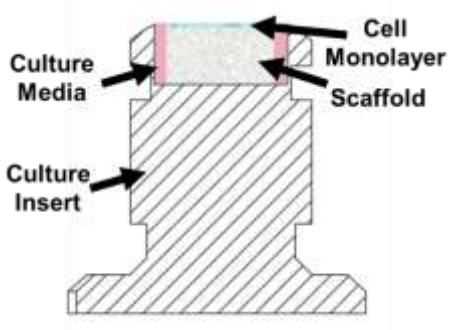

Figure 30 *A schematic of a BEC Insert with cells at an air-liquid interface on a scaffold.*

Cell Culture

3T3 fibroblasts were maintained in Dulbecco's Modified Eagle Medium /F-12 with 10% fetal bovine serum and 1% antibiotic-antimycotic at 37°C 5% CO_2 until 90% confluent. Corning® Transwell® inserts (ref: 3460 – Clear, Corning, NY) with 0.4 µm pores and polyester tissue culture treated membranes were conditioned with culture media at 37°C 5% CO_2 for at least 1 hour. Cells were detached from flasks with trypsin and seeded at 3×10^4 cells per cm^2 on either a Corning® Transwell® insert or on an alginate scaffold within a BEC Insert and incubated at 37°C 5% CO_2. After 24 hours, apical media was aspirated from Transwell inserts and cells were maintained at an air-liquid interface (ALI) for 24 hours. Media level in BEC Inserts with alginate scaffolds were monitored and replenished as needed.

Cytocompatibility

To study cytocompatibility of the alginate scaffold in a BEC Insert, cultures were maintained at an ALI in 37°C 5% CO_2 for 24 hours. Viability was analyzed with Invitrogen™ LIVE/DEAD™ Viability/Cytotoxicity Kit (Thermo Fisher Scientific) according to manufacturer instructions and imaged on an Olympus IX-81 inverted microscope with CellSens software (Olympus, Japan).

Exposure in a Biomimetic Aerosol Exposure System

A JUUL PCU, a BLANKZ!, pod and lab made e-liquid with nicotine, described in Section 5.3, Sample Preparation, were used for cell exposures. For samples exposed to lab air, an

empty BLANKZ! pod and an uncharged JUUL PCU were connected to BAES. Cell cultures in a 12-well plate were removed from the incubator and placed into BEC in a sterile environment. BEC was connected to BAES and Puff Only profile (Table 10) was run twice per plate, for a total of 50 cycles (puffs), with the PCU and pod switched between profiles to avoid a PCU running out of battery or a pod emptying during an exposure. Masses of pods were taken before and after each topography profile as described in Section 5.3, BAES Mass Balance section and masses of filter pads were taken before and after each plate was exposed. After exposure, plates were removed from BEC and placed back in 37°C 5% CO_2 for 3 hours. Positive controls were left unexposed. Negative Controls were treated with 100% ethanol. Plates with positive and negative controls were removed from the incubator and left at room temperature for ~30 minutes to avoid bias related to removing cultures from a controlled environment.

Cell Viability

To assess the effect of exposure in BAES, media was aspirated from the cell cultures and cells were washed with PBS. alamarBlue™ (LOT: 2409113, Invitrogen) was prepared in a 10% v/v solution in PBS. Next, 350 µl of alamarBlue was added to the apical the side of ALI cultures and incubated at 37°C 5% CO_2 for 3 hours. The following steps were conducted in a dark room to avoid light exposure to the light sensitive reagents. Samples of the digested alamarBlue cell solution were taken from each culture. Solution, PBS, and pure alamarBlue were placed in a 96-well plate and a SpectraMax iD3 (Molecular Devices) was used to measure absorbance at 550 and 595 nm. Viability of each sample was normalized to the positive control was calculated from absorbance values in Microsoft Excel (Version 16.73).

Aim 5: Report inferential statistics for the effect of input parameters and system response

Statistical Analyses

Statistical analyses were conducted in R using RStudio (2022.12.0+353). Data was tested for normality using a Shapiro-Wilk test. Hypothesis testing of non-normally distributed data sets was done using a Wilcoxon Rank Sum test. Otherwise, hypothesis testing was performed using a Student's t test. Graphics were produced in RStudio, Microsoft Excel, or a previously described Topography Analysis Program™ [85]. Error bars are 0.95 confidence intervals unless otherwise noted. Standard statistical notation for statistical significance is used in figures unless otherwise noted with one asterisk (*) denoting $p<0.05$, two asterisks (**) denoting $p<0.01$, and three asterisks (***) denoting $p<0.001$.

CHAPTER 6. RESULTS

6.1 Design and Fabrication of a Biomimetic Aerosol Exposure System (Aims 1& 2)

ENDS Adapter

Design and Fabrication

An electronic nicotine delivery system (ENDS) adapter with a streamlined flow path between device and emissions system inlet was developed to reduce aerosol deposition at the ENDS connection. Figure 31a shows an orthographic view of a cross section of the ENDS adapter model, cut on the axial center plane in computer aided design (CAD) software. Flow from ENDS to emissions system is left to right in the figure. The Fusion360 model is parametrically driven, with equations for a continuous spline curve programmed into the model and is available for use by Respiratory Technologies Lab personnel. A CAD user enters dimensions of an ENDS outlet and of a system inlet into the parameters table of the model and an ENDS adapter part and a mold for the part are automatically generated. Automated ENDS adapter CAD files are available for ENDS with circular cross sections, such as cig-a-likes, and for ENDS with a rectilinear mouth piece, such as pod style e-cigarettes.

An iterative process was used to develop a manufacturing protocol for the ENDS adapter. Figure 31b shows a photograph of the ENDS adapter mold during its first iteration; a three-part mold and fabricated via stereolithography (SLA). The part did not fully cure after three days. Investigation of specs available on materials indicate a material interaction between the platinum catalyzer in the silicone rubber and residue from uncured resin on the mold from its manufacturing process. A second iteration (Figure 31c-d) required redesign of the mold including additional part lines for the subtractive manufacturing in aluminum and use of fasteners. The part and its intended use is shown in Figure 31e where a blue positioning jig holds a JUUL e-cigarette, the translucent white adapter connects the e-cigarette to a filter pad holder at the emissions system inlet.

Leak Test

After fabrication, the ENDS adapter was leak tested to ensure an airtight seal. Figure 31f shows flow rate measurements taken by PES-2's system flow meter during a leak test of the ENDS adapter. The ENDs adapter inlet was obstructed by a "mock JUUL". The black line shows command flow and the red line is the measured flow rate from the system flow meter. Five puffs

were performed. The flow meter indicated a small signal at the start of the first puff when air was present in the flow path between the mock JUUL and the flow meter. Once that stagnant air was evacuated, observed flow rate remained under 0.5 mL/s, which is within the accuracy of the flow meter, indicating connections between components, including the ENDS adaptor, maintained an airtight seal.

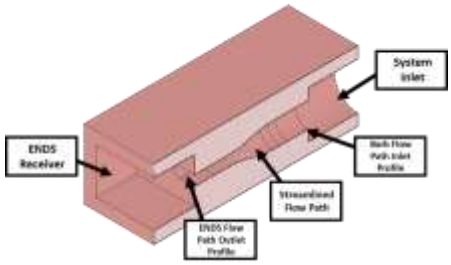

a) An orthographic cross section view of the CAD model of an ENDS adapter.

b) A photograph of a 3D printed ENDS adapter mold.

c) An aluminum mold with an ENDS adapter before removal.

d) An ENDS adapter and its mold disassembled.

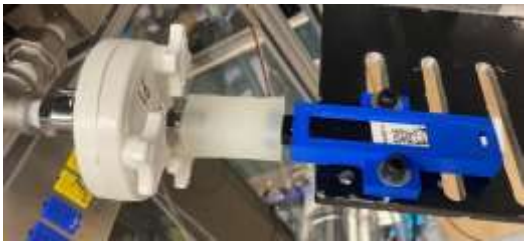

e) A photograph of the ENDs adapter with a JUUL e-cigarette assembled onto PES-2.

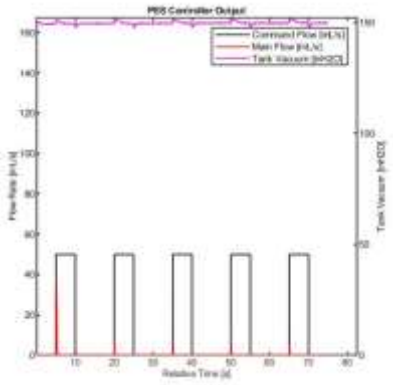

f) Measured and command flow of the ENDS adapter leak test. The black line gives command flow rate and red is the reading from the system flow meter.

Figure 31 *Photos from multiple steps of an iterative design process to develop a customizable ENDS adapter.*

Oral Cavity Module

Design and Fabrication

An Oral Cavity Module (OCM) was developed from a cast of a human oral cavity as an inlet to the biomimetic aerosol exposure system (BAES). Figure 32a-b shows a cross-sectional rendering (panel a) and a photograph (panel b) of the OCM labeled with components. The OCM provides geometric biomimicry at the inlet of BAES, acting as an inlet filter to quantify patient and behavior specific deposition in the oral cavity and to produce a realistic dose of aerosol downstream from the oral cavity. The OCM includes receivers that allow a positioning jig to be attached. The positioning jig holds an ENDS product securely during testing, preventing cantilevering between the PCU and pod, which has been shown to affect the operation of the e-cigarette [176]. The OCM Insert provides a sampling point within the OCM. Standardized hose connectors used at all inlets and exhaust points of the module allow connection with 0.5" flexible tubing, enabling a variety of upstream and downstream connections such as to a filter pad holder, as shown in Figure 32b, or to modules and instruments, such as flow meters, exposure chambers, and particle sensors. Alternate inlets allow modularity with the ability to connect alternative pumps to OCM.

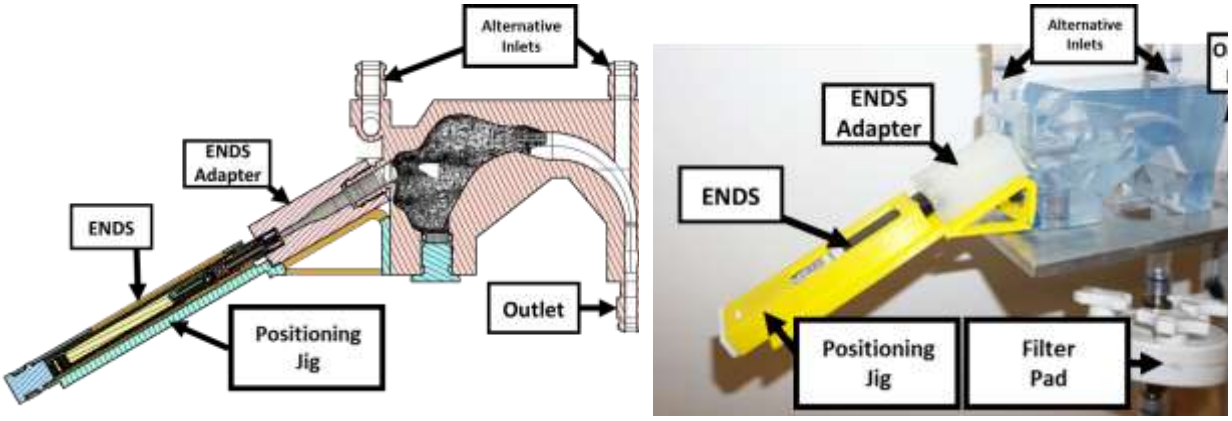

a) *A labeled cross-sectional rendering of the Oral Cavity Module assembled with an ENDS positioning jig and an ENDS adapter.*

b) *A labeled photograph of an Oral Cavity Module connected between a filter pad holder at the exit and ENDS at the inlet.*

Figure 32 *Graphics of an Oral Cavity Module with geometry from a 22-year-old white female.*

A process for preparing models for computational fluid dynamics (CFD) was developed and tested and is shown in Figure 33. The method results in geometry of the fluid space of a model that can be used for computer simulation of an empirical model. Autodesk Fusion360

software was used to develop the biomimetic oral cavity exposure chamber from the Respiratory Technologies Lab (RTL) lung model [91]. CFD analysis, not reported here, was conducted by others.

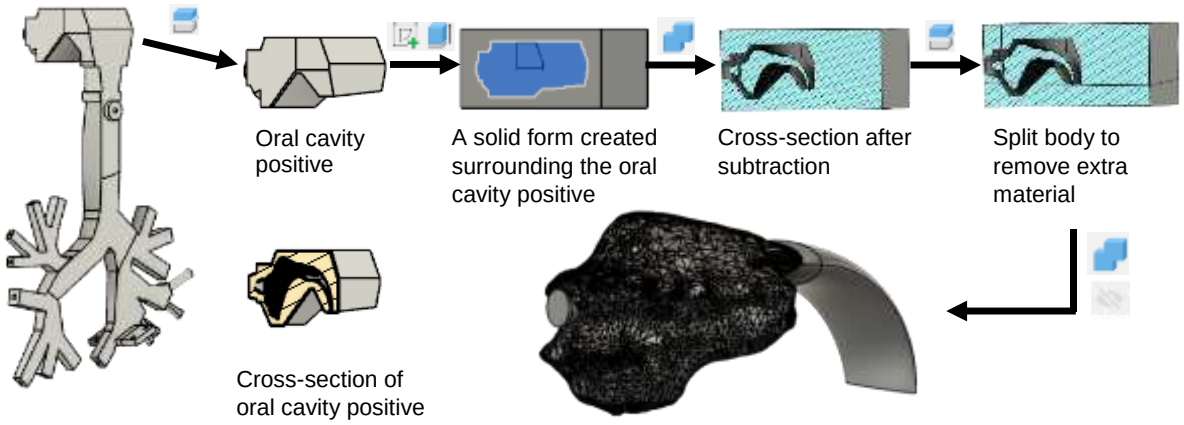

Figure 33 *A process to prepare a 3D flow model to a model suitable for Computational Fluid Dynamics.*

Usability Testing

An assembly protocol for OCM was performed by a lab technician and its' usability was evaluated using a Likert Scale. Results are given in Table 11.

Table 11 *Evaluation of the assembly procedure written for experiments with the Oral Cavity Module.*

	Definitely yes	**Probably yes**	**Might or might not**	**Probably not**	**Definitely not**
The procedure included enough detail that I was able to follow it without any other resources.	X				
I was able to complete the protocol start to finish.	X				
The images included in the procedure aided me in performing tasks correctly.	X				
The steps included in this procedure alone allowed me to assemble and disassemble the OCM, without any prior knowledge or experience with the apparatus.			X		
The procedure included details that distracted me from necessary tasks.				X	
Word choice was clear enough to indicate Which direction or side of a part a step refers to.		X			

Bifurcated Exposure Chamber

Design and Fabrication

The BEC mimics the fluid mechanics and geometry of the first lung bifurcation, creating a biomimetic instrument in which analytical studies and biological exposures can take place using identical geometry. The BEC is shown in Figure 34a-b. BEC accepts commercially available multiple well plates, shown in Figure 34a-b. The height of the bifurcated flow path part produces interference that acts together with the BEC gasket to ensure the chamber is airtight during operation, which was confirmed by leak testing the module. The bifurcated flow path part models a symmetrical lung with a rectilinear cross-section and branching angles based on prior work [87, 92]. The bifurcated flow path part was cast from a 3D printed core. A photo from the casting process is given in Figure 34c. After fabrication of the silicone rubber part for mass characterization studies, actual part dimensions were measured at a single location per branch. The observed overall length of the BEC flow path is 126.80 ± 0.01 mm. The length of the channel before the bifurcation (Figure 34b) is 53.50 ± 0.01 mm, the width of the channel is 16.45 ± 0.01 mm, and the height is 16.64 ± 0.01 mm. Downstream from the bifurcation, the length of the channel is 73.69 ± 0.01 mm, width of the channel is 14.32 ± 0.01 mm, and the height is 9.97 ± 0.01 mm. The branching angle of the lungs is 48 degrees from the center line of the bifurcation. Through-holes within the bifurcated flow path part accept BEC Inserts when placed into a 12-well plate and the bifurcated flow path part is placed on top of the multi-well plate, as shown in Figure 34b. BEC Inserts provide a culture system for monolayers at an air-liquid interface. Inserts are 19.05 mm tall with an outer diameter of 20.83 mm to fit into a standard 12-well plate. For analytical studies, samples can be taken from the inserts to quantify mass and chemical compound deposition within the BEC. Each BEC insert well has a volume of 0.97 mL, with a depth of 3.81 mm and a diameter of 18.03 mm. A labeled photograph of an assembled BEC connected to the OCM and to filter pads is given in Figure 34d.

a) *The Bifurcated Exposure Chamber consists of an aluminum enclosure, a multiple well plate, custom culture inserts, a bifurcated flow path part with its bottom up, and a lid (not shown).*

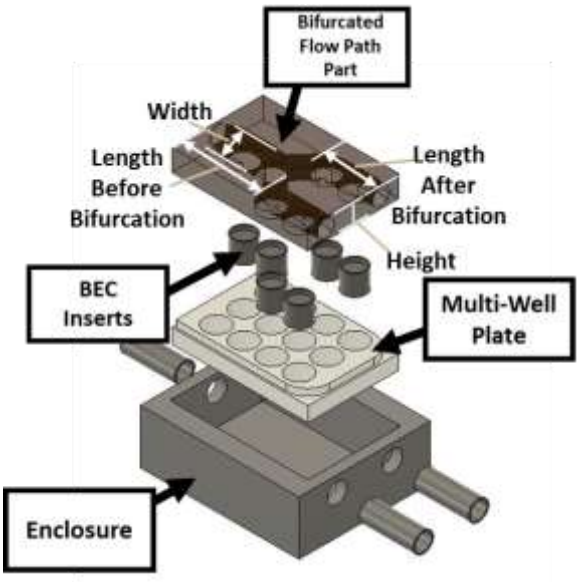

b) *An exploded view of a Bifurcated Exposure Chamber assembly that includes an enclosure, a multiple well plate, BEC Inserts and a bifurcated flow path part. A lid (not pictured) is placed over the flow path part to make the assembly airtight.*

c) *The bifurcated flow path part being cast in silicone rubber. The green part is a removable core that created the internal flow path of the part.*

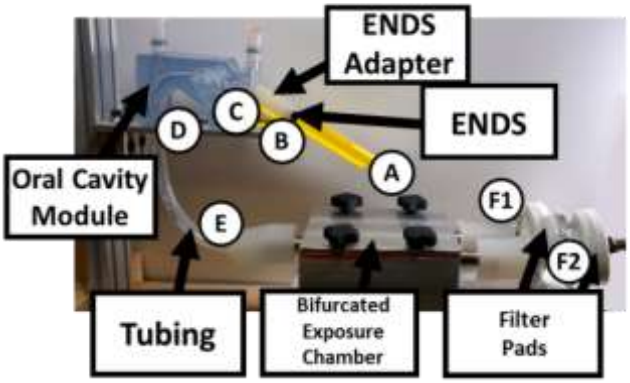

d) *An annotated photograph of the Full Assembly configuration of BAES.*

Figure 34 *Graphics describing the Bifurcated Exposure Chamber and Full Assembly of the Biomimetic Aerosol Exposure System.*

Clean Air Oral Inhale Subsystem

Current emissions systems are not capable of clean air inhales between puffs through the same system inlet. In BAES, lab air inhalation through the primary inlet between puffs was

achieved by using a servo programmed to retract the e-cigarette from the ENDS adapter at the inlet of OCM between puffs. The flow rate was measured at various locations in the BAES to illustrate the transient system response. Figure 35 illustrates the command system flow rate in comparison to the measured system exit flow rate downstream from the filter pads for one exemplar cycle, which consisted of a 25 mL/s puff with a duration of 3.5 secs, after which the ENDS was retracted from the inlet adapter, enabling clean air to enter the oral cavity module. A puff associated respiration (PAR) inhale of 450 mL/s and 3.33 s duration followed the puff, followed by five subsequent tidal inhalations of 350 mL/s and 3.33 s duration. At the end of each cycle, the ENDS was reinserted into the adapter, and the complete cycle was repeated 25 times to complete a single emissions trial.

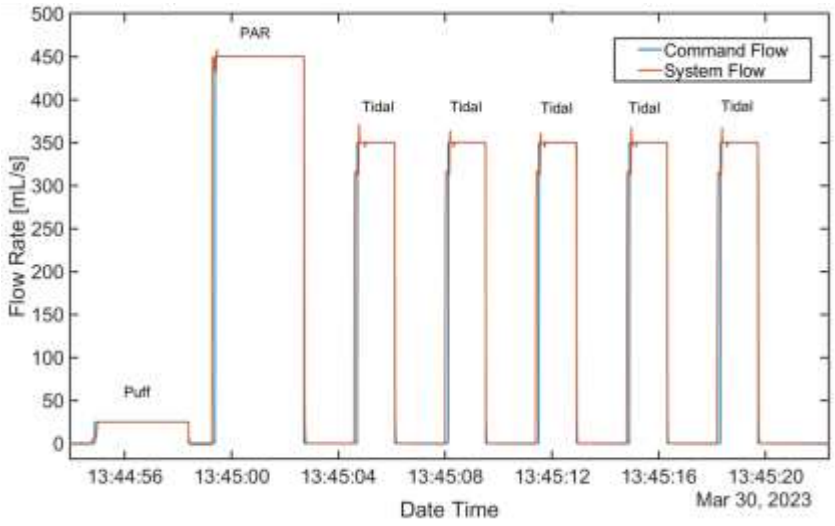

Figure 35 *A command system flow rate (blue line) in comparison to the measured system exit flow rate downstream from the filter pads (red line) for one exemplar PAR450 cycle.*

Adapt the PES-2 as Biomimetic Aerosol Exposure System

An existing emissions system, PES-2™ [80], was adapted into BAES through development of both hardware and software. The ENDS adapter, OCM, tubing, BEC, and two filter pad holders with filter pads in each make up a BAES Full Assembly, shown in Figure 34d. An ENDS (A) is placed in the positioning jig fixed to the OCM with its outlet in the ENDS adapter (B). The outlet of the ENDS adapter (C) exhausts to the OCM inlet. The positioning jig allows linear motion of the ENDS along its center axis when the Clean Air Oral Inhale Subsystem is in use. The distal end of an ENDS is connected to the arm of a linear servo using a 3D printed elastomeric adapter. Communication with the PES control software retracts the servo, breaking the seal between the ENDS and ENDS adapter during ambient air inhalation while the

positioning jig constrains motion in all other directions. Tubing of length 28.4 cm is connected between the exhaust of OCM (location D) and to the inlet of BEC (location E). The outlets (locations F1 and F2) of the BEC are each attached to a filter pad holder. Custom adapters that transition from the inner diameter of the BEC outlet to the inlet of 0.5” flexible tubing or to the mechanical connector of a filter pad holder were designed with the same methods as the ENDS adapter and allow modularity of the BEC.

6.2 Validation and Characterization of BAES (Aim 3)

Comparison of ENDS Adapter to a Traditional Emissions Set-Up

To validate the ENDS adapter, mass balances of the ENDS adapter and a traditional emissions system set up using flexible tubing were conducted. Results are given in Figure 36. Range of total particulate matter (TPM) per puff reflects the variation observed when using BLANKZ! Pods with a JUUL e-cigarette. The fraction of total aerosol produced by an electronic cigarette that was deposited in transit to a filter pad or lost as volatile matter was 0.116 ± 0.021 (0.95 CI, N= 37) in a traditional emissions testing setup and 0.098 ± 0.015 (0.95 CI, N= 60) in a streamlined adapter. Deposition in the ENDS adapter was ~2% less than in the traditional set up. Results were not statistically significant. Pearson Correlation Coefficients between Deposition Fraction and TPM per puff for the Baseline condition and for ENDS adapter were 0.729 and 0.736.

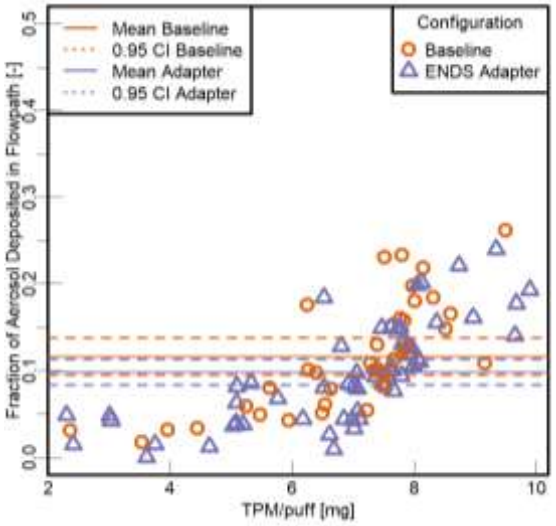

Figure 36 *The fraction of total aerosol produced by an electronic cigarette deposited between the device and a filter pad or lost as volatiles in a traditional emissions testing setup or an ENDS adapter. Results are not statistically significant.*

Flow Rate Characterization

Flow rate characterization was conducted by placing a calibrated orifice plate [41] in the BAES flow path at several locations. This characterizes accuracy and repeatability of the BAES' flow control subsystem, rather than relying on and reporting command flow rate, a practice common in emissions studies. During initial flow characterization that measured inlet flow rate at location B across the operating range of a JUUL e-cigarette, puff durations corresponded closely to command puff duration with mean duration error of 0.3 s with maximum duration error of ~0.45 s across 53 puffs. Figure 37a shows further characterization of accuracy and repeatability at a clinically relevant flow rate of 25 mL/s measured at locations B, E, F1, and F2 labeled in Figure 34d. System and observed flow rates at the e-cigarette at 25 mL/s command flow, 50 puffs, 3.5 s, 20 s period. Mean error for N=100 puffs was within accuracy of measurement instruments. The accuracy of flow rate was within 5% of both command flow and system flow rate. For all local flow rate measurement points before the flow bifurcation within BEC, nominal flow rate is equal to command flow rate. Downstream from BEC, the nominal flow rate is equal to one half the command flow rate. At all measurement points, nominal flow fell within local flow rate plus or minus the larger of the accuracy or repeatability of the measurement instrument.

Wall Shear Stress Characterization

Wall shear stress (WSS) is a critical parameter for maintaining a physiological environment during cell culture but is difficult to measure *in situ* for risk of disrupting flow. Flow rate is simple to measure at the inlet and outlet of an exposure chamber. The law of conservation of mass supports the assumption that flow rate is the same at multiple locations within a branch. Therefore, wall shear stress within BEC was modeled using local flow rate measurement and flow path dimensions. Figure 37b gives wall shear stress values in generations 1 and 2 modeled by the linear program (LP) using input parameters from Tables 8 and 9, minimum and maximum wall shear stress thresholds based on prior work [91, 174], and predicted wall shear stress within BAES for generations 1 and 2 based on local flow rate measurements taken at locations E, F1, and F2 and measurements of the polydimethylsiloxane (PDMS) bifurcated flow path part. Channel width was measured at a single location for each branch. Channel height is the mean channel height measured in B1 and B2 for the first generation and mean channel height measured in A3, C3, A4, and C4 for the second generation. The minimum puff flow rate that satisfies all constraints in the LP model is 17 mL/s. Puffing alone was insufficient to provide appropriate mechanical cues to cells as reflected by

Reynolds number between 31-86 and wall shear stress predictions between 0.0007-0.002 Pa. The optimum inhale flow rate that satisfies all constraints is ~510 mL/s resulting in Reynolds number between 726-2100 and wall shear stress between 0.02-0.04 Pa for generations 1-4. Calculated WSS based on local flow rate and channel dimension measurements were as follows: for puffing, 0.0005 ± 0.0001 Pa in the first generation, 0.0007 ± 0.0008 Pa in the left branch and 0.001 ± 0.0008 Pa in the right branch of generation 2. For tidal breathing shear stress was 0.007 ± 0.0007 Pa in the first generation and 0.013 ± 0.003 Pa in both branches in generation 2. PAR breaths at 429 mL/s produced WSS of 0.010 ± 0.0007 Pa in generation 1, 0.017 ± 0.003 Pa in the left branch and 0.019 ± 0.003 Pa in the right branch of generation 2. Asymmetry in the empirical model reflects the asymmetry in both measured flow rate and actual channel heights.

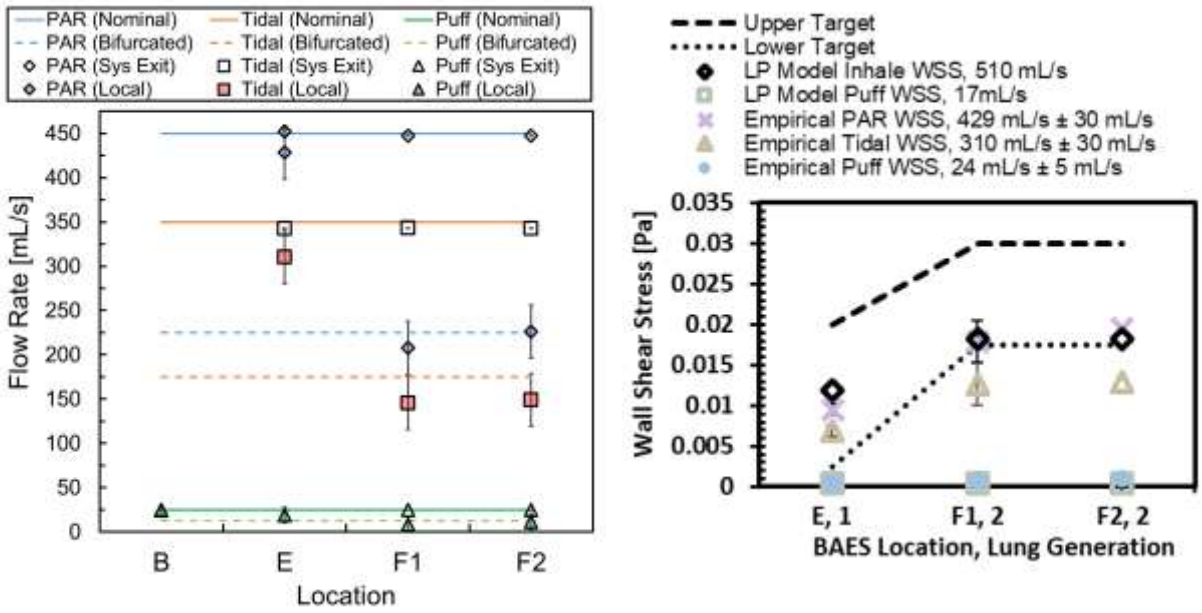

a) *Flow characterization using an internally calibrated orifice plate to measure local flow rate and a third-party calibrated flow meter to measure system flow rate.*

b) *WSS modeled at design target flow rates and estimated wall shear stress with 0.95 confidence intervals based on measured local flow rate and channel dimensions.*

Figure 37 *Local flow rate and corresponding wall shear stress (WSS) for each component of a breathing cycle: Puff from an ENDS, Puff Associated Respiration (PAR), and tidal breathing in a Biomimetic Aerosol Exposure System.*

Mass Dose Characterization

Effect of Emissions Topography Profile on Percent Yield Deposited in BAES with an Oral Cavity Module

Mass balance of BAES in the Adapter + OCM configuration was conducted to quantify flow path deposition as a function of emissions topography profile (ETP). Deposition of blue dyed e-liquid droplets was visually observed inside of OCM. An exemplary photo of the OCM is given in Figure 38a, which was taken following two repetitions of the Puff Only topography profile (50 puffs). Mass deposited between the e-cigarette and filter pad when the ENDS adapter and OCM make up the flow path was estimated by taking the mass of the e-cigarette's pod and a filter pad placed immediately downstream from the OCM outlet before and after a puffing profile with the assumption of conservation of mass to estimate approximate percent of total yield deposited in the ENDS adapter + OCM flow path. Here, mass in the volatile phase are included in the reported result. Fraction of mass that left the e-cigarette and deposited before the filter pad or exited the system as volatile matter when the flow path included an ENDS adapter and the OCM are given in Figure 38b. PAR450 data exhibited non-normality and a non-parametric test was used in comparing means to PAR450. Mean deposition fraction, df_{TPM} [-] was 0.13 ± 0.02, 0.16 ± 0.06, 0.19 ± 0.06, 0.20 ± 0.05 and 0.17 ± 0.01 for Puff only, PAR150, PAR250, PAR350, and PAR450 respectively. Deposition fraction for Puff Only (N=34) was significantly different from PAR250 (N=7, p=0.025), PAR350 (N=5, p=0.022), and PAR450 (N=53, p=0.001). There was not statistical significance between Puff Only and PAR150 (N=6) or between any profiles that include ambient air inhalation cycles between puffs.

Droplets could be visually observed on the OCM Insert following two topography profiles (50 cycles), shown in Figure 39a. Figure 39b gives dose per unit area in the OCM Insert for the five topography profiles studied. Statistical analyses for this data were done with deposition fraction for the OCM Insert to normalize data to device performance in a given trial. Samples sizes are smaller for OCM Insert data than OCM mass balance data because an absorbance plate reader was used to measure mass in the OCM Insert and any human error in the plate reader protocol led to data exclusion. OCM insert dose with the Puff Only ETP was Y''_{TPM} = 1.31 mg/cm^2 ± 0.956 (N=23) or df_{TPM} = 0.0023 ± 0.002. PAR150 OCM Insert dose was Y''_{TPM} = 0.041 ± 0.04 mg/cm^2 (N=3) or df_{TPM} = 7.04 x 10^{-5} ± 7.06 x 10^{-5}. PAR250 OCM Insert dose was Y''_{TPM} = 0.030 mg/cm^2 ± 0.03 (N=3) or df_{TPM} = 8.22 x 10^{-5} ± 1.27 x 10^{-4}. PAR350 OCM Insert dose was Y''_{TPM} = 0.073 mg/cm^2 ± 0.23 (N=3) or df_{TPM} = 9.33 x 10^{-5} ± 2.35 x 10^{-4}. PAR450 OCM Insert dose was Y''_{TPM} = 0.079 mg/cm^2 ± 0.22 (N=8) or df_{TPM} = 1.03 x 10^{-4} ± 2.33 x 10^{-4}. Difference in

deposition fraction between Puff Only and all ETPs with inhales was significant with a Wilcoxon rank-sum test. There was no statistical significance between deposition fractions of topography profiles that include inhalation breaths.

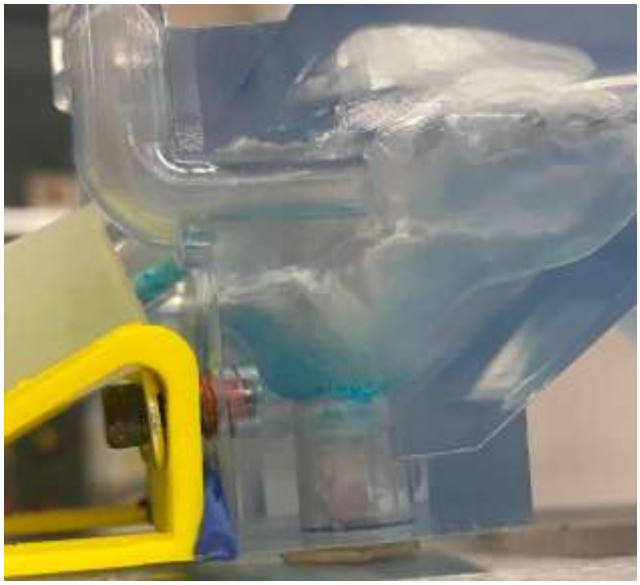

a) A photo of OCM taken was taken following two repetitions of a topography profile with clean air inhalation. Blue clouding is dyed e-liquid droplets

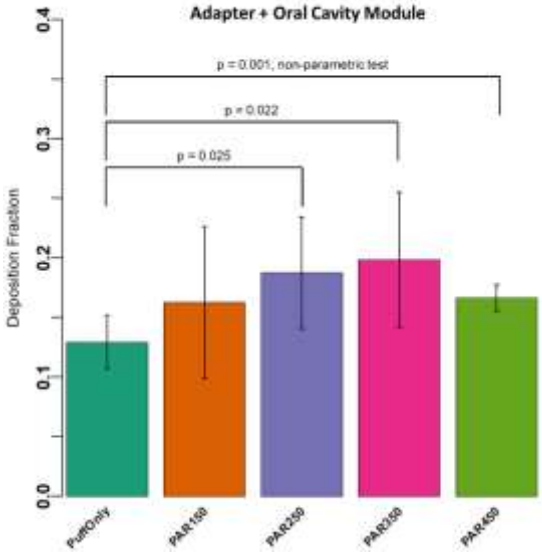

b) Deposition fraction between the e-cigarette exit and the filter pad when an adapter and an Oral Cavity Module made up the flow path for Puff Only (N=34), PAR150 (N=6), PAR250 (N=7), PAR350 (N=5), and PAR450 (N=53),

Figure 38 *Deposition in the ENDS Adapter + Oral Cavity Module (OCM) configuration of a Biomimetic Aerosol Exposure System for five emissions topography profiles.*

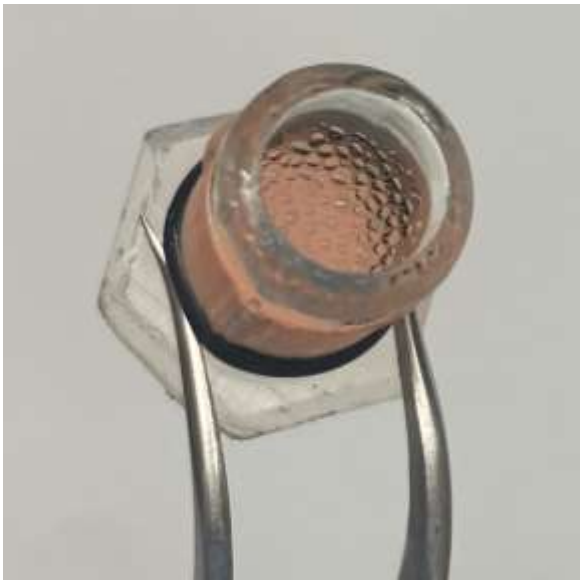

a) *Droplets visually observed inside of the OCM Insert after 50 puffs at 25 mL/s.*

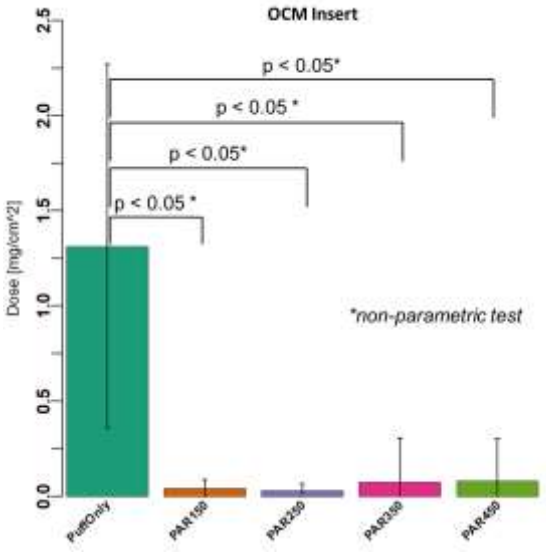

b) *Dose, Y''_{TPM}, in the OCM Insert for Puff Only (N=23), PAR150 (N=3), PAR250 (N=3), PAR350 (N=3), and PAR450 (N=8). Negative error bars are cut at 0 [mg/cm^2].*

Figure 39 *Deposition in the Oral Cavity Module Insert for five emissions topography profiles.*

Effect of Emissions Topography Profile on Percent Yield Deposited in the Flow Path of BAES Full Assembly

Mass balance of BAES Full Assembly configuration was conducted to study the effect of ETP on deposition in the system flow path. The Full Assembly configuration of BAES used a piece of flexible tubing to connect the exit of the OCM to the inlet of the BEC during all Full Assembly emissions and exposure trials. Exemplar images of tubing after 50 cycles of Puff Only and PAR450 are given in Figure 40a-b. When the blue dyed e-liquid was used a difference in aerosol deposition at the inlet of the tubing where it interfaces with the OCM outlet was observed visually as a function of topography profile, with the darkest staining present when PAR450.

a) *Inlet of the tubing connecting the OCM to the BEC after 50 puffs of the Puff Only topography profile. The inlet of the tubing appears clear, with minimal clouding of blue e-liquid droplets.*

b) *Inlet of the tubing connecting the OCM to the BEC after 50 puffs of the PAR450 topography profile. Blue clouding is dyed e-liquid droplets.*

Figure 40 *Photos of inlet of the tubing connecting the OCM to the BEC with two different emissions topography profiles.*

Mass deposited inside of the BAES Full Assembly flow path was estimated by taking the gross mass of the e-cigarette's pod and filter pads placed at each of the two outlets of BEC before and after a puffing profile and assuming conservation of mass to estimate approximate percent of total net yield deposited in the flow path between e-cigarette outlet and the filter pads. Here, mass of volatiles flowing through the pads are included in the reported effective deposition. The fraction of mass that left the e-cigarette and deposited before the filter pads or were lost as volatile matter when the flow path included an ENDS adapter, the OCM, 28.4 cm of tubing, and the BEC are given in Figure 41. The deposition fraction in the Full Assembly was 0.32 ± 0.04, 0.19 ± 0.06, 0.18 ± 0.05, 0.17 ± 0.04, and 0.22 ± 0.06 for Puff Only (N= 49), PAR150 (N= 7), PAR250 (N=12), PAR350 (N=10), and PAR450 (N=20) respectively. The deposition fraction for Puff Only was significantly different from all profiles that included clean air inhalation cycles between puffs. There was no statistical significance between profiles that included ambient air inhalation cycles between puffs. The significant difference in deposition as a function of ETP in both BAES configurations supports the Aim 2 hypothesis that particle deposition depends upon puff and respiration topography, independent of flow path geometry.

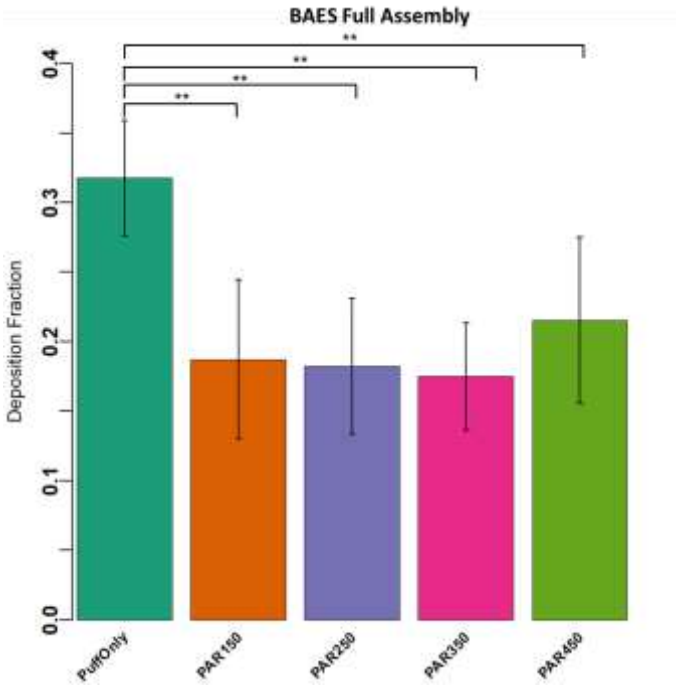

Figure 41 *Deposition fraction between the e-cigarette exit and the filter pad when a streamlined adapter, an Oral Cavity Module, and a Bifurcated Exposure Chamber made up the flow path for Puff Only (N=49), PAR150 (N=7), PAR250 (N=12), PAR350 (N=10), and PAR450 (N=20). A non-parametric test was used for all hypothesis tests in this figure.*

BEC Symmetry

The BEC was designed such that flow would be split evenly at the bifurcation thus creating two symmetric flow paths, assuming conservation of mass. Manufacturing tolerance, imperfections in the mold used to create the bifurcated flow path part, or non-uniform vacuum pressure between inlets to vacuum may lead to non-symmetric flow between the two branches. To test if the BEC performed as intended, mean deposition fraction for each pad at the outlets of BEC were compared for the Puff Only condition. Mean deposition fraction on the pad at location F1 was 0.39 (±0.020 CI, N=49). Mean deposition fraction on the pad at location F2 was 0.31 (±0.019 CI, N=49), given in Figure 42. Initially, deposition fraction data from both pads exhibited non-normality. A Wilcoxon signed rank test found a significant difference between pad deposition fractions ($p<0.001$). To verify this with a parametric hypothesis test, a Box Cox transformation [177] was applied to each data set. A Student's t test was conducted on transformed data. The difference between the transformed means was significant ($p<0.001$).

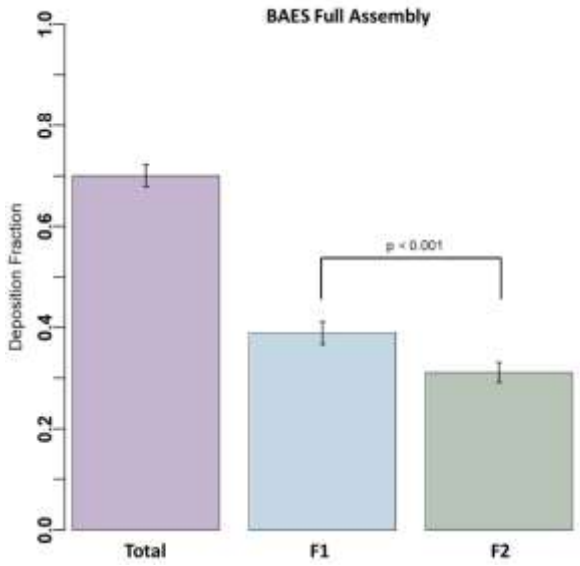

Figure 42 *Fraction of total yield from the electronic cigarette that was deposited on each filter pad at system exit and total mass that exited the system (F1 Pad + F2 Pad) in the Full BAES configuration with a streamlined adapter, an Oral Cavity Module, tubing, and a Bifurcated Exposure Chamber included in the flow path for Puff Only (25 puffs).*

Tunable Scaffolds to Control Fluid Shear

Scaffold Dimensions

A process for fabricating 3D alginate scaffolds with tunable height [169] was adapted for use in BEC Inserts. The cell culture system uses the alginate scaffold as a substrate that places a monolayer of cells cultured on top of the coated scaffold on the wall of the BEC flow path. Scaffolds were fabricated by crosslinking alginate in a petri dish in a Calcium Chloride bath, forming a 55 mm alginate disc, and punching out individual ~14 mm scaffolds with a cork bore punch. For cell culture, each alginate scaffold is placed into the well of a BEC Insert, shown in Figure 43. The difference between the Insert Well Diameter and the Scaffold Diameter provides an annular space for culture media, which feeds the cells through absorption into the alginate scaffold matrix. To assess repeatability of the fabrication method and to quantify exposure area, three scaffolds were removed from a sterile environment for photos to be taken and images analyzed. Images were processed in ImageJ2. Each scaffold diameter was measured on three different axis, demonstrated in the example image in Figure 43. Table 12 gives descriptive statistics of scaffold dimensions.

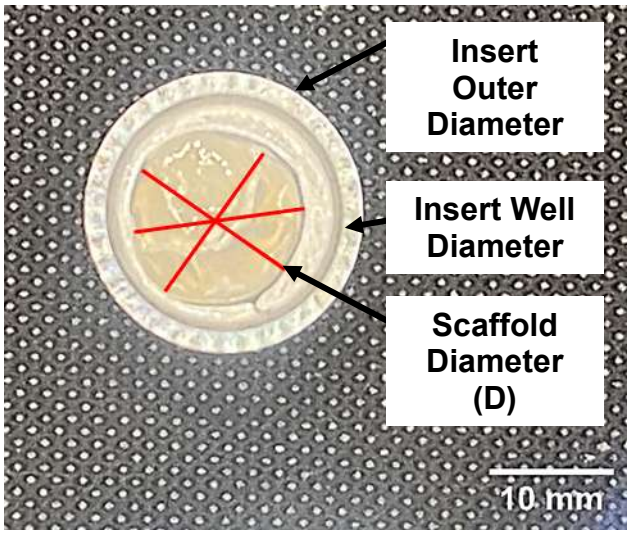

Figure 43 *Scaffold diameters were measured using ImageJ2. Repeated measures were taken for each scaffold, shown with lines drawn on an exemplar scaffold image.*

Table 12 *Descriptive statistics of diameters (D) of punched alginate scaffolds.*

Sample	D1	D2	D3	Mean	SD
	[mm]	[mm]	[mm]	[mm]	[mm]
Scaffold 1	13.322	13.564	13.736	13.54067	0.207984
Scaffold 2	13.448	14.2	14.647	14.09833	0.605931
Scaffold 3	14.431	14.508	14.572	14.50367	0.0706
Grand Mean				14.04756	0.483504

Cytocompatibility

Cell viability of 3T3 fibroblasts cultured at an air-liquid interface (ALI) on a fibronectin coated alginate scaffold in a BEC Insert was assessed with a Live/Dead assay and compared to ALI culture on a Corning® Transwell® insert. Figure 44 shows exemplar images of each condition with the Transwell insert culture in panel a and the custom culture system in panel b. Green areas are live cells stained with calcein-AM ethidium. Qualitative assessment indicates that cells did not attach to the alginate scaffold, reflected by the lack of cells visible in Figure 44b. Cells on the Transwell insert in Figure 44a, appear elongated. Cells visible on the alginate insert in Figure 44b appear round and smaller in diameter than cells on a Transwell insert.

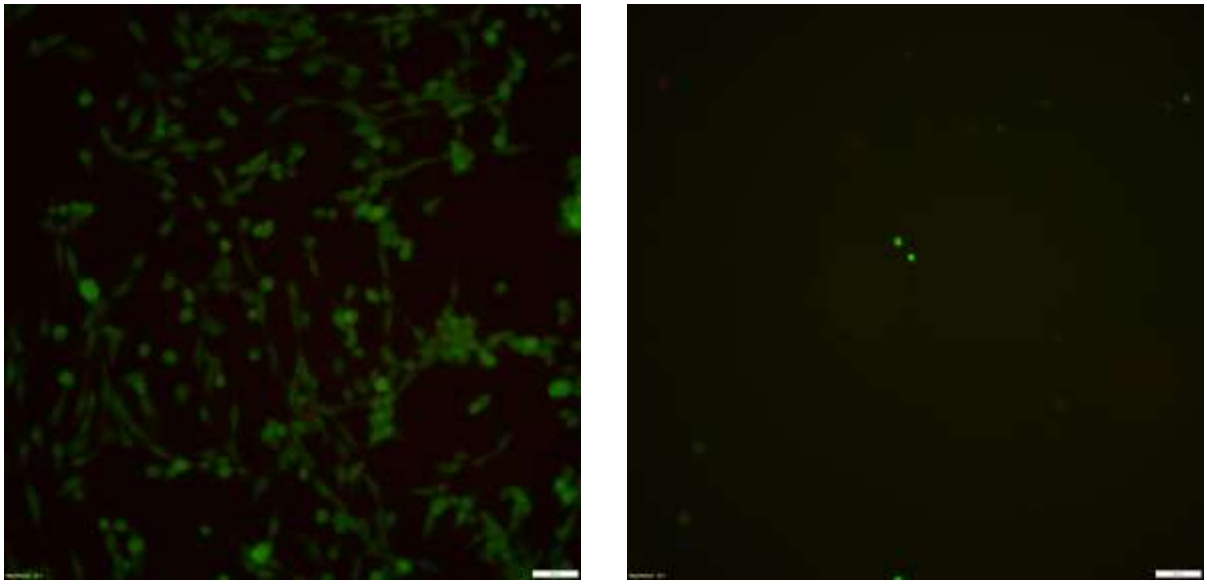

a) *Cells cultured on a Corning ® Transwell® insert with a polyester membrane a 0.4 µm pores.*

b) *Cells cultured on 7% alginate coated in 0.01 mg/mL fibronectin. Alginate scaffolds kept inside of stainless steel BEC Inserts.*

Figure 44 *3T3 fibroblasts cultured at an air-liquid interface. Fluorescence imaging on an Olympus IX-81 inverted microscope with CellSens software (Olympus, Japan) at 20x stained with calcein-AM ethidium/ homodimer-1. Scale bars are 50µm.*

6.3 Demonstrate Emissions Testing Capability of a Biomimetic Aerosol Exposure System (Aim 3 cont.)

Effect of Third Party Products

During BAES characterization using a BLANKZ! Pod with a JUUL e-cigarette, qualitative observations indicated that greater mass was aerosolized from a pod in a single trial than in previous work using the JUUL e-cigarette with a JUULpod [173]. Therefore, BAES was used to compare yield and flow path deposition fraction of BLANKZ! Pods and JUULpods with a JUUL e-cigarette. In a configuration that included an ENDS, ENDS adapter, and filter pad holder connected to the vacuum subsystem inlet, BAES was exercised to assess the effect of a third party product. Using the Puff Only emissions topography profile (Table 10), a JUUL power control unit (PCU) was puffed with either a JUUL brand pod with 5% nicotine (tobacco favor) or lab made 50:50 Propylene (PG): Glycerin (GL) e-liquid. Total particulate matter (TPM) per puff was calculated from mass change of the pod and number of puffs in a topography profile and is shown in Figure 45. Mean TPM/puff from a JUUL brand pod was 2.17 ± 0.25 mg/puff (0.95 CI,

N=23). Mean TPM/puff from a BLANKZ! Pod with 50:50 PG:GL was 6.89 ± 0.44 mg/puff (0.95 CI, N=60). Results were statically significant with a p-value less than 0.001.

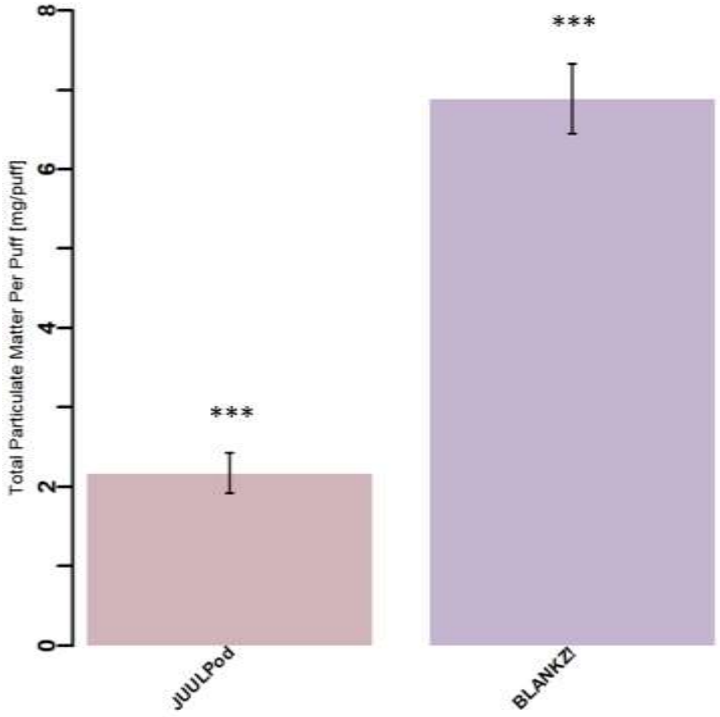

Figure 45 *Total particulate matter per puff for a JUUL brand pod (N=23) and a BLANKZ! Pod with lab made e-liquid (N=60, p< 0.001).*

Estimation of Volatile Mass Fraction During BAES Trials

Mass characterization of BAES (Section 6.2) compared the effect of ETP on deposition in two BAES configurations. For the purpose of studying effect of ETP, an assumption was made that the difference between ENDS decrease and filter pad increase was mass deposited in the flow path. However, a fraction of mass undergoes a phase change during aerosolization by thermal decomposition [178] and exits the system as volatile matter. To account for this and to precisely map deposition throughout the entire BAES system, additional mass balance was performed with the Puff Only ETP.

The fraction of mass deposited in the ENDS adapter, Cambridge filter pad (CFP) holder inlet (geometry given in Figure 14b-c in Section 4.1.1), and filter pad were measured directly by taking the mass of each flow path component before and after a trial and calculating the mass increase. In the Adapter Only BAES configuration, every component of the flow path was measured. Therefore, the difference between the mass decrease of the e-cigarette (Δm_{ENDS})

and the combined mass increase of the Adapter, CFP holder inlet, and CFP ($m_{Deposited} = \Delta m_{Adapter} + \Delta m_{CFP\_Inlet} + \Delta m_{CFP}$) is the mass that underwent a phase change during aerosolization and exited the system as volatile matter ($m_{Volatile} = \Delta m_{ENDS} - m_{Deposited}$). Direct mass measurements and volatile estimates were normalized to the quantity of mass that left the ENDS in each trial and are given in Figure 46. Mean mass deposition fractions are as follows: Adapter = 0.018, CFP holder inlet = 0.043, CFP = 0.865, from which the mass fraction of volatiles = 0.074 was computed.

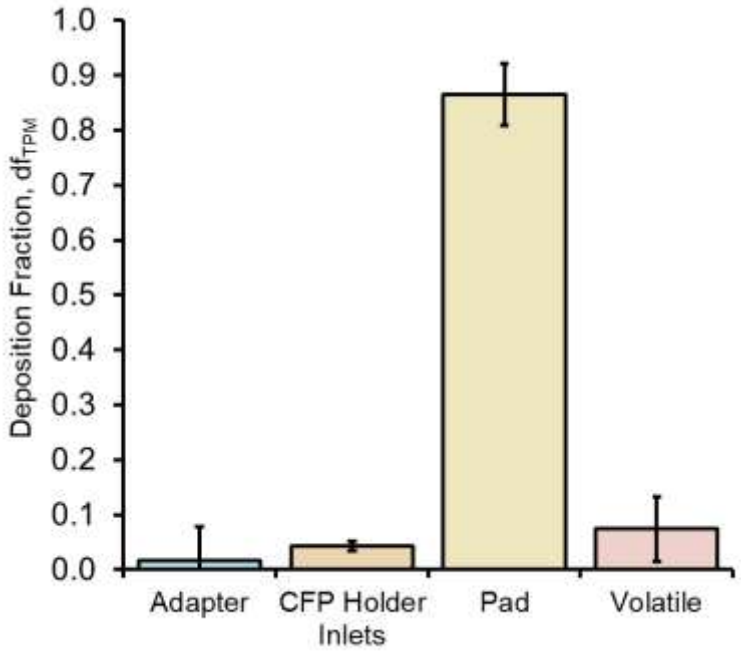

Figure 46 *Direct mass measurements of all flow path components in a simplified BAES configuration allowed estimation of fraction of aerosol in the volatile phase.*

Distribution of Aerosol Deposition in a Biomimetic Aerosol Exposure System

Using known mass deposition in the Adapter, CFP holder inlet, CFP, and volatiles, mass distribution in each BAES region was inferred. Gross distribution of aerosol throughout BAES was inferred by mass balance of BAES in Adapter + OCM and Full Assembly configurations while accounting for the sources of aerosol loss in the Puff Only ETP. We assume that the fraction of mass that undergoes a phase change is constant for trials conducted under the same conditions (device, pod, consumable, ETP) and utilize this fraction along with the direct measurements of the adapter, CFP holder inlet, and CFP. Figure 47 provides an inter-module analysis of deposition fraction, df_{TPM} [-], distribution in BAES, accounting for fraction of mass deposited in transit to a module and for volatile matter. Deposition in OCM was 0.027 while

deposition fraction in the tubing and BEC was 0.248. In the Full Assembly configurations two CFPs are used, therefore CFP Holder Inlet deposition fraction was doubled to df_{TPM} = 0.087 deposited in the left and right CFP holder inlets F1 and F2. The white triangular data point with a bright pink border represents actual measurements at the system exit in the Full Assembly configuration and allows us to compare our inferred model to actual filter pad data. The inferred model agrees within 0.11 of the observed deposition that exits the system. These results support the Aim 1 hypothesis that aerosol particle deposition in aerosol exposure systems depend upon the flow path geometry.

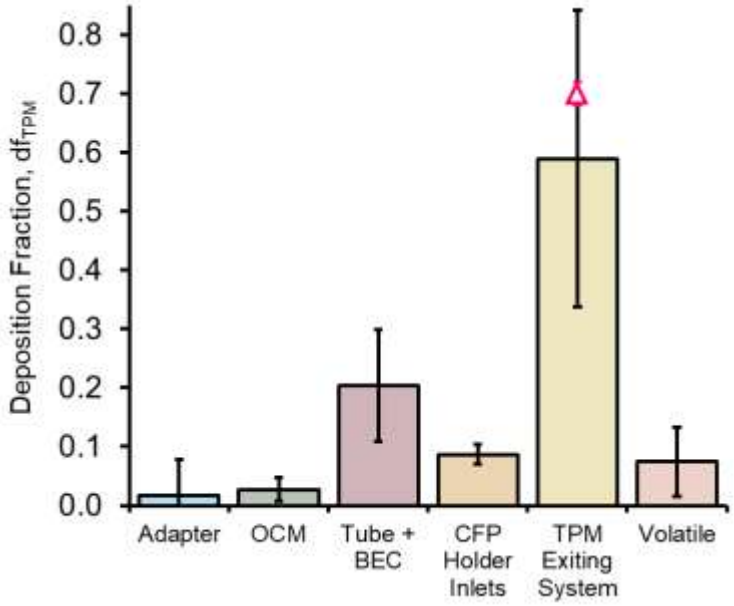

Figure 47 *An inter-module analysis of distribution of mass via deposition fraction, df_{TPM} [-], in BAES. The triangular data point represents direct measurements at the system exit in the Full Assembly configuration and allows comparison of the inferred model to actual filter pad data.*

Distribution of Aerosol Deposition within Regions of a Biomimetic Aerosol Exposure System

High resolution mass distribution within BAES modules was quantified using blue dyed e-liquid and an absorbance plate reader. Figure 48a provides intra-module estimates of dose per unit area. These are direct measurements of mass concentration of e-liquid [mg/mL] at each sampling point after two rounds of Puff Only exposure. Concentrations were converted into mass dose per unit area, Y''_{TPM} [mg/cm^2]. Samples sizes were not equal for all sampling points due to data exclusion from systematic errors (i.e., Forgetting to take a sample, no signal detected in plate reader) or because taking OCM samples was time consuming and often

skipped to preserve throughput. Sample sizes were: N=23 for the OCM Insert (OCI), N=2 for OCM, N=21 for tubing, N=25 for B1 and B2, and N=26 for wells A3, C3, A4, and C4. The OCI is the closest sampling point to the system inlet. Dose in the OCI was mean Y''_{TPM} 1.31 ± 0.956 mg/cm^2. Dose within the OCM was 0.12 ± 0.03 mg/cm^2. There was 0.078 ± 0.026 mg/cm^2 in the tubing connecting OCM and BEC. Dose in each well in BEC was: 0.066 ± 0.020 mg/cm^2 in B1, 0.067 ± 0.022 mg/cm^2 in B2, 0.036 ± 0.016 mg/cm^2 in A3, 0.037 ± 0.013 mg/cm^2 in C3, 0.036 ± 0.014 mg/cm^2 in A4, and 0.04 ± 0.012 mg/cm^2 in C4. A paired t test found statistical difference between OCI and OCM (p=0.010), OCI and Tube (p=0.014), and between OCI and all wells in BEC ($p < 0.05$). There were also significant differences between the OCM and Tube (p<0.001) and OCM and all wells in BEC (p<0.001). Interestingly the dose in Tubing and samples in the first generation of BEC did not exhibit a statistical difference. Meanwhile Tubing was statistically different than all wells after the bifurcation: Tube and A3 (p= 0.028), Tube and C3 (p=0.016), Tube and A4 (p=0.03), Tube and C4 (p=0.008). Between wells (Figure 48b), there were significant differences between wells before the bifurcation and wells in the C3-C4 branch: B1 and C3 (p=0.046), B1 and C4 (p=0.022), B2 and C3 (p=0.045), and B2 and C4 (p=0.023).

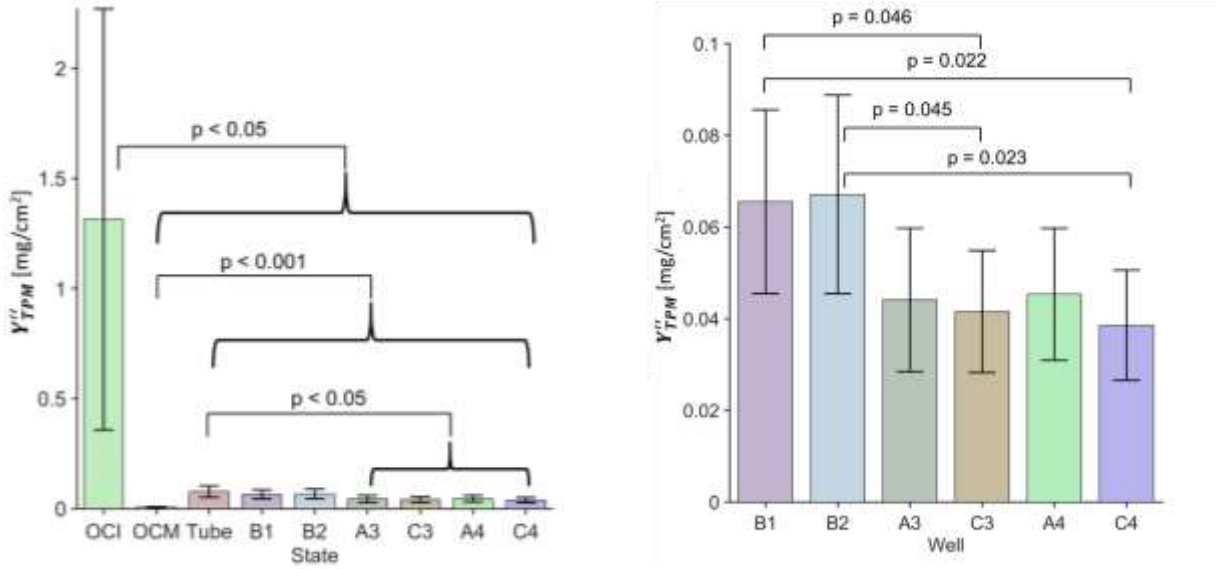

a) Intra-module analysis of deposition fraction under Puff Only conditions. Brackets denote statistical significance.

b) A zoomed in version of panel a and analysis with paired t tests.

Figure 48 *High resolution analysis of deposition fraction throughout the biomimetic aerosol exposure system, including intra-module analyses, with a Puff Only topography profile.*

Significant differences between the OCI and other system locations and significance between samples from generation 1 and samples from generation 2 support the Aim 3 hypothesis that aerosol particle deposition, which naturally occurs in machine-puffing systems, can be used to mimic particle deposition in the human respiratory tract.

6.4 Demonstrate Toxicology Testing Capability of a Biomimetic Aerosol Exposure System (Aim 4)

Exposure in a Biomimetic Aerosol Exposure System

3T3 cells were cultured at an ALI and exposed to lab air or e-cigarette aerosol in the BAES. Protocol efficiency was analyzed to inform improvements to the exposure protocol. Samples were outside of the incubator for 34 ± 7 minutes (standard deviation (SD)). Controls were outside of the incubator for 21 ± 19 minutes (SD). Samples remained inside of BAES for 18 ± 2 minutes (SD). Descriptive statistics are given in Table 13. Plate 3 were not captured.

Table 13 *Descriptive statistics for amount of time samples were outside of environmental control and inside of the BAES during an exposure study.*

Condition	Plate Label	Outside of Environmental Control	Time inside of BAES
[-]	[-]	[min]	[min]
Dirty Puff	**1**	50	18
Dirty Puff	**2**	37	20
Dirty Puff	**3**	NA	NA
Dirty Puff	**4**	38	15
Dirty Puff	**5**	33	21
Dirty Puff	**6**	37	19
Clean Puff	**7**	30	16
Clean Puff	**8**	24	17
Clean Puff	**9**	23	18
Mean	**Test**	34	18
SD	**Test**	8.7	2
Control	**Control Dirty Puff**	0	
Control	**Control Dirty Puff2**	38	
Control	**Control Clean Puff**	25	
Mean	**Control**	21	
SD	**Control**	19.3	

The Effect of Transverse Flow

Due to lack of compatibility on the alginate scaffold in a BEC Insert, proof-of-concept toxicology testing was performed using cultures on Corning ®Transwell® inserts and multi-well plates in BEC. To assess the effect of transverse flow on cells, 3T3 fibroblasts cultured at an ALI using Transwell inserts were exposed to lab air in the BEC, puffed with the Puff Only ETP through BAES. The ETP was performed twice per sample. This exposure is referred to as "Clean Puff" exposure. Viability of exposed cells was assessed with an alamarBlue™ assay and normalized to an incubator control. Viability results are given in Figure 49a. Clean Puff viability data from well A4 exhibited non-normally distributed data with N=9, per a Shapiro Wilks test. All other Clean Puff datasets were normally distributed. A one-tailed t-test was performed between viability of an incubator control (N=19) and Clean Puff exposed cells (N=9) for each well with the alternative hypothesis that the viability of was sample is less than the incubator control. All wells were significantly less than the control ($p<0.001$). Two-tailed paired t tests (or a pair non-parametric test for analyses involving well A4 data) were performed to assess whether location within the BEC had a significant effect on cell viability in the Clean Puff condition. Statistical differences were found between wells B1 and C3 ($p=0.003$), B2 and C3 ($p=0.002$), A3 and C3 ($p=0.01$), and A3 and C4 ($p=0.046$). A heat map of viability per well location for Clean Puff exposure in BEC is given in Figure 49b.

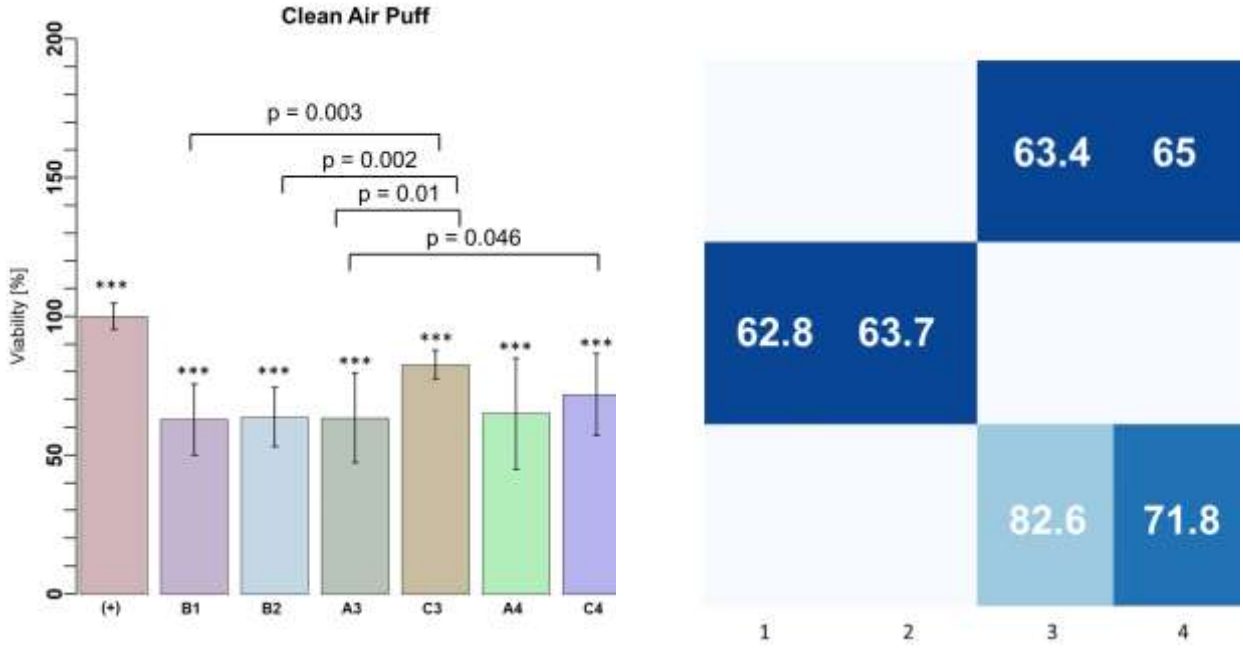

a) Viability in BEC with Clean Puff exposure and an incubator control. Asterisks denote statistical significance to the control with a one-tailed unpaired t test. Brackets denote significant difference with a two-tailed paired t test.

b) Means of viability in wells in BEC after Clean Puff exposure. Darker blue indicates lower viability. Light blue wells without labels were covered by the bifurcated flow path part and not exposed. Flow is left to right.

Figure 49 *Lab air exposed to 3T3 fibroblasts puffed in BAES using two the Puff Only topography profile. The topography profile was performed twice per sample.*

The Effect of Dose at the First Lung Bifurcation

Figure 50 illustrates the underlying cell viability data upon which subsequent inferences are conducted. To assess the effect of e-aerosol exposure on cell viability, 3T3 fibroblasts cultured at an ALI using Transwell inserts were exposed to 50:50 PG:GL with 5% nicotine (by mass) in a BLANKZ! Pod with a JUUL e-cigarette in the BEC with the Puff Only topography profile. The topography profile was performed twice per sample. This exposure is referred to as "Dirty Puff" exposure. Viability of exposed cells was assessed with an alamarBlue™ assay and normalized to an incubator control. Data points are labeled with Plate-Replicate format. The left digit denotes which plate the sample was in when it was exposed. Data from the same plate use the same style data marker. The right digit denotes the repeated measure of the data. Plates 1-3 did not have repeated measures while Plates 5 and 6 included three repeated measures for

each well. Plate 4 was excluded due to a systematic error and data for this plate is not included. Plate numbers given in Figure 50 correspond with Plate labels in Table 13.

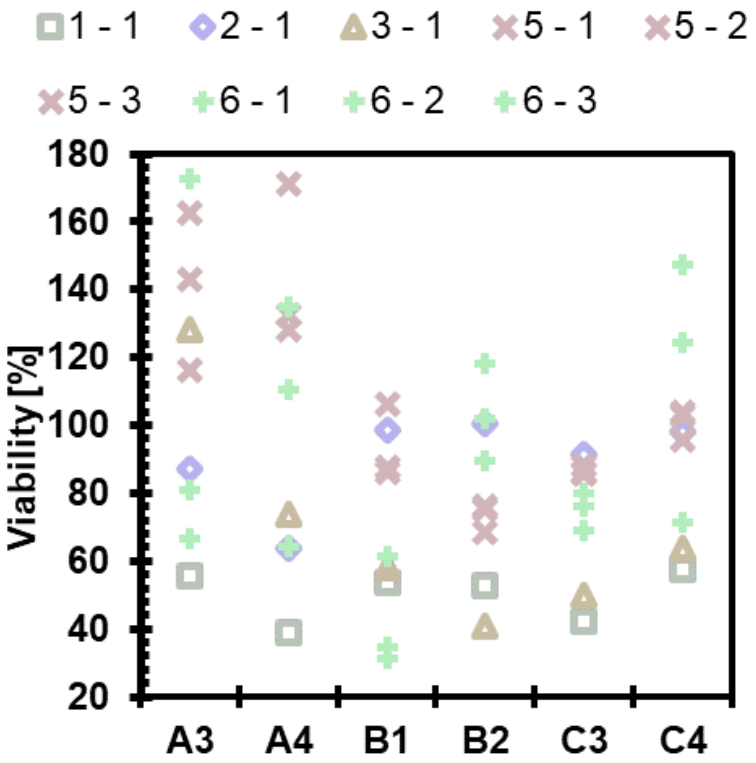

Figure 50 *Raw Dirty Puff viability data by plate location with repeated measures. Data points are labeled Plate-Replicate. Plates 1-3 did not have repeated measures. Plates 5 and 6 included 3 repeated measures for each well.*

Figure 51 shows mean viability of Dirty Puff exposure for each exposed well. All data was normally distributed per a Shapiro Wilks test with a sample size of 5 for each well. For Dirty Puff exposure, well B1 (p= 0.004) and C3 (p=0.0009) were significantly different than the positive control. A pairwise t test was conducted between each well of the Dirty Puff exposure dataset. There were statistical differences between wells B1 and A3 (p=0.009), B2 and C4 (p=0.04), A3 and C3 (p=0.02), and C3 and C4 (p=0.02).

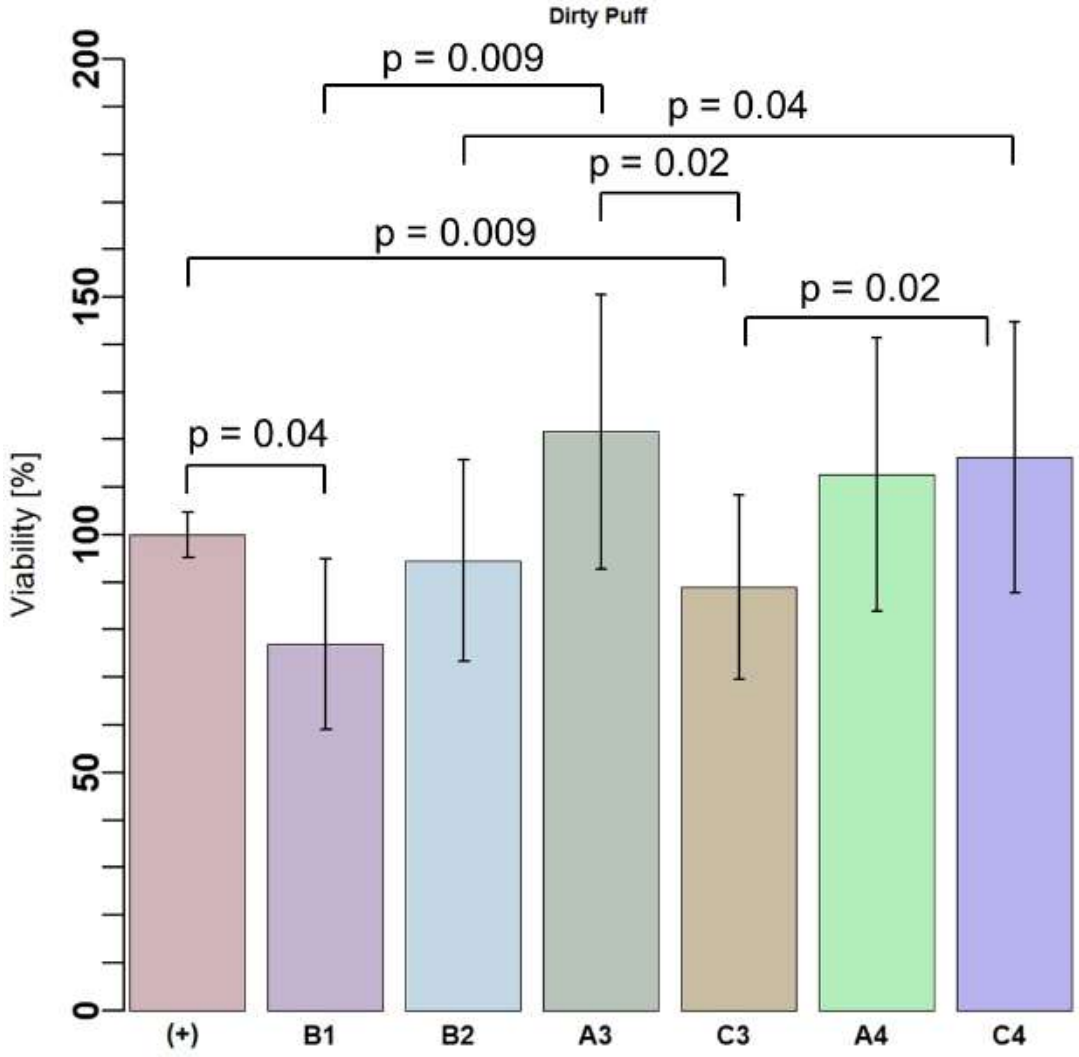

Figure 51 *Statistical comparisons of Dirty Puff viability data by plate location.*

Figure 52a gives a heat map of dose [mg/cm^2] in a 12-well plate in BEC measured in the mass characterization experiment described in Section 6.3. Figure 52b shows a corresponding heat map of viability of cells exposed under the same conditions, with the exception that mass measurements were taken in a BEC Insert in a 12-well plate in BEC while cells were cultured on Transwell inserts in a 12-well plate in BEC due to biocompatibility issues of the BEC Insert culture system described in Section 6.2.

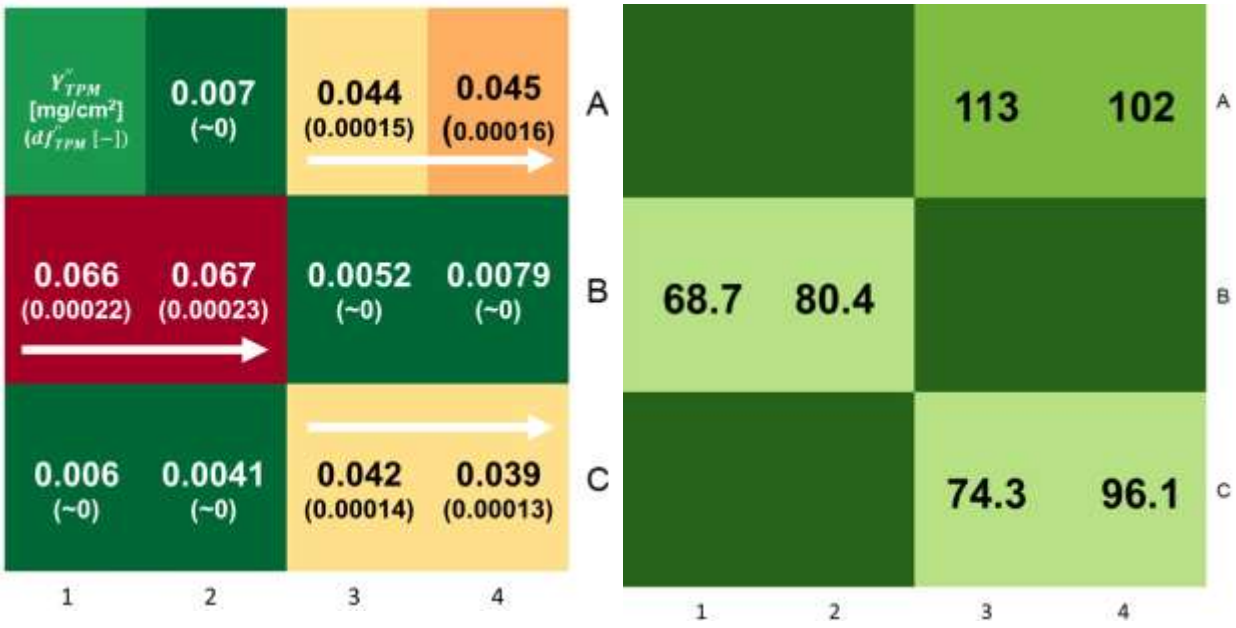

a) A heat map of mean mass deposition Y''_{TPM} [mg/cm^2] and mean df''_{TPM} [1/cm^2] in a 12-well plate within BEC. Arrows show flow direction of exposed wells.

b) A heat map of mean cell viability [%] in a 12-well plate within BEC. Dark green wells without labels were covered by the bifurcated flow path part and did not contain cultures. Flow is left to right.

Figure 52 *Dirty Puff dose and viability results presented as a heat map of a 12-well plate.*

Figure 53 shows a double bar graph of viability data comparing Clean Puff and Dirty Puff conditions. At all locations in BEC, viability was higher in the Dirty Puff condition than the Clean Puff condition, though only A3 (p=0.009) and A4 (p=0.047) exhibited statistical significance. Both datasets exhibited wide variability, with repeated measures of well viability ranging two-fold in some cases. This results support the Aim 4 hypothesis: “The viability of cells under no flow conditions, transverse flow of clean air, and transverse flow of ENDS aerosol will not be equal.”

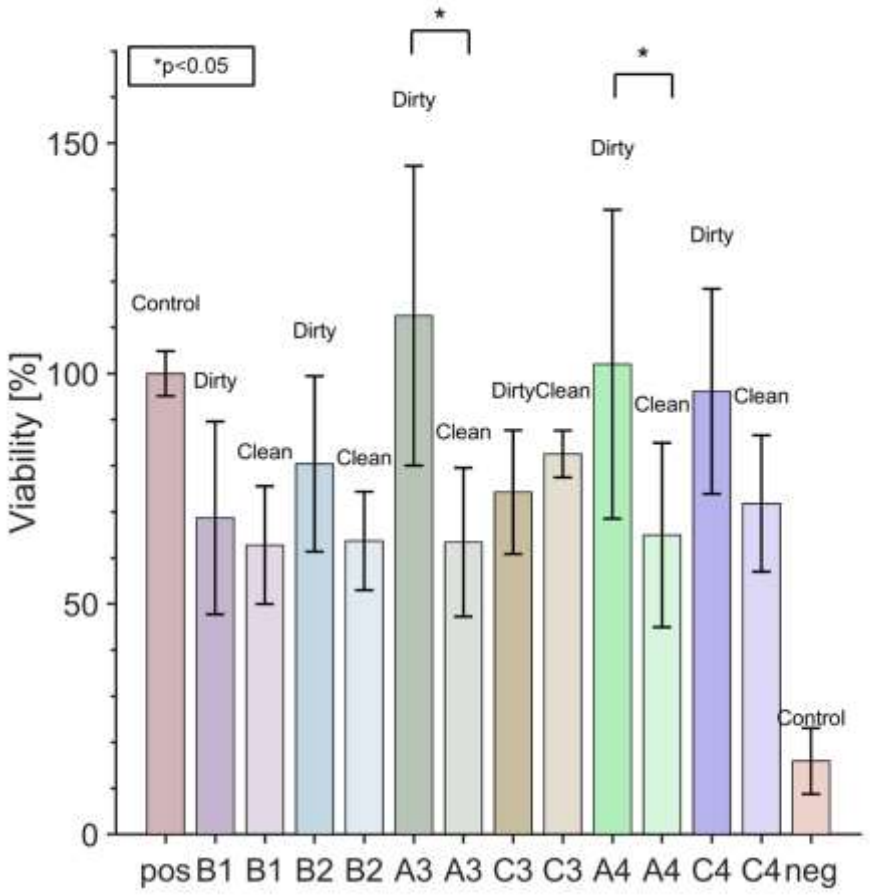

Figure 53 *A double bar graph showing mean cell viability per well for Clean Puff and Dirty Puff exposures. Error bars are 95% confidence intervals.*

In both types of exposure, cells in well C3 responded differently than those in other wells, including significant difference from well A3, which is symmetric to C3. This prompted examination of the bifurcated flow path part. Figure 54a is a photograph of the PDMS bifurcated flow path part after a Dirty Puff exposure. The photograph shows the cell-facing side of the bifurcated flow. Small bubbles (white arrows) throughout the part are a result of air trapped during the manufacturing process. Clouded, irregular blemishes between wells (black arrows) are condensation from aerosol exposure in the bifurcated flow path of the part. The condensation around well C3 (tan arrow) appears different than the other wells; the blemish extends around the top of the well, while other wells do not have any condensation around them, only between wells.

The bifurcated flow path part was fabricated by casting silicone rubber around a 3D printed core to form a flow path. The 3D printing process and the casting process each have a

manufacturing tolerance; in fused deposition modeling the primary source of error is related to the printer's nozzle diameter and z-step of the print bed, while in casting error is related to elastomer shrink during curing. Both processes are susceptible to part warping during material solidification. These tolerances add up to results in a larger deviation from nominal design in the resulting part. Therefore, channel height, the driving dimension in determining WSS in a rectangular channel (Equation 4), was measured above each well. Observed channel heights are given in Figure 54b. The channel in the C3-C4 branch was taller than the A3-A4 branch. The channel in the A3-A4 branch was more than 1 mm less than nominal (10 mm).

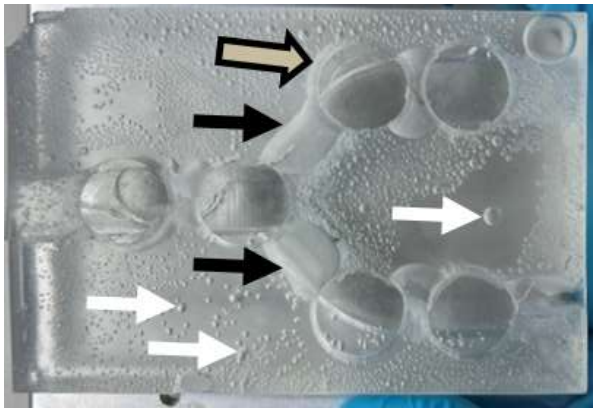

a) *The cell-facing side of the bifurcated flow path part after an exposure. Small bubbles (white arrows) throughout the part are a result of air trapped during the manufacuring process. Clouded, irregular blemishes between wells are condensation left from aerosol exposure in the flow path of the part (black arrows). The geometry of the condensation around C3 (tan arrow) appears different than other wells.*

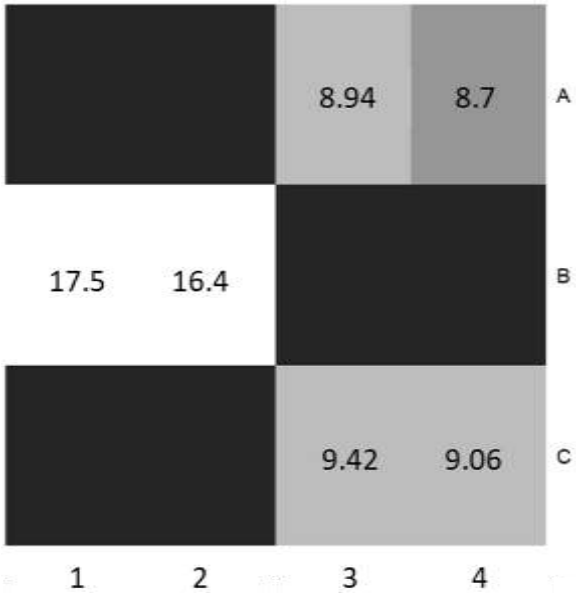

b) *A heat map of channel height [mm] in the PDMS bifurcated flow path part used for biological exposures. Lighter shading indicates a larger channel height over a well. Black wells without labels were not part of the flow path. Flow is left to right.*

Figure 54 *Qualitative and quantitative analyses of the BEC bifurcated flow path part.*

Figure 55 examines the multifactor relationship between viability, nicotine dose, and wall shear stress. Cell viability is affected by both dose (shown above) and wall shear stress (a function of flow rate). Meanwhile dose is dependent on puff flow rate [104]. Statistically

significant ($p<0.05$) Pearson Correlation r values, given on the figure, were found between all factors. Though the magnitudes of the Pearson r values are modest, their significance suggests the importance of these preliminary findings.

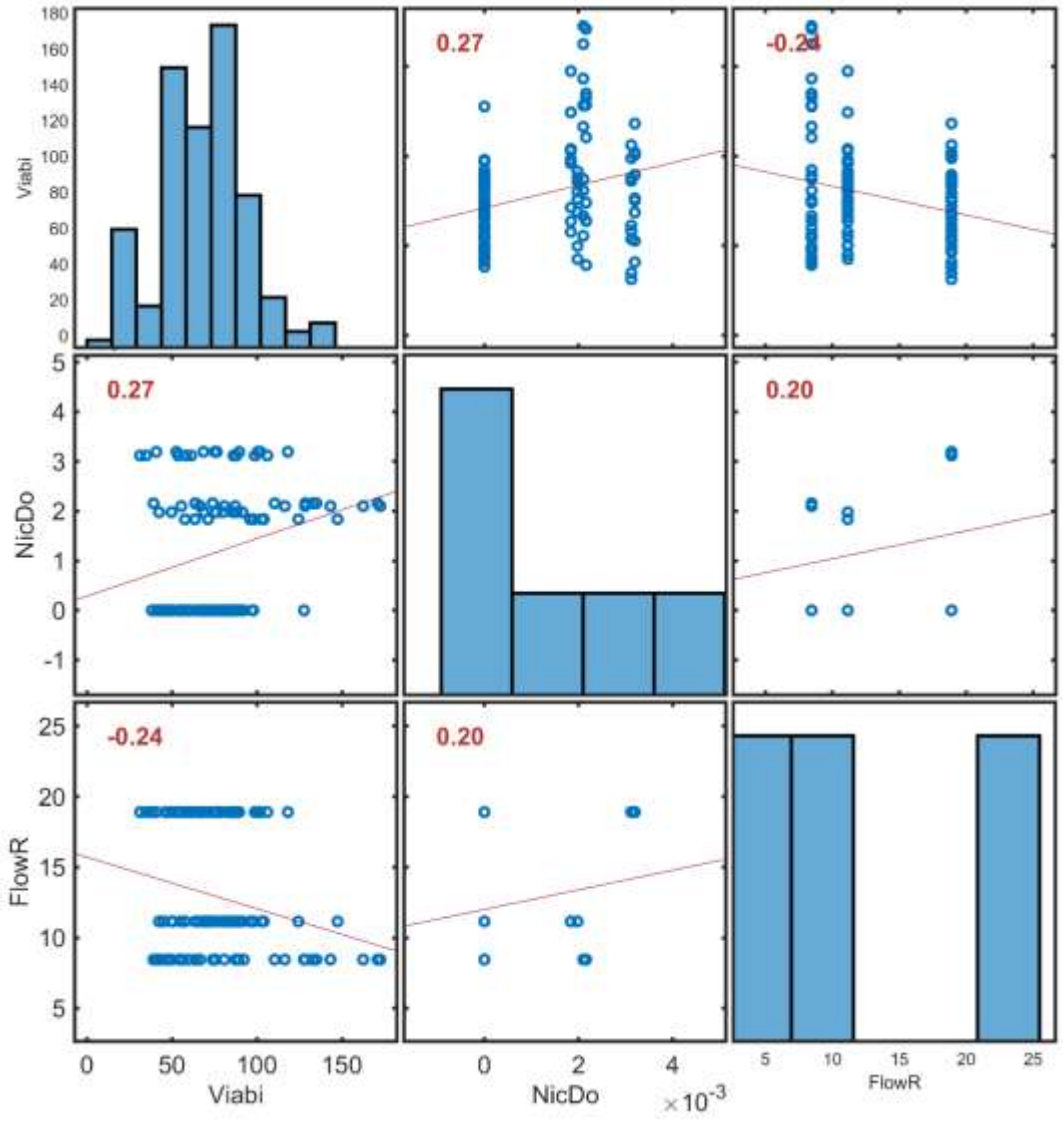

Figure 55 *A correlation matrix between viability [%], nicotine mass dose [mg /cm^2], and flow rate [mL/s]. Red r values indicate a significant correlation at alpha < 0.05.*

Figure 56 graphically shows the confounding effect of local flow rate on viability in both Clean Puff and Dirty Puff conditions. Raw Data is grouped by three mean channel flow rates (BEC inlet, left and right), with straight line regression models corresponding to the three

channel mean flow rates. The multiple linear regression predictive analysis was modeled using all viability (v [%]), nicotine yield per unit area (Y''_{NIC} [$\frac{mg}{cm^2}$]), and flow rate (Q [mL/s]) data:

$$v = 95.553 + 7730.8\,Y''_{NIC} + -2.04\,Q \quad (5)$$

Y''_{NIC} [mg/cm^2] is nicotine yield per unit area and is calculated from observed Y''_{TPM} by multiplying the mass fraction of nicotine in the e-liquid:

$$Y''_{NIC} = Y''_{TPM} \times f_{NIC} \quad (6)$$

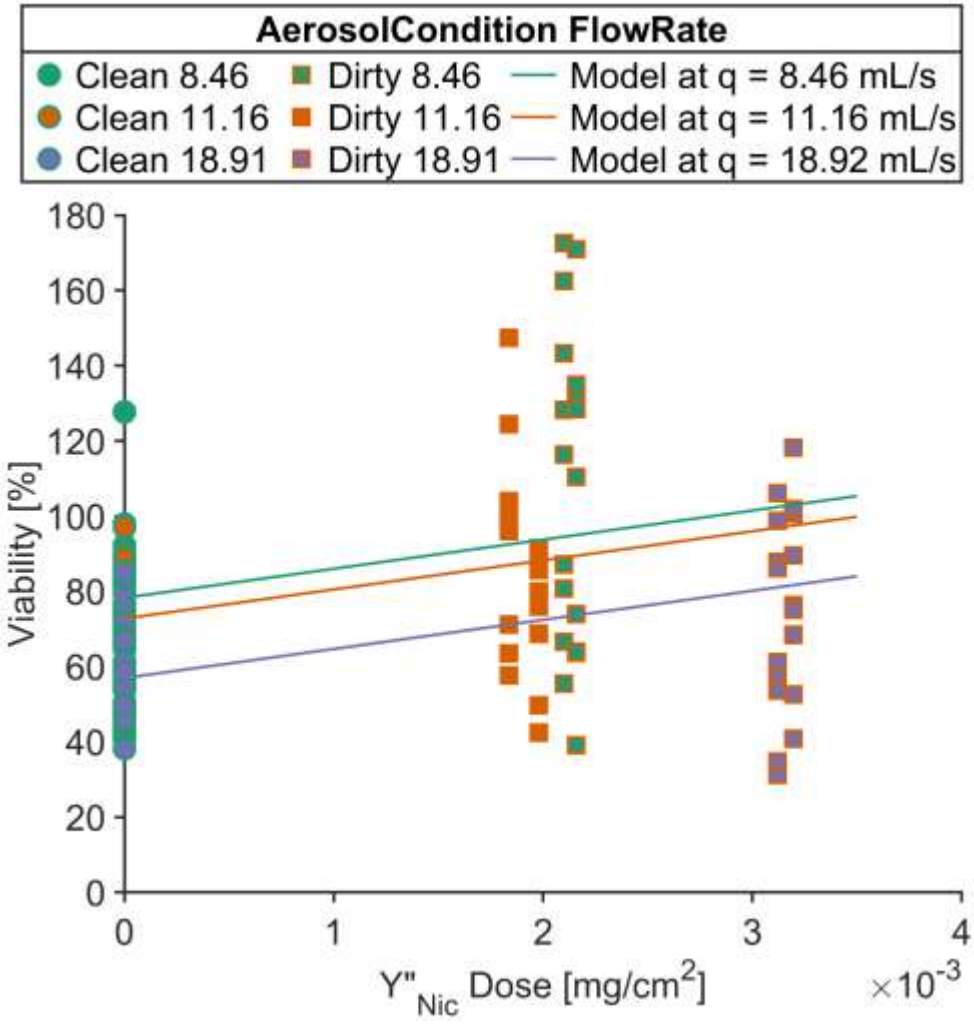

Figure 56 *Raw Data grouped by three mean channel flow rate (BEC inlet, left and right), with straight line regression models corresponding to the three channel mean flow rates.*

6.5 Summary of Use and Outcomes (Aim 5)

Constructing a Dose Response Curve from BAES Output

Figure 57 illustrates how datasets produced using BAES are interpreted to produce a dose response of 3T3 fibroblasts exposed to e-liquid composed of 50:50 PG:GL with 5% nicotine when aerosolized with a JUUL e-cigarette at 25 mL/s for 50 puffs, without clean air inhalation. BAES enables high-throughput aerosol exposure to several samples at multiple doses in a single trial. Data output from BAES studies allows construction of a dose response curve by delivery of a dose of aerosol dependent on axial system location. Figure 57a gives dose distribution, Y''_{TPM} [mg/cm^2], as a function of system location. Figure 57b gives cell viability, an exemplar biological endpoint, as a function of system location. Figure 57c shows how the datasets combine to produce an abbreviated dose response curve for the first generation, where flowrate was measured at 18.92 mL/s at the BEC inlet. Figure 57d shows cell viability as a function of dose normalized to deposition fraction of total particulate matter, df_{TPM} [1/cm^2] per unit area. Each data point represents cell viability when exposed to a fraction of the total aerosol produced by this product-geometry-behavior combination. Computational models of aerosol inhalation often report dose as deposition efficiency at an airway location [179]. This proposed input measure, df''_{TPM} [1/cm^2], enables seamless comparison between *in silico* and *in vitro* models. Results given in Figure 57 support the Aim 5 hypothesis: “The BAES can be used for acute exposures of cell cultures under higher fidelity dose, geometry and flow conditions in comparison to traditional machine puffing emissions systems.”

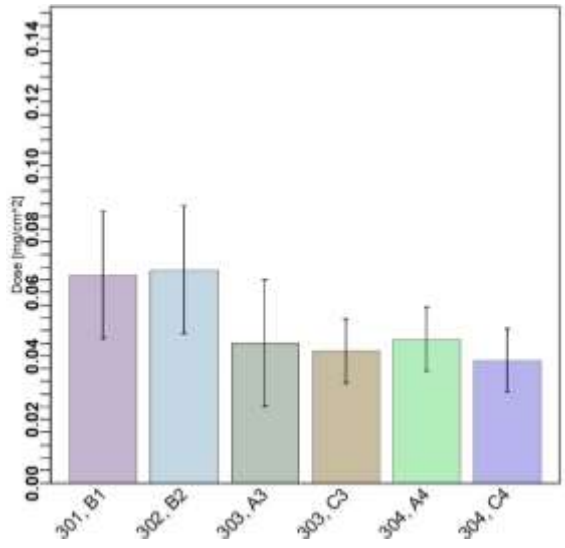

a) *Dose, Y''_{TPM} [mg/cm^2], as a function of axial location (state number, well).*

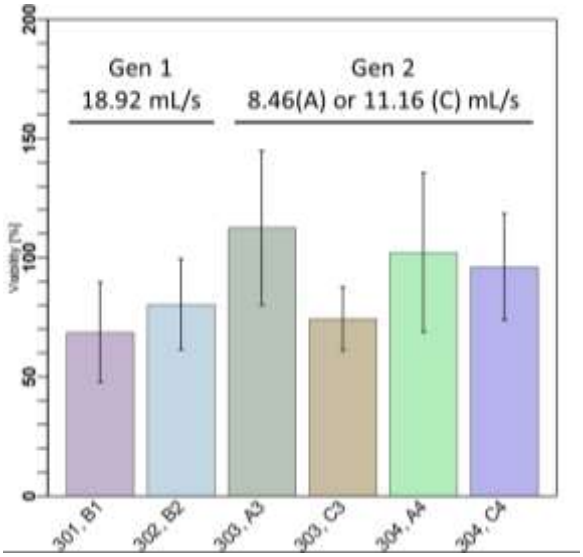

b) *Cell viability as a function of axial location (state number, well).*

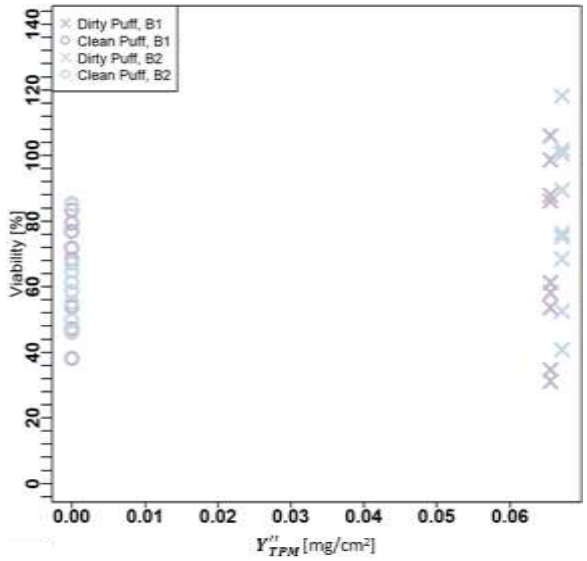

c) *Cell viability as a function of dose, Y''_{TPM} [mg/cm^2] at 18.92 mL/s.*

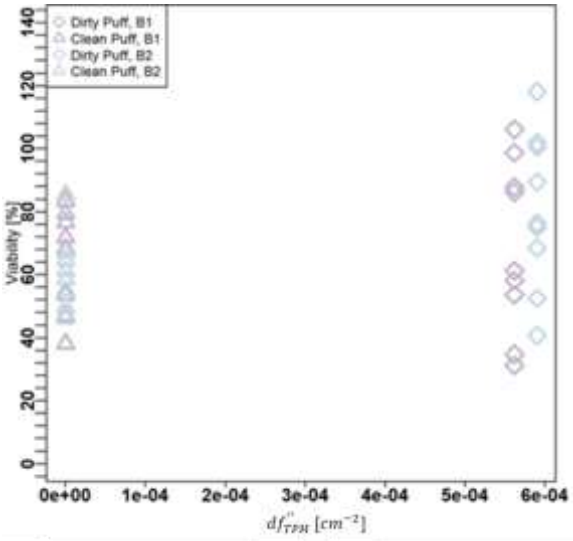

d) *Cell viability as a function of deposition fraction per unit area, df''_{TPM}, [1/cm^2] at 18.92 mL/s.*

Figure 57 *Viability and mass dose data sets from BAES are used to product dose response curves for a given product-geometry-behavior combination.*

CHAPTER 7. DISCUSSION

Current emissions systems do not concurrently mimic both user behavior and airway geometry. This work documents what appears to be the first aerosol generation and integrated emissions exposure and capture system with high fidelity geometric and puffing/respiration biomimicry, with inhalation of lab air through the same inlet as the puff, closely mimicking the flow path of e-cigarette aerosol and accompanying clean air inhalation by users.

7.1 Design and Fabrication of a Biomimetic Aerosol Exposure System

A variety of exposure systems have previously been used for toxicology testing of aerosols; some *in vitro* toxicology testing systems bear little resemblance to the geometric and flow conditions of the human airway [44, 76, 138]. Conversely, organ-on-a-chip systems [84] seek to achieve high fidelity local conditions, but do not capture a systems level view of either the airway or the flow conditions. Current emissions systems do not mimic both user behavior and geometric biomimicry. The Biomimetic Aerosol Exposure System (BAES) achieves a middle ground between two extremes, while incorporating many appealing attributes previously reported.

This work demonstrates a novel biomimetic Oral Cavity Module (OCM) (to act as an “inlet filter”) based on medical imaging data. Further, when the OCM is accompanied by the inhalation subsystem, the result represents a first of its kind emissions and exposure system. The OCM’s alternate inlets offer modularity by providing the ability to connect additional lines to the module for alternative breathing patterns, including bidirectional breathing. While the oral cavity geometry used in the OCM was from a 3D scan of a cast [91], prior work [180, 181] has demonstrated the ability to convert medical imaging data from computed topography scans into a digital format that can be manipulated in CAD software and 3D printed. The modular design of the BAES readily permits the OCM to be interchanged for the purpose of conducting studies on the effect of oral cavity geometry (accounting for biological sex, age, number of teeth, and other factors) on dose delivered within the oral cavity and down-stream. Prior computational work has suggested anatomical variability e-aerosol deposition [179]; BAES provides the tools to model this empirically with patient specific anatomies.

The Bifurcated Exposure Chamber, BEC, provides the ability to expose samples to transverse flow, placing them in the free stream of flowing aerosol resembling a mesoscale analog to lung-on-a-chip. The meso-scale model proposed here offers promise for such future

innovation in 3D tissue modeling and tissue engineering. Shortcomings of organ-on-a-chip platforms include high cost and a need for specialized equipment. This technology for transverse flow exposure at an air-liquid interface (ALI) uses low cost and commercially available materials to address these shortcomings. The modular design allows a variety of culture systems to be used within BEC. Design of a novel ALI culture insert was described. Commercially sold inserts, such as Transwell® inserts, are compatible with the module. At the same time, the BAES offers the ability to integrate lung-on-chip models down-stream from the exit of the BAES, using side stream sampling, so the benefits of micro-scale lung on a chip models can be leveraged in addition to the system flow conditions provided by BAES.

Results of this dissertation support that respiratory topography has a significant impact on particle deposition in an emissions system. Many emissions systems do not support variable flow rates that mimic human puffing topography or the ability to inhale ambient air between puffs as a user would. The development of the clean air inhalation subsystem enables ambient air inhalation through the primary system inlet. A straight-forward but valuable extension to the BAES presented here would include addition of an exhaled breath system.

The manner in which a device under test is connected to an emissions system is undervalued and may have important implications on the results obtained. Standard emissions protocols [141, 142] describe an airtight seal between a device being tested and the emissions system, but do not comment on this connection as a source of deposition in the system. The length and geometry of this connector may be particularly important when conducting emissions testing of condensing aerosols such as those generated by ENDS. We describe a streamlined device specific adapter for a JUUL e-cigarette. By applying the given equations to the exit geometry of other e-cigarettes, the component can be adapted for other products. The BAES ENDS adapter was compared to a traditional emissions setup that used flexible tubing to connect the electronic nicotine delivery system (ENDS) under test to the emissions system inlet. Results indicate that ~12% of aerosol in a traditional emissions testing setup was deposited between the e-cigarette and the filter pad or were volatiles which exited the system exhaust. That number was reduced to 10% when using the ENDS adapter. Though the difference in deposition fraction between the ENDS adapter and a short tubular connector was not significant, the ENDS adapter reduces risk of operator error and inconsistent assembly. The methods and results demonstrated herein provide a means for quantifying the impact of the connector geometry, and its flow path length, on the emissions results reported. The device specific adapter controls the distance an e-cigarette can be inserted into it, enhancing

repeatability between emissions trials. Further, the device specific adapter eliminates the need for laboratory film to seal joints between tubing, therefore reducing assembly steps, increasing throughput.

Pearson Correlation Coefficients between Deposition Fraction and TPM per puff for the Baseline and ENDS adapter conditions show that there is a correlation between the amount of e-liquid a device aerosolizes in a puff and deposition early in the flow path when using a third-party pod with the e-cigarette. This phenomenon suggests that device performance may affect particle size distribution, therefore where aerosol deposits in an emissions system and in the human airway. Future work should study the effect of device parameters (power, temperature, coil resistance) on aerosol particle size, the variation in these parameters within a single device and a single manufacturer, and if this variability changes with use of third-party products such as BLANKZ!. Particle size of vaping products has been analyzed using optical particle sensors [54] and could be easily integrated into BAES.

7.2 Validation and Characterization of BAES

Mass characterization quantified deposition fraction in each BAES configuration as a function of emissions topography profile (ETP). The hypothesis of Aim 2 was: “Aerosol particle deposition and local flow conditions in machine puffing systems depend upon puff and respiration topography, referred to as the ‘system flow conditions’. This is true both in simple and complex system geometry flow paths.” The Puff Only ETP was significantly different from ETPs with clean air inhalation following puffs in both the Adapter + OCM and Full Assembly BAES configuration. Deposition fraction in the Adapter + OCM configuration increased as a function of PAR flow rate/duration from Puff Only (0mL/s, 0s) to PAR350 (350mL/s, 4.3s PAR), then decreased with PAR450 (450mL/s. 3.33 s PAR). Deposition fraction in the Full Assembly configuration decreased as a function of PAR flow rate/duration from Puff Only (0mL/s, 0s) to PAR350 (350mL/s, 4.3s PAR) then increased with PAR450 (450mL/s. 3.33 s PAR). There may be a trend when flow rate of the PAR is varied, but results were not statistically significant and more data is needed before conclusions can be made regarding differences between ETPs with ambient air inhalation between puffs. The physics of particle deposition suggests that there will be a difference in deposition by impaction as a function of flow rate [182]. The significance of this difference in BAES geometry should be assessed in future work. This result supports the premise that inhalation topography should be included in emissions and biological exposure studies. This is the first time that the impact of clean air inhalation through a primary system inlet has been reported.

The large difference in deposition in the OCM Insert between topography profiles highlights the importance of simulating user puffing and respiration behavior through a system's primary inlet instead of in a dilution chamber as other systems have done [84]. There was dramatically higher deposition in the Puff Only condition compared to all conditions with ambient air inhales, especially those with long PAR flow durations. These results demonstrate how clean air oral inhalation through the same inlet as a puff impacts aerosol distribution. The duration of the post-puff breath hold may also have an impact on deposition in the Oral Cavity Module and should be investigate further with clinically relevant breath hold durations.

The computational model of BAES suggests that cultures on custom inserts inside of BEC would experience WSS between 0.010-0.019 Pa. WSS in the lung during inhalation has been estimated with CFD to be between 0.01 and 0.5 Pa in early lung generations, depending on lung location, geometry, and inhalation flow rate [91, 174]. Flitney and colleagues demonstrated that exposure to shear stress as low as 0.7 Pa resulted to cytoskeletal morphological changes in alveolar epithelial cells, indicating that these predictions are the correct order of magnitude [183]. Work from Mahto 2014 showed that cells remained viable after exposure to 2 Pa of shear stress for 20 minutes [172] indicating that the magnitude of fluid shear presented to cells inside of BEC will not lead to acute cell death. With BAES paired with the linear program (LP), wall shear stress can be fine-tuned by identifying desired wall shear stress and system geometry, then utilizing inlet flow rate prescribed by the LP model. The BAES LP model helps optimize how to operate and guide design of the *in vitro* system.

The computational model of BAES provides a tool to determine the inlet flow rate of an *in vitro* aerosol exposure system, subject to constraints related to operation of an aerosol generator, puff/inhalation topography, wall shear stress, flow regime, and lung model geometry. The result of this model prescribes the input parameters for a given *in vitro* system. The LP model showed that the optimal flow rate to maintain a physiological environment, given the described constraints, is ~510 mL/s. The upper limit for flow rate in BAES is limited by the system flow meter that provides real time feedback to the controller to maintain command flow rate. The system flow meter used has a reported upper limit of 500 mL/s, however we observed significant deviation from command flow rate above 450 mL/s. Therefore, the maximum inhalation flow rate reported in this study was 450 mL/s puff associated respiration (PAR). Due to the limitation of the system flow meter, the current system configuration is just shy of maintaining physiological wall shear stress in generation 2. Empirically modeled wall shear stress in generation 2, which had a lower target of 0.02 Pa, was 0.017 ± 0.003 Pa in the left

branch and 0.019 ± 0.003 in the right branch. The actual dimensions of the second generation branch channel part were less than the nominal channel width and height. This can be attributed to poor resolution in the z-direction of fuse deposition modeling 3D printing used to fabricate the mold's core and shrink of the elastomer upon curing. The decreased channel height resulted in a higher wall WSS than predicted in the LP model and the upper limit of uncertainty fell within the target range for WSS. Future work can ensure the physiological WSS is maintained by replacing the system flow meter in BAES with an instrument with a higher detection limit or by reducing the height of the flow channel in generation 2. This work demonstrates the utility of computer simulation using a LP model, which requires less time and computational power than computational fluid dynamics. Correlating *in silico* models of the human respiratory tract with *in silico* models of the BAES may provide a mechanistic foundation for relating *in vitro* biological outcomes obtained in the BAES with anticipated human outcomes.

A BEC Insert with alginate scaffolds was introduced as a novel cell culture system that places a cell monolayer in the free stream of flowing aerosol. 7% alginate in a petri dish was cured in a Calcium Chloride ($CaCl_2$) bath, then punched from the 55 mm disc created from the curing process. Surface topography of the alginate disc varied based on how slowly and evenly the alginate containing petri dish was lowered into the $CaCl_2$ bath. If the petri dish was not even with the surface of the bath, the alginate disc was thicker on the side that was lower. If the alginate began to splash or mix as it was lowered into the bath, still in its liquid form, the resulting disc exhibited uneven surface topography. When selecting areas of the disc to punch into cell culture scaffolds, areas of uneven topographies were avoided in order to achieve macroscopically smooth scaffolds. When making scaffolds, a good rule was to make two alginate discs per 12 scaffolds (enough to fill a 12-well plate). Two alginate discs allowed selectiveness in areas scaffolds were punched from the disc. The scaffold fabrication process described provides a low-cost, high throughput method for fabricating hydrogel scaffolds at a defined height and diameter.

Cells did not attach to the alginate scaffold in the BEC insert. Cells cultured on the Transwell® insert attached to the substrate and morphology appeared elongated, typical of a healthy fibroblast [184]. Meanwhile, the few cells cultured on alginate that did attach appeared round and smaller in diameter than cells on the Transwell insert. This round morphology is indicative that the cell traction force on the alginate scaffold, which is related to substrate stiffness and surface topography, inhibited cell spreading [185]. Prior work that utilizes alginate concentrations ranging between 2.5% and 15% as a scaffold material and showed adequate

cell attachment and survival with cell proliferation decreasing as alginate concentration increased [186]. The source of non-compatibility of alginate scaffolds in BEC Inserts should be investigated further in future work. Parameters to investigate include alginate concentration (both increase and decrease from 7%), protein coatings, surface modifications, and addition of solutes, such as metallic nanoparticles, in alginate solution to enhance cell health. Utility of culture inserts with the ability to place cell monolayer in the free stream of flowing aerosol would be a significant contribution to the fields of environmental medicine, pulmonary toxicology, pulmonary pathology, and tissue engineering/regenerative medicine.

7.3 Demonstrate Emissions Testing Capability of a Biomimetic Aerosol Exposure System

Specification of fraction of aerosol deposited in each emissions system region, including accounting for matter that exits the system exhaust as volatile matter, has never been published. We provide analysis that maps the distribution of aerosol throughout BAES. Many emissions studies use the assumption that all mass leaving the device under test travels to an emissions exposure or capture subsystem [44], which is treated as the control volume. This poor assumption skews both analytical and topological results [187]. The entire system from inlet to exhaust should be treated as the control volume. Mapping mass distribution within the system is necessary to understand doses deposited in an emissions capture or exposure module. The deposition fractions given in Section 6.3 account for aerosol that was deposited in the adapter, tubing, or inlet of the filter pad holder and for volatile matter. Mass balance using direct measurements of several components allowed us to estimate mass that underwent a phase change during aerosolization and account for mass deposition in transit to an exposure module. We estimate that the fraction of mass that exits BAES in the gas phase is 7.4%. This is consistent with other work that estimates that thermal decomposition of PG yields ~14% of PG in the gas phase, compared to that of the e-liquid. With e-liquid containing 50:50 PG:GL, this is consistent with loss of ~7% [188]. The biomimetic geometry of BAES is designed to create mass deposition along the flow path similar to aerosol dynamics in the airway.

We observed a larger range in emissions from a third-party pod compared to a JUUL brand pod (Figure 45) when both were aerosolized by a JUUL e-cigarette. The mass of e-liquid aerosolized when using the BLANKZ! pod was more than threefold compared to a JUUL brand pod. The Food and Drug Administration (FDA) must consider the variability in device performance of products available to users, especially when used with products unintended by

manufacturers. Variability in product combinations and device performance will make it nearly impossible to isolate factors during outbreaks of e-cigarette related disease, such as e-cigarette and vaping associated lung injury (EVALI), which is still not fully understood four years after initial outbreak [189].

A variety of third-party products are available on the market to be used with a JUUL e-cigarette, many of which allow users to fill pods with their choice e-liquid. The market for refillable pods increased when the FDA banned the sale of flavored e-liquid in 2020 [20]. BLANKZ! pods are one of several third-party products compatible with the JUUL device. Other examples include YOUFILL (https://youfillpods.com) and CROWN (https://heat-tobaccos.com/product/crown-refillable-JUUL-pods/). YOUFILL offers multipacks of pods that claim to be refillable up to seven times, while CROWN pods are marketed as BLANKZ! pod alternatives that can be refillable 2-3 times. Even more concerning, JUUL compatible pods filled with fruit flavored CBD-containing e-liquid are available for purchase. One manufacture is called HEMPZILLA and markets ”JUUL-compatible…pods… formulated with our 300mg line of broad-spectrum, non-GMO CBD” (https://hempzillacbd.com/product/cbd-JUUL-pods/). A high throughput system that allows dose and biological endpoints as a function of product and puffing and respiration topography provides realistic and translatable toxicity results. BAES provides a platform to study the effects of product, behavior, and human geometry.

7.4 Demonstrate Toxicology Testing Capability of a Biomimetic Aerosol Exposure System

A correlation matrix between viability, flow rate, and mass dose showed significant correlations between all factors. Flow rate confounds the effect of aerosol dose on viability with flow rate being negatively correlated with viability and mass dose being positively correlated at the doses we tested. Our multiple linear regression model provides an estimate of viability based on nicotine yield, Y''_{NIC} [mg/cm^2] and flow rate. These findings support that flow rate is an important factor to mimic in *in vitro* airway models and should be held constant at a physiologically relevant magnitude and reported when studying the effect of dose on a biological endpoint. The modularity and multiple analysis capabilities of BAES allows control over mass dose and flow rate.

NIH 3T3 cells were exposed to lab air with Puff Only topography parameters. Viability of all Clean Air exposed samples were significantly lower than an incubator control. Cells in well C3 in BEC exhibited statistically significant higher viability than cells in wells B1, B2, and A3.

Cells in C4 exhibited higher viability than in A3. Meanwhile, the channel height above cells in row C of the multi-well plate was slightly larger than those in row A. This is consistent with higher observed flow rate at location F2, the outlet of the C-C4-F2 branch. Despite the flowrate and channel height asymmetry, WSS calculated in each branch with the PDMS bifurcated flow path part was near identical. Since viability was higher in wells C3 and C4, WSS alone was not responsible for decreased viability in the Clean Puff exposure. Prior work speculates that the geometry of commercial culture inserts, such as the ones used in this work, cause recirculation and turbulence that cause non-physiological stress on cells [1]. Local flow conditions arising from exposure geometry may have had an impact on Cean Puff viability results.

When exposed to e-cigarette aerosol, cells in wells B1 and C3 exhibited significantly lower viability than the positive control. While viability was significantly higher in C3 and C4 than other BEC locations in Clean Puff exposure, mean viability of cells in well C3 was lower than A3 in the Dirty Puff condition. Wells C3 and C4 are on the side of the flow path of measurement point F2, which showed a significantly lower deposition fraction than F1 in Section 6.3. Additionally, doses measured in wells C3 and C4 were lower than dose in A3 and A4, though not statistically significant. Nitrosamines from tobacco aerosol activate nicotinic acetylcholine receptors, which promote cell proliferation, cell-cycle progression, and angiogenesis [190, 191]. Lower deposition with lower viability in the C3-C4-F2 branch supports that nicotine exposure was responsible for higher viability of cells in the Dirty Puff condition compared to the positive control and to the Clean Puff condition. This also supports that cytotoxicity as a sole endpoint does is not adequate for risk assessment of tobacco related disease and injury caused by e-cigarettes. Additionally, commercial e-liquid contains additives other than nicotine. Investigations of ENDS induced oxidative stress, extracellular matrix stiffness, and gene expression will enhance investigations of the safety profile of ENDS.

The range of doses demonstrated is insufficient for a full dose response curve. The general approach remains valid, and even more so, in the presence of additional downstream BECs in series and/or in parallel. A roadmap for continued development is available in Figure 27 in Section 5.2.1, including the addition of two BEC beta modules intended to model generation three and generation four in a 96-well plate. A digital model of a preliminary BEC beta design is available to the Respiratory Technologies Lab for further development. Wall shear stress and nominal flow rates in BEC beta are predicted using the linear programming model with results given in Figure 28 in Section 5.2.1. The addition of BEC beta will enhance the utility of BAES by

producing an additional 64 data points in a single trial, accounting for two additional lung generations, and resulting in a greater number of observable doses and repeated measures.

Viability data showed high variability, especially in the Dirty Puff condition. This may be attributed to exposure occurring with samples in different stages of their cell cycles, therefore nicotine induced upregulation of cell proliferation led to variable observable effects. In the future, cells should be starved in serum free media for two hours before e-aerosol exposure. Additionally, a two-part viability study should be employed, such as with alamarBlue™ and lactate dehydrogenase assay. Despite high variability in viability data, we did obtain significantly significant results that are consistent with dose and flow rate data.

A limitation of viability results is that dose measurements were taken in a BEC Insert in a 12-well plate (Figure 58a-b) in BEC while cells were cultured on Transwell insert inserts in a 12-well plate (Figure 58c-d) in BEC due to biocompatibility issues of the BEC Insert culture system described in Section 6.2. The depth of the BEC culture insert is 3.81 mm (Figure 58b). The nominal height of an alginate scaffold is 3.81 mm, leaving the cell monolayer flush with the top of the well and directly on the wall of the flow path of the BEC. During mass characterization, BEC inserts were filled with deionized water to achieve the same geometry as with a scaffold. The culture surface of a Transwell insert is 17.37 mm below the top of a well (Figure 58d). This is a 22% difference and may lead to discrepancies in predicted dose. Figure 58e shows the possible effect of free stream angle and culture surface height on aerosol concentration on the culture surface. Panel 58e-i shows submerged culture, which the field of pulmonary toxicology has largely moved past given available technologies [83]. Panel 58e-ii shows an ALI culture using commercial culture inserts with aerosol flow normal to the cell monolayer, a method typically used in the field, such as with Vitrocell systems [158], but does not consider mechanical cues on cells. Panel 58e-iii shows air-liquid interface culture using a commercial culture insert with aerosol flow transverse to a cell monolayer. This level of biomimicry was achieved in this work. Panel 58e-iv shows an illustration of the BEC Insert with a cell monolayer in the free stream of aerosol, a goal of future development of the culture system. This graphic was adapted from an artist rendering that depicted an objective of this work: to culture cells in the stream of flowing aerosol.

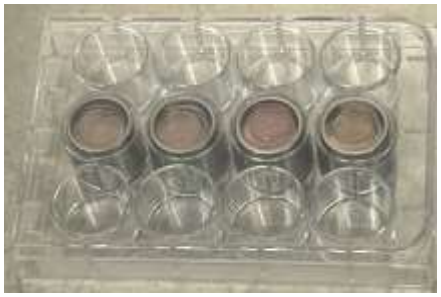

a) A photograph of BEC inserts with cells seeded on alginate scaffolds in a 12-well plate.

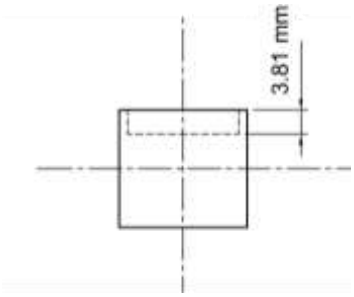

b) A schematic of a section view of a BEC insert well.

c) A photograph of cells seeded on Transwell inserts in a 12-well plate.

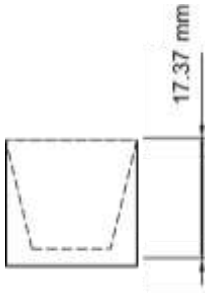

d) A schematic of a Transwell® insert in a 12-well plate well.

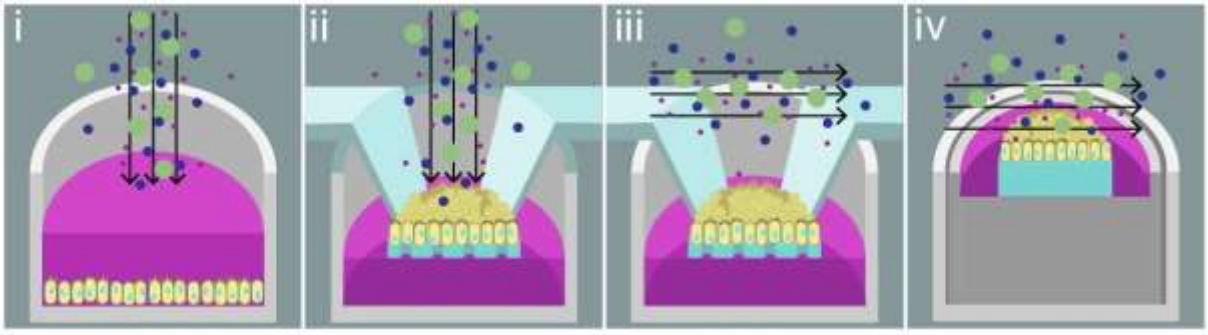

e) Panel i shows submerged culture, panel ii shows air-liquid interface culture using commercial culture inserts with aerosol flow normal to the cell monolayer, iii shows air-liquid interface culture using commercial culture inserts with aerosol flow transverse to a cell monolayer. Panel iv shows a rendering of the BEC Insert with cell monolayer in the free stream of aerosol. Adapted from a graphic by Tirzah Pilet.

Figure 58 *A comparison to BEC inserts and Transwell® inserts in a 12-well plate and how utilization of each compare to the objective of this work.*

Proof-of-concept studies demonstrate the toxicology testing capabilities of BAES. To allow optimization of the exposure protocol in future work, the amount of time cell cultures spent outside of a controlled environment was measured (Table 13). The time samples spent outside of the tissue incubator is longer than time spent in BAES. Time outside of environmental control but not in BAES reflects the amount of time it takes to place multi-well plates inside of BEC, seal the chamber, transfer samples from the cell culture lab to the emissions lab, commence puffing using the BAES software's graphical user interface, and transport cultures back to the cell culture lab. In rare cases, such as with Plate 1, unanticipated software issues stall the experiment. Differences in "Time in BAES" between samples reflect the amount of time it takes to change the e-cigarette between topography profiles and interact with BAES software. "Clean Puff" condition samples used an empty pod and discharge PCU, therefore the device did not need to be changed between puffing profiles, reflected by shorter "Time in BAES" for this condition. The protocol for biological exposure to e-cigarette aerosol ("Dirty Puff") requires two operators: one to measure pod and pad weights and one to handle biological samples and operate BAES. During air only exposures, mass measurements are not necessary and one operator is sufficient. Overall, the exposure process is quite streamlined and is limited by transferring samples between locations and waiting for computer processes. The main source of "slack" is in transferring samples between physical locations, which could be significantly decreased by having cell culture capabilities closer in proximity to BAES. A long-term goal of BAES is to integrate environmental control into the system, enabling sub-chronic ENDS exposure.

7.5 Summary of Recommended Use and Outcomes

An objective of this dissertation, given in Section 2.4.1, was to recommend standard input measures for toxicology testing of inhaled tobacco products. We recommend reporting dose as:

- Y''_{TPM} [mg/cm^2], total particulate matter per unit area
- df''_{TPM} [1/ cm^2], deposition fraction of TPM per unit area

Given the ability to measure and calculate mass per unit area in BAES, the practice of seeding cell monolayers at a known cell concentration based on unit area, and the morphology of the human airway, dose per unit area, Y''_{TPM} [mg/cm^2], may enable better repeatability and translation. In biological work, understanding mass dose is important. However, to understand the distribution of aerosol exposure throughout the airway and to account for the variability in e-

cigarette performance, both between products and for a given product, normalization is necessary. We present biological response of exposure to a fraction of the total aerosol produced by a specific product-geometry-behavior combination, deposition fraction per unit area, df''_{TPM} [1/ cm^2]. This data provides insight into toxicity of ENDS aerosol distributed throughout the airway, building upon the traditional method of reporting toxic response to an entire dose of aerosol from an e-cigarette. Normalized reporting metrics better captures the non-homogenous distribution of aerosol throughout the respiratory tract and represents a first step in identifying mechanisms of disease, particularity understanding where initiation of disease or injury may occur.

In a narrative review, Polosa 2019 states "*in vitro* exposures need to be contextualized with normal conditions (user exposures) and require the assessment of key dosimetry markers, such as nicotine or glycerol ratio, to 'normalize' exposures [192]." While normalization to a dosimetry marker is critical for baseline toxicology work, studying realistic behaviors and physiologically relevant exposures is needed to understand health effects of ENDS use. We observed a vast range in performance of the e-cigarette products studied (Figure 36, Figure 45), especially when used with a third-party product, which aerosolized between 2-10 mg of e-liquid per puff. As a result, normalizing to a particular dosimetry parameter would prohibit researchers from aerosolizing e-liquid with e-cigarette devices users actually use during exposure studies. This supports use of a normalized parameter, df''_{TPM} [1/cm^2], as an input measure reported in toxicology studies and facilitates correlations between *in vitro* results and *in silico* models.

A novel aspect of BAES is that analytical work and biological experiments are performed using an identical set up. Generation of a dose response curve requires two steps. First, exposure of dyed e-liquid to BAES with BEC Inserts filled with deionized water to conduct mass measurements on each insert using an absorbance plate reader. Next, exposure to cell cultures in BEC, under identical conditions other than absence of dye in e-liquid, and analysis of a biological endpoint of interest. With these two data sets are obtained from exercising a single exposure protocol, a dose response curve with doses relevant to the upper airway and first two lung generations are generated.

CHAPTER 8. CONCLUSIONS AND FUTURE DIRECTIONS

This work demonstrated proof of concept for a novel Biomimetic Aerosol Exposure System (BAES) useful for analytical and biological testing of inhaled tobacco products under realistic use and exposure conditions. Eleven experiments, some with up to five levels, and one computer simulation were performed to characterize and validate the system. While the number of dose and flow rate conditions and sample replicates were insufficient to achieve outcome measures with statistical power exceeding 0.8, the results presented herein demonstrate clear feasibility of the investigation premise: “An *in vitro* Biomimetic Aerosol Exposure System (BAES) will enhance the ability of respiratory health experts to better understand causes of e-cigarette associated lung injuries and other adverse health impacts associated with inhaled nicotine, cannabidiol (CBD), gases, solvents, chemicals, pathogens, and irritants.”

A BAES, which includes an electronic cigarette adapter, an Oral Cavity Module, and a Bifurcated Exposure Chamber, was designed, manufactured, and validated for analytical and biological investigation of tobacco product aerosol. Mass deposition distribution, flow rate, and cell viability were studied as a function of puffing and respiration topography and system location. The system improved upon the state-of-the-art to increase biomimicry at three levels: the systems level, the macroscale level, and the cellular level. Biomimicry was enhanced at the systems level by sequentially puffing the e-cigarette and inhaling clean air between puffs, mimicking how a human uses an electronic cigarette. The combined puff and inhalation patterns contributed to human mimicry of product use and deposition flow patterns. Biomimicry was enhanced at the macroscopic level by incorporating geometries that model the human airway, including surface topographies, turns, and a bifurcation, for both analytical characterization and biological exposures. Biomimicry was enhanced at the cellular level by manipulating the free stream angle of aerosol flow, inducing fluid shear on cells, more representative of physiological conditions experienced by airway tissues than traditional exposure systems. This system may broaden the utility of an emissions system to generate physiologically relevant *in vitro* models of exposure to inhaled aerosols.

Mass deposition was significantly different between the Puff Only condition and topography profiles that include ambient air breathing cycles between puffs. Future emissions and biological exposure studies must consider respiration topography in addition to human puffing topography for realistic results and to maintain a physiological environment for cell cultures. Mass deposition was mapped throughout the system, including accounting for mass

deposited in transit to a capture or exposure subsystem and mass in the volatile phase, creating high fidelity dose estimates. Proof of concept cell culture was performed with 3T3 fibroblasts cultured at an air-liquid interface and exposed to transverse aerosol flow in the BAES' Bifurcated Exposure Chamber (BEC). Cell viability exhibited joint dependence on nicotine yield, Y''_{NIC} [mg/cm^2], with a positively correlated trend, and local flow rate [mL/s], with a negatively correlated trend. A bivariate linear regression predictive cell viability model, when combined with the behavior-based yield model [159] for emissions, provides a foundation for predicting cell viability *in vitro* under realistic product characteristic and behavioral use conditions.

Based on this work and available literature, two standard input measures for biological studies of next generation tobacco products were recommended: Y''_{TPM} [mg/cm^2], total particulate matter per unit area, and df''_{TPM} [1/ cm^2], deposition fraction of TPM per unit area. Y''_{TPM} gives a precise dose based on surface area, appropriate for pseudostratified tissue types such as lung epithelium. df''_{TPM} normalizes dose to the quantity of aerosol produced by an electronic cigarette in a study trial, which is variable between products and within a product. Similarly, the yield and deposition fraction of any toxicant species under study should be reported. Use of standard input measures will enhance reproducibility of results within and between labs, even in the presence of the confounding factor of variation in device performance.

An *in vitro* BAES enhances the ability of respiratory health experts to better understand causes of e-cigarette associated lung injuries and other adverse health impacts associated with inhaled nicotine, cannabinoids, gases, chemicals, pathogens, and irritants. Traditional dose response curves fail to sufficiently describe where in the airway doses occur, under which use conditions they occur, and whose geometric configurations these conditions occur in. BAES provides, for the first time, methods to quantify dose and biological response as a function of product characteristics, user puffing and inhalation behavior, user airway geometry, and axial airway location. Future work that incorporates an *in silico* model of this *in vitro* system will bridge the gap between *in vitro* and *in vivo* models. Further, with greater physiological realism in exposure and response, the BAES enables reduction in the number of animals needed for pre-clinical testing saving time, money, and animals.

Future work was discussed in detail in Chapter 7. Broadly, near-term recommended future work includes:

- Study particle size distribution as a function of axial location and topography profile at several BAES flow path locations.
- Investigate how puff associated respiration flow rate affects deposition by impaction and sedimentation in BAES.
- Decrease channel height in generation 2 to maintain physiological wall shear stress throughout BAES.
- Investigate and mitigate the source of non-compatibility of alginate scaffolds in BEC Inserts to culture cell monolayers in the free stream of aerosol in the BEC.
- Refine, fabricate, and integrate BEC beta.

Long term goals of BAES development include:

- Correlate the *in vitro* system to the human lung using empirical regional deposition fractions and computational fluid dynamics.
- Correlate viability as a function of deposition fraction reported here to *in vivo* response.
- Repeat biological exposure with cell types phenotypically similar to human airway tissue and with additional endpoints (permeability assay, immunology).
- Integrate environmental control into BAES, enabling sub-chronic exposure.
- Use the comprehensive system architecture and control code logic given in Section 5.2 to incorporate bidirectional breathing with realistic exhalation topography into BAES.

Broadly, in the future, BAES should be used to continue to investigate and understand biological consequences of inhaled aerosols including toxicants, irritants, chemicals, and environmental agents including tobacco and non-tobacco vaping products.

BIBLIOGRAPHY

[1] S. Steiner, et al., "Development and testing of a new-generation aerosol exposure system: The independent holistic air-liquid exposure system (InHALES)," Toxicology in vitro : an international journal published in association with BIBRA, vol. 67, p. 104909, 2020/09// 2020.

[2] M. Winstanley, S. Woodward, and N. Walker, Tobacco in Australia: facts and issues 1995: Victorian Smoking and Health Program (Quit Victoria), 1995.

[3] S. G. Schnittman, SLAVERY IN VIRGINIA'S URBAN TOBACCO INDUSTRY-1840-1860 (SOUTH, LABOR, RICHMOND): University of Rochester, 1987.

[4] A. W. Musk and N. H. De Klerk, "History of tobacco and health," Respirology, vol. 8, pp. 286-290, 2003.

[5] US FDA, "FDA takes new steps to address epidemic of youth e-cigarette use, including a historic action against more than 1,300 retailers and 5 major manufacturers for their roles perpetuating youth access | FDA," ed: US FDA, 2018.

[6] M. E. Cornelius, C. G. Loretan, T. W. Wang, A. Jamal, and D. M. Homa, "Tobacco product use among adults—United States, 2020," Morbidity and Mortality Weekly Report, vol. 71, p. 397, 2022.

[7] World Health Organization. (2021, February 21). Tobacco. Available: https://www.who.int/news-room/fact-sheets/detail/tobacco

[8] P. G. Porter, "Origins of the American Tobacco Company," The Business History Review, vol. 43, pp. 59-76, 1969.

[9] B. Virgin, "As Dow turns 100, investors wonder about future," in Austin American Statesman, ed. Austin, Tex., 1996, p. 1.

[10] US Surgeon General. Smoking, Smoking and Health: Report of the Advisory Committee to the Surgeon General of the Public Health Service: US Department of Health, Education, and Welfare, Public Health Service, 1964.

[11] R. Fisher, "CIGARETTES, CANCER, AND STATISTICS," The Centennial Review of Arts & Science, vol. 2, pp. 151-166, 1958.

[12] R. A. Fisher, "Lung Cancer and Cigarettes?," Nature, vol. 182, pp. 108-108, 1958/07/01 1958.

[13] J. Cornfield, W. Haenszel, E. C. Hammond, A. M. Lilienfeld, M. B. Shimkin, and E. L. Wynder, "Smoking and Lung Cancer: Recent Evidence and a Discussion of Some Questions," JNCI: Journal of the National Cancer Institute, vol. 22, pp. 173-203, 1959.

[14] L. Breslow, L. Hoaglin, G. Rasmussen, and H. K. Abrams, "Occupations and cigarette smoking as factors in lung cancer," American journal of public health and the nations health, vol. 44, pp. 171-181, 1954.

[15] P. Stocks and J. M. Campbell, "Lung cancer death rates among non-smokers and pipe and cigarette smokers; an evaluation in relation to air pollution by benzpyrene and other substances," British medical journal, vol. 2, pp. 923-929, 1955.

[16] K. M. Cummings, C. P. Morley, and A. Hyland, "Failed promises of the cigarette industry and its effect on consumer misperceptions about the health risks of smoking," Tobacco control, vol. 11, pp. i110-i117, 2002.

[17] US Dept of Health and Human Services, "The Health and Consequences of Smoking," Nicotine addiction: a report of the Surgeon General, 1988.

[18] World Health Organization, WHO report on the global tobacco epidemic, 2008: the MPOWER package: World Health Organization, 2008.

[19] US FDA. (2009, Family Smoking and Tobacco Control Act.

[20] S. E. Sarles, E. C. Hensel, and R. J. Robinson, "Surveillance of U.S. Corporate Filings Provides a Proactive Approach to Inform Tobacco Regulatory Research Strategy," International Journal of Environmental Research and Public Health, vol. 18, 2021.

[21] US FDA. (2018, January 31). 2018 NYTS Data: A Startling Rise in Youth E-cigarette Use. Available: https://www.fda.gov/TobaccoProducts/PublicHealthEducation/ProtectingKidsfromTobacco/ucm625887.htm

[22] US FDA, "81 FR 28973 - Deeming Tobacco Products to Be Subject to the Federal Food, Drug and Cosmetic Act, as Amended by the Family Smoking Prevention and Tobacco Control Act," vol. 81, FDA, Ed., ed. https://www.federalregister.gov/articles/2016/05/2016-10658/deeming-tobacco-produicts-to-be-subject-to-the-federal-food-drug-and-cosmetic-act-as-amended-by-the: Food and Drug Administration, US Dept of Health and Human Services, 2016, pp. 28973-29106.

[23] "SOTTERA, INC., doing business as NJOY, Appellee v. FOOD & DRUG ADMINISTRATION, et al., Appellants.," in Circuit Judge Garland, Circuit Judge Kavanaugh, Senior Circuit Judge Williams vol. 121, ed: United States Court of Appeals,District of Columbia Circuit, 2010, pp. 1-25.

[24] US CDC, "Youth and Tobacco Use | CDC," 2021-04-22T08:05:27Z 2021.

[25] T. W. House, "Bill Signed: H.R. 2471," ed, 2022.

[26] V. Bahl, S. Lin, N. Xu, B. Davis, Y. H. Wang, and P. Talbot, "Comparison of electronic cigarette refill fluid cytotoxicity using embryonic and adult models," Reprod Toxicol, vol. 34, pp. 529-37, Dec 2012.

[27] R. Z. Behar, Y. Wang, and P. Talbot, "Comparing the cytotoxicity of electronic cigarette fluids, aerosols and solvents," Tobacco Control, vol. 27, p. 325, 2018.

[28] L. Neilson, C. Mankus, D. Thorne, G. Jackson, J. DeBay, and C. Meredith, "Development of an in vitro cytotoxicity model for aerosol exposure using 3D reconstructed human airway tissue; application for assessment of e-cigarette aerosol," 20150828 DCOM- 20160622 2015.

[29] G. Romagna, E. Allifranchini, E. Bocchietto, S. Todeschi, M. Esposito, and K. E. Farsalinos, "Cytotoxicity evaluation of electronic cigarette vapor extract on cultured mammalian fibroblasts (ClearStream-LIFE): comparison with tobacco cigarette smoke extract," Inhal Toxicol, vol. 25, 2013// 2013.

[30] S. Sancilio, M. Gallorini, A. Cataldi, and V. di Giacomo, "Cytotoxicity and apoptosis induction by e-cigarette fluids in human gingival fibroblasts," Clinical Oral Investigations, vol. 20, pp. 477-483, 2016/04/01 2016.

[31] P. Vasanthi Bathrinarayanan, J. E. P. Brown, L. J. Marshall, and L. J. Leslie, "An investigation into E-cigarette cytotoxicity in-vitro using a novel 3D differentiated co-culture model of human airways," Toxicology in Vitro, vol. 52, pp. 255-264, 2018/10/01/ 2018.

[32] C. A. Lerner, et al., "Vapors Produced by Electronic Cigarettes and E-Juices with Flavorings Induce Toxicity, Oxidative Stress, and Inflammatory Response in Lung Epithelial Cells and in Mouse Lung," PLOS ONE, vol. 10, p. e0116732, 2015.

[33] R. Bengalli, E. Ferri, M. Labra, and P. Mantecca, "Lung Toxicity of Condensed Aerosol from E-CIG Liquids: Influence of the Flavor and the In Vitro Model Used," Int J Environ Res Public Health, vol. 14, 10 2017.

[34] G. Kaur, T. Muthumalage, and I. Rahman, "Mechanisms of toxicity and biomarkers of flavoring and flavor enhancing chemicals in emerging tobacco and non-tobacco products," Toxicology Letters, vol. 288, pp. 143-155, 2018/05/15/ 2018.

[35] N. J. Leigh, R. I. Lawton, P. A. Hershberger, and M. L. Goniewicz, "Flavourings significantly affect inhalation toxicity of aerosol generated from electronic nicotine delivery systems (ENDS)," Tob Control, vol. 25, pp. ii81-ii87, 11 2016.

[36] C. J. Stewart, et al., "Effects of tobacco smoke and electronic cigarette vapor exposure on the oral and gut microbiota in humans: a pilot study," PeerJ, vol. 6, p. e4693, 2018/04/30 2018.

[37] C. Troiano, Z. Jaleel, and J. H. Spiegel, "Association of Electronic Cigarette Vaping and Cigarette Smoking With Decreased Random Flap Viability in Rats," JAMA Facial Plastic Surgery, vol. 21, pp. 5-10, 2019.

[38] S. C. Desai, "Is e-Cigarette Vaping a New Clinical Challenge to Wound Healing?," JAMA Facial Plastic Surgery, vol. 21, pp. 10-11, 2019.

[39] S. Kligerman, et al., "Radiologic, Pathologic, Clinical, and Physiologic Findings of Electronic Cigarette or Vaping Product Use–associated Lung Injury (EVALI): Evolving Knowledge and Remaining Questions," Radiology, p. 192585, 2020.

[40] N. Malek, et al., "A Transdisciplinary Approach to Understanding Characteristics of Electronic Cigarettes," Tobacco Regulatory Science, vol. 4, pp. 47-72, // 2018.

[41] S. Sarles, "Development of Topography Monitors for Inhaled Nicotine Delivery Systems," 2019.

[42] J. P. Allem, L. Dharmapuri, J. B. Unger, and T. B. Cruz, "Characterizing JUUL-related posts on Twitter," Drug Alcohol Depend, vol. 190, pp. 1-5, Jun 23 2018.

[43] Truth Initiative. (2018, 2/24/2019). truth initiative. Available: https://web.archive.org/web/20201030053229/https://truthinitiative.org/who-we-are/our-missionAvailable: https://truthinitiative.org

[44] J. Adamson, T. Jaunky, D. Thorne, and M. D. Gaça, "Characterisation of the borgwaldt LM4E system for in vitro exposures to undiluted aerosols from next generation tobacco and nicotine products (NGPs)," Food Chem Toxicol, vol. 113, pp. 337-344, Mar 2018.

[45] D. Azzopardi, et al., "Electronic cigarette aerosol induces significantly less cytotoxicity than tobacco smoke," Toxicol Mech Methods, vol. 26, pp. 477-491, Jul 2016.

[46] J. F. Ureña, L. A. Ebersol, A. Silakov, R. J. Elias, and J. D. Lambert, "Impact of Atomizer Age and Flavor on," Chem Res Toxicol, vol. 33, pp. 2527-2537, Oct 2020.

[47] D. Grady, "Vaping Kills a 15-Year-Old in Texas," in New York Times, ed: nytimes, 2020.

[48] J. F. Etter and C. Bullen, "Saliva cotinine levels in users of electronic cigarettes," in Eur Respir J. vol. 38, ed England, 2011, pp. 1219-20.

[49] US CDC. (2019, November 4). Outbreak of Lung Injury Associated with the Use of E-Cigarette, or Vaping, Products. Available: https://www.cdc.gov/tobacco/basic_information/e-cigarettes/severe-lung-disease.html

[50] G. A. Triantafyllou, et al., "Long-term outcomes of EVALI: a 1-year retrospective study," The Lancet Respiratory Medicine, vol. 9, pp. e112-e113, 2021.

[51] B. C. Blount, et al., "Vitamin E Acetate in Bronchoalveolar-Lavage Fluid Associated with EVALI," New England Journal of Medicine, 2019.

[52] M. DiPasquale, et al., "A mechanical mechanism for vitamin E acetate in E-cigarette/vaping associated lung injury (EVALI)," Chemical Research in Toxicology, 2020/08/26 2020.

[53] V. B. Mikheev, T. P. Klupinski, A. Ivanov, E. A. Lucas, E. D. Strozier, and C. Fix, "Particle size distribution and chemical composition of aerosolized vitamin E acetate," Aerosol Science and Technology, vol. 54, pp. 993-998, 2020/09/01 2020.

[54] A. J. Kaiser, et al., "A robotic system for real-time analysis of inhaled submicron and microparticles," iScience, vol. 24, p. 103091, 2021/10/22/ 2021.

[55] K. McKelvey, et al., "IQOS labelling will mislead consumers," Tobacco Control, vol. 27, p. s48, 2018.

[56] M. C. Jaklevic, "First Tobacco Product Receives “Reduced Exposure” Authorization," JAMA, vol. 324, pp. 622-622, 2020.

[57] G. S. Helen, P. Jacob Iii, N. Nardone, and N. L. Benowitz, "IQOS: examination of Philip Morris International’s claim of reduced exposure," Tobacco Control, vol. 27, pp. s30-s36, 2018.

[58] E. Simonavicius, A. McNeill, L. Shahab, and L. S. Brose, "Heat-not-burn tobacco products: a systematic literature review," Tobacco control, vol. 28, pp. 582-594, 2019.

[59] P. Nabavizadeh, et al., "Vascular endothelial function is impaired by aerosol from a single IQOS HeatStick to the same extent as by cigarette smoke," Tobacco control, vol. 27, pp. s13-s19, 2018.

[60] K. E. Farsalinos, N. Yannovits, T. Sarri, V. Voudris, and K. Poulas, "Nicotine delivery to the aerosol of a heat-not-burn tobacco product: comparison with a tobacco cigarette and e-cigarettes," Nicotine and Tobacco Research, vol. 20, pp. 1004-1009, 2018.

[61] K. Bekki, Y. Inaba, S. Uchiyama, and N. Kunugita, "Comparison of chemicals in mainstream smoke in heat-not-burn tobacco and combustion cigarettes," Journal of University of Occupational and Environmental Health, vol. 39, pp. 201-207, 2017.

[62] J.-P. Schaller, et al., "Evaluation of the Tobacco Heating System 2.2. Part 2: Chemical composition, genotoxicity, cytotoxicity, and physical properties of the aerosol," Regulatory Toxicology and Pharmacology, vol. 81, pp. S27-S47, 2016.

[63] J.-P. Schaller, J. P. M. Pijnenburg, A. Ajithkumar, and A. R. Tricker, "Evaluation of the Tobacco Heating System 2.2. Part 3: Influence of the tobacco blend on the formation of harmful and potentially harmful constituents of the Tobacco Heating System 2.2 aerosol," Regulatory Toxicology and Pharmacology, vol. 81, pp. S48-S58, 2016.

[64] G. Jaccard, D. T. Djoko, O. Moennikes, C. Jeannet, A. Kondylis, and M. Belushkin, "Comparative assessment of HPHC yields in the Tobacco Heating System THS2. 2 and commercial cigarettes," Regulatory Toxicology and Pharmacology, vol. 90, pp. 1-8, 2017.

[65] A. A. Ruprecht, et al., "Environmental pollution and emission factors of electronic cigarettes, heat-not-burn tobacco products, and conventional cigarettes," Aerosol science and technology, vol. 51, pp. 674-684, 2017.

[66] M. I. Mitova, et al., "Comparison of the impact of the Tobacco Heating System 2.2 and a cigarette on indoor air quality," Regulatory Toxicology and Pharmacology, vol. 80, pp. 91-101, 2016.

[67] N. J. Leigh, P. L. Tran, R. J. O'Connor, and M. L. Goniewicz, "Cytotoxic effects of heated tobacco products (HTP) on human bronchial epithelial cells," Tobacco control, vol. 27, pp. s26-s29, 2018.

[68] M. The Lancet Respiratory, "The EVALI outbreak and vaping in the COVID-19 era," The Lancet. Respiratory medicine, pp. S2213-2600(20)30360-X, 2020.

[69] R. Krishnamoorthi, "Letter from Chairman Raja Krishnamoorthi, Subcommittee on Economic and Consumer Policy,Committee on Oversight and Reform, to Dr. Stephen Hahn, Commissioner, Food and Drug Administration," C. Dr. Stephen Hahn, Food and Drug Administration, Ed., Available online at http://cdn.cnn.com/cnn/2020/images/08/11/2020.08.11.rk.to.fda.re.vaping.and.coronavirus.pdf ed. Washington DC: Congress of the United States House of Representatives, 2020, p. 2.

[70] Q. Wang, et al., "E-cigarette-induced pulmonary inflammation and dysregulated repair are mediated by nAChR α7 receptor: role of nAChR α7 in SARS-CoV-2 Covid-19 ACE2 receptor regulation," Respiratory Research, vol. 21, p. 154, 2020/06/18 2020.

[71] K. S. Tan and D. Y. Wang, "Vaping and Respiratory Viruses: The End for ENDS?," American Journal of Respiratory Cell and Molecular Biology, 2020.

[72] S. M. Gaiha, J. Cheng, and B. Halpern-Felsher, "Association Between Youth Smoking, Electronic Cigarette Use, and Coronavirus Disease 2019," Journal of Adolescent Health, 2020/08/11/ 2020.

[73] K. M. Bozkanat, D. Rao, T. J. Lieu, and Y. M. Rivera-Sanchez, "The perfect storm: A Case of COVID-19 infection in an adolescent patient with EVALI," Respiratory Medicine Case Reports, p. 101306, 2020/11/25/ 2020.

[74] US FDA, "Premarket Tobacco Product Applications for Electronic Nicotine Delivery Systems - Guidance for Industry," U. S. D. o. H. a. H. Services, Ed., ed, 2019.

[75] M. Aufderheide, S. Scheffler, N. Möhle, B. Halter, and D. Hochrainer, "Analytical in vitro approach for studying cyto- and genotoxic effects of particulate airborne material," Analytical and Bioanalytical Chemistry, vol. 401, pp. 3213-3220, 2011/12/01 2011.

[76] J. Adamson, D. Azzopardi, G. Errington, C. Dickens, J. McAughey, and M. D. Gaca, "Assessment of an in vitro whole cigarette smoke exposure system: The Borgwaldt RM20S 8-syringe smoking machine," Chem Cent J, vol. 5, p. 50, Aug 26 2011.

[77] W. Fields, A. Maione, B. Keyser, and B. Bombick, "Characterization and Application of the VITROCELL VC1 Smoke Exposure System and 3D EpiAirway Models for Toxicological and e-Cigarette Evaluations," Applied In Vitro Toxicology, vol. 3, pp. 68-83, 2017/03/01 2017.

[78] M. Aufderheide and U. Mohr, "CULTEX--an alternative technique for cultivation and exposure of cells of the respiratory tract to airborne pollutants at the air/liquid interface," Exp Toxicol Pathol, vol. 52, pp. 265-70, Jun 2000.

[79] M. Aufderheide, J. W. Knebel, and D. Ritter, "A Method for the In Vitro Exposure of Human Cells to Environmental and Complex Gaseous Mixtures: Application to Various Types of Atmosphere," Alternatives to Laboratory Animals, vol. 30, pp. 433-441, 2002/07/01 2002.

[80] E. C. Hensel, S. Jayasekera, and R. J. Robinson, "Accounting for effects of system dynamics to improve accuracy of emissions reported in e-cig vaping machines," Inhal Toxicol, pp. 1-11, Oct 17 2018.

[81] K. Hubert, B.-N. Barbara, and M. Lutz, "Cigarette Mainstream Smoke: The Evolution of Methods and Devices for Generation, Exposure and Collection," Beiträge zur Tabakforschung International/Contributions to Tobacco Research, vol. 27, pp. 137-274, 2016.

[82] TWG, PROTOCOL FOR THE PREPARATION OF SMOKE CONDENSATE FOR MOUSE SKIN BIOASSAY. Lorillard Records, 1968.

[83] X. Li, "In vitro toxicity testing of cigarette smoke based on the air-liquid interface exposure: A review," Toxicology in Vitro, vol. 36, pp. 105-113, 2016/10/01/ 2016.

[84] K. H. Benam, R. Novak, T. C. Ferrante, Y. Choe, and D. E. Ingber, "Biomimetic smoking robot for in vitro inhalation exposure compatible with microfluidic organ chips," Nat Protoc, vol. 15, pp. 183-206, 02 2020.

[85] E. C. Hensel, et al., "Proposed Standard Test Protocols and Outcome Measures for Quantitative Comparison of Emissions from Electronic Nicotine Delivery Systems," Int. J. Environ. Res. Public Health, vol. 19, p. 2144, 2022.

[86] E. C. Hensel, et al., "A Proposed Waterpipe Emissions Topography Protocol Reflecting Natural Environment User Behaviour," Int J Environ Res Public Health, vol. 17, Dec 2019.

[87] E. R. Weibel, A. F. Cournand, and D. W. Richards, Morphometry of the human lung vol. 1: Springer, 1963.

[88] E. R. Weibel, "Morphometry of the human lung: the state of the art after two decades," Bulletin europeen de physiopathologie respiratoire, vol. 15, pp. 999-1013, 1979.

[89] K. Horsfield, G. Dart, D. E. Olson, G. F. Filley, and G. Cumming, "Models of the human bronchial tree," Journal of Applied Physiology (1948), vol. 31, p. 207, 1971.

[90] J. Choi, M. H. Tawhai, E. A. Hoffman, and C.-L. Lin, "On intra-and intersubject variabilities of airflow in the human lungs," Physics of Fluids, vol. 21, p. 101901, 2009.

[91] B. Sul, et al., "Assessing airflow sensitivity to healthy and diseased lung conditions in a computational fluid dynamics model validated in vitro," Journal of biomechanical engineering, vol. 140, 2018.

[92] F. Lizal, J. Elcner, P. K. Hopke, J. Jedelsky, and M. Jicha, "Development of a realistic human airway model," Proceedings of the Institution of Mechanical Engineers, Part H: Journal of Engineering in Medicine, vol. 226, pp. 197-207, 2012.

[93] F. S. Stylianou, J. Sznitman, and S. C. Kassinos, "Direct numerical simulation of particle laden flow in a human airway bifurcation model," International Journal of Heat and Fluid Flow, vol. 61, pp. 677-710, 2016.

[94] P. G. Koullapis, S. C. Kassinos, M. P. Bivolarova, and A. K. Melikov, "Particle deposition in a realistic geometry of the human conducting airways: Effects of inlet velocity profile, inhalation flowrate and electrostatic charge," Journal of biomechanics, vol. 49, pp. 2201-2212, 2016.

[95] J. Wedel, P. Steinmann, M. Štrakl, M. Hriberšek, and J. Ravnik, "Can CFD establish a connection to a milder COVID-19 disease in younger people? Aerosol deposition in lungs of different age groups based on Lagrangian particle tracking in turbulent flow," Computational Mechanics, vol. 67, pp. 1497-1513, 2021/05/01 2021.

[96] A. Ghosh, D. Sen, N. K. Manna, and S. Sarkar, "Multiphase dynamics in a three dimensional branching network," Institute of Physics Conference Series: Materials Science and Engineering. p. 012041. 2021. Conference Proceedings.

[97] J. Jedelsky, F. Lizal, and M. Jicha, "Characteristics of turbulent particle transport in human airways under steady and cyclic flows," International journal of heat and fluid flow, vol. 35, pp. 84-92, 2012.

[98] E. R. Weibel, G. S. Kistler, and W. F. Scherle, "Practical stereological methods for morphometric cytology," The Journal of cell biology, vol. 30, pp. 23-38, 1966.

[99] A. Schmidt, S. Zidowitz, A. Kriete, T. Denhard, S. Krass, and H.-O. Peitgen, "A digital reference model of the human bronchial tree," Computerized Medical Imaging and Graphics, vol. 28, pp. 203-211, 2004.

[100] J. Xi, P. W. Longest, and T. B. Martonen, "Effects of the laryngeal jet on nano-and microparticle transport and deposition in an approximate model of the upper tracheobronchial airways," Journal of Applied Physiology, vol. 104, pp. 1761-1777, 2008.

[101] S. Steiner, P. Herve, S. Majeed, C. Pak, S. Frentzel, and J. Hoeng, "Development of a novel in vitro aerosol exposure system: The Independent Holistic Air-Liquid aerosol exposure system (InHALES)," Toxicology Letters, vol. 295, pp. S252-S253, 2018/10/10/ 2018.

[102] R. J. Robinson, et al., "A Comparison between Cigarette Topography from a One-Week Natural Environment Study to FTC/ISO, Health Canada, and Massachusetts Department of Public Health Puff Profile Standards," International Journal of Environmental Research and Public Health, vol. 17, 2020.

[103] E. C. Hensel, A. A. al Olayan, S. E. Sarles, N. C. Eddingsaas, and R. R. Robinson, "Hookah and Dual-Use Behavior in the Natural Environment," in Tobacco Regulatory Science Meeting, Baltimore, MD, 2018.

[104] E. Hensel, et al., "Understanding the Association Between Pod-Style Electronic Cigarette Aerosol Emissions and User Topography Behavior," presented at the SRNT 2020 Annual Meeting, New Orleans, LA, 2020.

[105] S. Jayasekera, E. Hensel, and R. Robinson, "Feasibility of Using the Hexoskin Smart Garment for Natural Environment Observation of Respiration Topography," International Journal of Environmental Research and Public Health, vol. 18, p. 7012, 2021.

[106] N. C. Eddingsaas, E. C. Hensel, S. O'Dea, P. Kunselman, and A. G. DiFrancesco, "Effect of user puffing topography on total particulate matter, nicotine, and volatile carbonyl emissions from Narghil waterpipes," Tobacco Control, vol. doi: 10.1136/tobaccocontrol-2019-054966, pp. tobaccocontrol-2019-054966, 2019.

[107] R. J. Robinson, E. C. Hensel, A. A. al-Olayan, J. M. Nonnemaker, and Y. O. Lee, "Effect of e-liquid flavor on electronic cigarette topography and consumption behavior in a 2-week natural environment switching study," PLoS ONE, vol. 13, p. e0196640, 11/29/2017 received, 04/17/2018 accepted. 2018.

[108] W. Zhang, et al., "Salivary Microbial Dysbiosis is Associated with Systemic Inflammatory Markers and Predicted Oral Metabolites in Non-Small Cell Lung Cancer Patients," J Cancer, vol. 10, pp. 1651-1662, 2019.

[109] F. D'Aiuto, F. Graziani, S. Tete, M. Gabriele, and M. S. Tonetti, "Periodontitis: from local infection to systemic diseases," International journal of immunopathology and pharmacology, vol. 18, pp. 1-11, 2005.

[110] D. A. Granger, M. K. Taylor, and SpringerLink, Salivary Bioscience: Foundations of Interdisciplinary Saliva Research and Applications, 1st 2020. ed. Cham: Springer International Publishing, 2020.

[111] A. C. Schamberger, C. A. Staab-Weijnitz, N. Mise-Racek, and O. Eickelberg, "Cigarette smoke alters primary human bronchial epithelial cell differentiation at the air-liquid interface," Scientific Reports, vol. 5, p. 8163, 2015/02/02 2015.

[112] E. Bishop, L. Haswell, J. Adamson, S. Costigan, D. Thorne, and M. Gaca, "An approach to testing undiluted e-cigarette aerosol in vitro using 3D reconstituted human airway epithelium," Toxicol In Vitro, vol. 54, pp. 391-401, Feb 2019.

[113] L. Czekala, L. Simms, M. Stevenson, N. Tschierske, A. G. Maione, and T. Walele, "Toxicological comparison of cigarette smoke and e-cigarette aerosol using a 3D in vitro human respiratory model," Regul Toxicol Pharmacol, vol. 103, pp. 314-324, Apr 2019.

[114] D. Thorne, et al., "Genotoxicity evaluation of tobacco and nicotine delivery products: Part One. Mouse lymphoma assay," Food Chem Toxicol, vol. 132, p. 110584, Oct 2019.

[115] H. Yao and I. Rahman, "Current concepts on oxidative/carbonyl stress, inflammation and epigenetics in pathogenesis of chronic obstructive pulmonary disease," Toxicol Appl Pharmacol, vol. 254, pp. 72-85, Jul 2011.

[116] S. Cirillo, et al., "Impact of electronic cigarette heating coil resistance on the production of reactive carbonyls, reactive oxygen species and induction of cytotoxicity in human lung cancer cells in vitro," Regul Toxicol Pharmacol, vol. 109, p. 104500, Dec 2019.

[117] A. J. Ross, L. A. Dailey, L. E. Brighton, and R. B. Devlin, "Transcriptional Profiling of Mucociliary Differentiation in Human Airway Epithelial Cells," American Journal of Respiratory Cell and Molecular Biology, vol. 37, pp. 169-185, 2007/08/01 2007.

[118] L. E. Ostrowski and P. Nettesheim, "Inhibition of Ciliated Cell Differentiation by Fluid Submersion," Experimental Lung Research, vol. 21, pp. 957-970, 1995/01/01 1995.

[119] H. Chen, et al., "Evaluation of the cytotoxicity of cigarette smoke condensate by a cellular impedance biosensor," Food and Chemical Toxicology, vol. 50, pp. 612-618, 2012/03/01/ 2012.

[120] D. Thorne, J. Whitwell, J. Clements, P. Walker, D. Breheny, and M. Gaca, "The genotoxicological assessment of a tobacco heating product relative to cigarette smoke using the in vitro micronucleus assay," Toxicology Reports, 2020/08/15/ 2020.

[121] Y. Zhou, et al., "Extracellular matrix in lung development, homeostasis and disease," Matrix biology : journal of the International Society for Matrix Biology, vol. 73, pp. 77-104, 2018/11// 2018.

[122] C. Tapparel, K. Sobo, S. Constant, S. Huang, S. Van Belle, and L. Kaiser, "Growth and characterization of different human rhinovirus C types in three-dimensional human airway epithelia reconstituted in vitro," Virology, vol. 446, pp. 1-8, 2013/11/01/ 2013.

[123] A. W. Orr, B. P. Helmke, B. R. Blackman, and M. A. Schwartz, "Mechanisms of Mechanotransduction," Developmental Cell, vol. 10, pp. 11-20, 2006/01/01/ 2006.

[124] A. O. Stucki, et al., "A lung-on-a-chip array with an integrated bio-inspired respiration mechanism," Lab on a Chip, vol. 15, pp. 1302-1310, 2015.

[125] D. Huh, B. D. Matthews, A. Mammoto, M. Montoya-Zavala, H. Y. Hsin, and D. E. Ingber, "Reconstituting Organ-Level Lung Functions on a Chip," Science, vol. 328, p. 1662, 2010.

[126] A. Balijepalli and V. Sivaramakrishan, "Organs-on-chips: research and commercial perspectives," Drug Discov Today, vol. 22, pp. 397-403, 02 2017.

[127] M. H. Lee, J. E. Szulejko, and K. H. Kim, "Determination of carbonyl compounds in electronic cigarette refill solutions and aerosols through liquid-phase dinitrophenyl hydrazine derivatization," Environ Monit Assess, vol. 190, p. 200, Mar 8 2018.

[128] M. C. Brinkman, et al., "Comparison of True and Smoothed Puff Profile Replication on Smoking Behavior and Mainstream Smoke Emissions," Chem Res Toxicol, vol. 28, pp. 182-90, Feb 16 2015.

[129] M. Delaval, D. Egli, P. Schüpfer, C. Benarafa, M. Geiser, and H. Burtscher, "Novel instrument to generate representative e-cigarette vapors for physicochemical particle characterization and in-vitro toxicity," Journal of Aerosol Science, vol. 129, pp. 40-52, 2019/03/01/ 2019.

[130] D. Thorne, et al., "Extreme testing of undiluted e-cigarette aerosol in vitro using an Ames air-agar-interface technique," Mutation Research/Genetic Toxicology and Environmental Mutagenesis, vol. 828, pp. 46-54, 2018/04/01/ 2018.

[131] K. E. Farsalinos and G. Gillman, "Carbonyl Emissions in E-cigarette Aerosol: A Systematic Review and Methodological Considerations," Frontiers in Physiology, vol. 8, p. 1119, 2018.

[132] T. Cheng, "Chemical evaluation of electronic cigarettes," Tobacco Control, vol. 23, p. ii11, 2014.

[133] F. Zanetti, et al., "Assessment of the impact of aerosol from a potential modified risk tobacco product compared with cigarette smoke on human organotypic oral epithelial cultures under different exposure regimens," Food Chem Toxicol, vol. 115, pp. 148-169, May 2018.

[134] Z. Wu, et al., "E-cigarette Aerosols Versus Cigarette Smoke: Harm Reduction in Levels of Harmful and Potentially Harmful Constituents and Cytotoxicity," 2021.

[135] R. Z. Behar, W. Luo, K. J. McWhirter, J. F. Pankow, and P. Talbot, "Analytical and toxicological evaluation of flavor chemicals in electronic cigarette refill fluids," Scientific Reports, vol. 8, p. 8288, 2018/05/29 2018.

[136] J. Singh, E. Luquet, D. P. T. Smith, H. J. Potgieter, and P. Ragazzon, "Toxicological and analytical assessment of e-cigarette refill components on airway epithelia," Science progress, vol. 99, pp. 351-398, 2016.

[137] R. J. Robinson, J. Russo, and R. L. Doolittle, "3D Airway reconstruction using visible human data set and human casts with comparison to morphometric data," Anatomical Record-Advances in Integrative Anatomy and Evolutionary Biology, vol. 292, pp. 1028-1044, Jul 2009.

[138] S. Soulet, C. Pairaud, and H. Lalo, "A Novel Vaping Machine Dedicated to Fully Controlling the Generation of E-Cigarette Emissions," International Journal of Environmental Research and Public Health, vol. 14, p. 1225, 10/14 07/28/received 10/06/accepted 2017.

[139] J. Zhao, G. Pyrgiotakis, and P. Demokritou, "Development and characterization of electronic-cigarette exposure generation system (Ecig-EGS) for the physico-chemical and toxicological assessment of electronic cigarette emissions," Inhalation Toxicology, vol. 28, pp. 658-669, 2016/12/05 2016.

[140] S. Hosseini, V. Gholap, M. S. Halquist, and L. Golshahi, "Effects of device settings and e-liquid characteristics on mouth-throat losses of nicotine delivered with electronic nicotine delivery systems (ENDS)," Journal of Aerosol Science, vol. 171, p. 106178, 2023/06/01/ 2023.

[141] ISO/TC-126/SC-3, "ISO 20768:2018 Vapour product - Routine analytical vaping machine - definitions and standard conditions," ed. Geneva, Switzerland: International Organization for Standardization, 2018, p. 7.

[142] C. No, "81-Routine Analytical Machine for E-Cigarette Aerosol Generation and Collection-Definitions and Standard Conditions," CORESTA Recommended Method Number, vol. 81, 2015.

[143] N. A. Saliba, et al., "Surface chemistry of electronic cigarette electrical heating coils: Effects of metal type on propylene glycol thermal decomposition," Journal of Analytical and Applied Pyrolysis, vol. 134, pp. 520-525, 2018/09/01/ 2018.

[144] J. H. Hwang, et al., "Electronic cigarette inhalation alters innate immunity and airway cytokines while increasing the virulence of colonizing bacteria," J Mol Med (Berl), vol. 94, pp. 667-79, 06 2016.

[145] M. M. Roushdy, "Association of dental caries, Streptococcus mutans counts and secretory IgA with tobacco smoking," Australian Journal of Basic and Applied Sciences, vol. 3, pp. 3224-3229, 2009.

[146] S. Pushalkar, et al., "Electronic Cigarette Aerosol Modulates the Oral Microbiome and Increases Risk of Infection," iScience, vol. 23, p. 100884, 2020/03/27/ 2020.

[147] K. L. Ying, et al., "Abstract 1163: Lung and salivary microbiome in electronic cigarette users, never-smokers, and smokers: A pilot cross-sectional study," Cancer Research, vol. 80, p. 1163, 2020.

[148] S. Bashiardes, G. Zilberman-Schapira, and E. Elinav, "Use of Metatranscriptomics in Microbiome Research," Bioinformatics and biology insights, vol. 10, pp. 19-25, 2016.

[149] J. H. Cho, "The association between electronic-cigarette use and self-reported oral symptoms including cracked or broken teeth and tongue and/or inside-cheek pain among adolescents: A cross-sectional study," PLOS ONE, vol. 12, p. e0180506, 2017.

[150] X. Zhao, et al., "Effects of different discoloration challenges and whitening treatments on dental hard tissues and composite resin restorations," J Dent, vol. 89, p. 103182, 10 2019.

[151] S. Kumar, R. S. Prasad, K. K. Atulya, G. Kedia, and N. B. Kedia, "Assessment of effect of cigarette smoking effects on the surface roughness of different denture base materials," Journal of Advanced Medical and Dental Sciences Research, vol. 8, 2020.

[152] G. Moschos, N. Nikolaidis, and L. Pitas, "Anatomically-based 3D face and oral cavity model for creating virtual medical patients," in 2004 IEEE International Conference on Multimedia and Expo (ICME) (IEEE Cat. No.04TH8763), 2004, pp. 867-870 Vol.2.

[153] Y. Liang, et al., "OralViewer: 3D Demonstration of Dental Surgeries for Patient Education with Oral Cavity Reconstruction from a 2D Panoramic X-ray," pp. 553-563.

[154] N. Al Mortadi, D. Eggbeer, J. Lewis, and R. J. Williams, "CAD/CAM/AM applications in the manufacture of dental appliances," American journal of orthodontics and dentofacial orthopedics, vol. 142, pp. 727-733, 2012.

[155] E. Taneva, B. Kusnoto, and C. A. Evans, "3D scanning, imaging, and printing in orthodontics," Issues in contemporary orthodontics, vol. 148, 2015.

[156] R. J. Robinson, P. Snyder, and M. J. Oldham, "Comparison of particle tracking algorithms in commercial CFD packages: sedimentation and diffusion," Inhalation toxicology, vol. 19, pp. 517-531, 2007.

[157] Vitrocell. (2022, April 7). Smoking Robot VC 10. Available: https://www.vitrocell.com/inhalation-toxicology/smoking-machines/vc-10

[158] Vitrocell. (2022, March 7). VC 1. Available: https://www.vitrocell.com/inhalation-toxicology/smoking-machines/vc-1

[159] E. C. Hensel, N. C. Eddingsaas, A. G. DiFrancesco, S. Jayasekera, S. O'Dea, and R. J. Robinson, "Framework to Estimate Total Particulate Mass and Nicotine Delivered to E-cig Users from Natural Environment Monitoring Data," Scientific Reports, 2019.

[160] J. Adamson, D. Thorne, B. Zainuddin, A. Baxter, J. McAughey, and M. Gaça, "Application of dosimetry tools for the assessment of e-cigarette aerosol and cigarette smoke generated on two different in vitro exposure systems," Chemistry Central Journal, vol. 10, p. 74, 2016/12/09 2016.

[161] J. Adamson, X. Li, H. Cui, D. Thorne, F. Xie, and M. D. Gaca, "Nicotine Quantification In Vitro: A Consistent Dosimetry Marker for e-Cigarette Aerosol and Cigarette Smoke Generation," Applied In Vitro Toxicology, vol. 3, pp. 14-27, 2017/03/01 2017.

[162] S. Anthérieu, et al., "Comparison of cellular and transcriptomic effects between electronic cigarette vapor and cigarette smoke in human bronchial epithelial cells," Toxicology in Vitro, vol. 45, pp. 417-425, 2017/12/01/ 2017.

[163] M. Taylor, et al., "A comparative assessment of e-cigarette aerosols and cigarette smoke on in vitro endothelial cell migration," Toxicology Letters, vol. 277, pp. 123-128, 2017/08/05/ 2017.

[164] CORESTA. (2015, 2014 Electronic Cigarette Aerosol Parameters Study. Available: https://www.coresta.org/2014-electronic-cigarette-aerosol-parameters-study-29232.html

[165] T. R. Sosnowski and K. Kramek-Romanowska, "Predicted Deposition of E-Cigarette Aerosol in the Human Lungs," Journal of Aerosol Medicine and Pulmonary Drug Delivery, vol. 29, pp. 299-309, 2016/06/01 2016.

[166] A. Peters, et al., "Translocation and potential neurological effects of fine and ultrafine particles a critical update," Particle and fibre toxicology, vol. 3, pp. 1-13, 2006.

[167] K. Rudd, et al., "Chemical Composition and In Vitro Toxicity Profile of a Pod-Based E-Cigarette Aerosol Compared to Cigarette Smoke," Applied In Vitro Toxicology, vol. 6, pp. 11-41, 2020/03/01 2020.

[168] Health Canada - Tobacco Reporting Regulations, Part 3 - Emissions from Designated Tobacco Products, H. Canada, 2000.

[169] S. E. Sarles, E. Lazarus, L. Widom, W.-K. Karin, and I. Rivero, "Hydrogel Composite Layering Process for Full Thickness Skin Models," presented at the IISE Annual Conference and Expo, Seattle, WA, 2022.

[170] A. Mata, A. J. Fleischman, and S. Roy, "Characterization of polydimethylsiloxane (PDMS) properties for biomedical micro/nanosystems," Biomedical microdevices, vol. 7, pp. 281-293, 2005.

[171] V. K. Sidhaye, K. S. Schweitzer, M. J. Caterina, L. Shimoda, and L. S. King, "Shear stress regulates aquaporin-5 and airway epithelial barrier function," Proceedings of the National Academy of Sciences, vol. 105, pp. 3345-3350, 2008.

[172] S. K. Mahto, J. Tenenbaum-Katan, A. Greenblum, B. Rothen-Rutishauser, and J. Sznitman, "Microfluidic shear stress-regulated surfactant secretion in alveolar epithelial type II cells in vitro," American Journal of Physiology-Lung Cellular and Molecular Physiology, vol. 306, pp. L672-L683, 2014.

[173] E. C. Hensel, et al., "Nominal Operating Envelope of Pod and Pen Style Electronic Cigarettes," Frontiers in Public Health, vol. 9, p. 1201, 17 Aug 2021 2021.

[174] A. S. Green, "Modelling of peak-flow wall shear stress in major airways of the lung," Journal of Biomechanics, vol. 37, pp. 661-667, 2004/05/01/ 2004.

[175] R. Robinson, S. Jayasekera, E. Sarles, S. Godleski, G. Difrancesco, and E. Hensel, "Juul Puff Topography From Real-world Ambulatory Measurement," ed. San Antonio River Rivercenter in San Antonio, TX: Society For Research On Nicotine & Tobacco, 2023.

[176] Q. M. Saleh, "Methods for Quantifying Power Characteristics and Chronic Patterns of Use Behavior of Electronic Vaping Products," 2022.

[177] M. Bicego and S. Baldo, "Properties of the Box–Cox transformation for pattern classification," Neurocomputing, vol. 218, pp. 390-400, 2016/12/19/ 2016.

[178] O. Geiss, I. Bianchi, and J. Barrero-Moreno, "Correlation of volatile carbonyl yields emitted by e-cigarettes with the temperature of the heating coil and the perceived sensorial quality of the generated vapours," 20160319 DCOM- 20161213 2016.

[179] L. Pichelstorfer, R. Winkler-Heil, M. Boy, and W. Hofmann, "Aerosol dynamics simulations of the anatomical variability of e-cigarette particle and vapor deposition in a stochastic lung," Journal of Aerosol Science, vol. 158, p. 105706, 2021.

[180] M. Y. Weiss, R. Melnyk, D. Mix, A. Ghazi, G. E. Vates, and J. J. Stone, "Design and Validation of a Cervical Laminectomy Simulator using 3D Printing and Hydrogel Phantoms," Operative Neurosurgery, vol. 18, pp. 202-208, 2019.

[181] T. M. Bücking, E. R. Hill, J. L. Robertson, E. Maneas, A. A. Plumb, and D. I. Nikitichev, "From medical imaging data to 3D printed anatomical models," PLoS One, vol. 12, p. e0178540, 2017.

[182] R. J. Robinson, P. Snyder, and M. J. Oldham, "Comparison of analytical and numerical particle deposition using commercial CFD packages: Impaction and sedimentation," Inhalation toxicology, vol. 20, pp. 485-497, 2008.

[183] E. W. Flitney, E. R. Kuczmarski, S. A. Adam, and R. D. Goldman, "Insights into the mechanical properties of epithelial cells: the effects of shear stress on the assembly and remodeling of keratin intermediate filaments," The FASEB Journal, vol. 23, pp. 2110-2119, 2009/07/01 2009.

[184] A. M. Rahimi, M. Cai, and S. Hoyer-Fender, "Heterogeneity of the NIH3T3 Fibroblast Cell Line," Cells, vol. 11, p. 2677, 2022.

[185] S. Weng and J. Fu, "Synergistic regulation of cell function by matrix rigidity and adhesive pattern," Biomaterials, vol. 32, pp. 9584-9593, 2011/12/01/ 2011.

[186] A. Svanström, et al., "Optimized alginate-based 3D printed scaffolds as a model of patient derived breast cancer microenvironments in drug discovery," Biomedical Materials, vol. 16, p. 045046, 2021.

[187] T. Jaunky, et al., "Assessment of tobacco heating product THP1.0. Part 5: In vitro dosimetric and cytotoxic assessment," Regul Toxicol Pharmacol, vol. 93, pp. 52-61, Mar 2018.

[188] C. R. Polgampola Ralalage, "Analysis of the aerosol composition, its deposition and uptake in electronic cigarette users," MS, Department of Chemistry and Materials Science, Rochester Institute of Technology, Rochester, NY, 2023.

[189] N. L. Benowitz, C. Havel, P. Jacob, D. F. O'Shea, D. Wu, and J. Fowles, "Vaping THC-O Acetate: Potential for Another EVALI Epidemic," Journal of Medical Toxicology, vol. 19, pp. 37-39, 2023/01/01 2023.

[190] C. Schaal and S. P. Chellappan, "Nicotine-Mediated Cell Proliferation and Tumor Progression in Smoking-Related CancersCell Cycle Alterations in Lung Cancer," Molecular Cancer Research, vol. 12, pp. 14-23, 2014.

[191] P. Dasgupta, et al., "Nicotine induces cell proliferation, invasion and epithelial-mesenchymal transition in a variety of human cancer cell lines," International Journal of Cancer, vol. 124, pp. 36-45, 2009.

[192] R. Polosa, R. O'Leary, D. Tashkin, R. Emma, and M. Caruso, "The effect of e-cigarette aerosol emissions on respiratory health: a narrative review," Expert review of respiratory medicine, vol. 13, pp. 899-915, 2019.